

EXHIBIT 5

Thermal and Mechanical Optimisation of Diode Laser Bar Packaging

**Von der Fakultät für Maschinenwesen der
Rheinisch-Westfälischen Technischen Hochschule Aachen
zur Erlangung des akademischen Grades eines
Doktors der Naturwissenschaften
genehmigte Dissertation**

vorgelegt von

**Diplom-Physiker
Christian Scholz
aus Duisburg**

Berichter:

Universitätsprofessor Dr. rer. nat. R. Poprawe M.A.

Universitätsprofessor Dr. rer. nat. P. Loosen

Tag der mündlichen Prüfung:

23. Mai 2007

Diese Dissertation ist auf den Internetseiten der Hochschulbibliothek online verfügbar

Bibliografische Information der Deutschen

Bibliothek:

Die Deutsche Bibliothek verzeichnet diese
Publikation in der Deutschen Nationalbibliografie;
detaillierte bibliografische Daten sind im Internet
über <http://dnb.d-nb.de> abrufbar.

© July 2007 Christian Scholz

Herstellung und Verlag: Books on Demand GmbH, Norderstedt

ISBN-13: 9783837002607

"If we knew what it was we were doing, it would not be called, research, would it?"

Albert Einstein (1879-1966)
German Physicist, Nobel prize winner

I Introduction and Technical Basics

1.	Introduction.....	3
2.	Components of Diode Laser Bar Package and Packaging Process	7
2.1.	Laser Bar	7
2.1.1.	Temperature Dependent Properties of Laser Bar	9
2.1.2.	Influence of Mechanical Stress.....	11
2.2.	Heat Sink	14
2.2.1.	Conductively Cooled Heat Sink.....	15
2.2.2.	Actively Cooled Heat Sink.....	17
2.2.3.	Expansion Matched Heat Sink	17
2.3.	Solder.....	19
2.3.1.	Indium.....	20
2.3.2.	Indium-Tin.....	21
2.3.3.	Gold-Tin	22
2.3.4.	Oxidation and Reduction of Solder	23
2.3.5.	Plating and Diffusion Barrier	25
2.4.	N-Contact Sheet and Isolation Foil.....	28
2.5.	Packaging of Diode Laser Bars	28
3.	Properties of Diode Laser Bars and Measurement Methods.....	30
3.1.	Electro-Optical Properties	30
3.2.	Measurement Methods of Electro-Optical Properties.....	34
3.3.	Lifetime of Diode Laser Bars.....	35
3.4.	Thermal Properties of Heat Sinks.....	37
3.5.	Measurement Methods for Packaging Induced Stress.....	40
3.5.1.	Photo-Current Spectroscopy (PCS).....	42
3.5.2.	Micro-Photoluminescence Spectroscopy	43
3.5.3.	DoP-Electroluminescence.....	44
3.6.	Metallurgical Analysis	46
3.6.1.	Analysis of Solder Cross Section	46
3.6.2.	Shear Tests	49

II Analysis

4.	Thermal Influence of the Packaging	53
4.1.	Thermal Resistance	53
4.1.1.	Simulation.....	53
4.1.2.	Experiment.....	56
4.2.	Thermal Contact between Heat Sink and Laser Bar.....	57
4.2.1.	Avoiding Oxidation of Solder	58
4.2.2.	Solder Voids Experiment.....	63
4.2.3.	Simulation of Solder Voids	66
4.3.	Influence of Solder Layer Thickness	69
4.3.1.	Simulation.....	69
4.3.2.	Experiment.....	71
4.4.	Thermal Influence on Degradation.....	75
5.	Mechanical Influence of the Packaging	76
5.1.	Basic Principal of Mechanical Load	76
5.2.	Expansion-Matched Heat Sinks.....	78
5.2.1.	Design and Simulation	79
5.2.2.	Fabrication and Properties.....	85
5.2.3.	Stress Level of Laser Bar on Expansion-Matched Heat Sinks.....	87
5.3.	Metallurgy of the Solder Interface	90
5.3.1.	Stress Reduction by Solder Creeping	90
5.3.2.	Diffusion Barrier	97
5.3.3.	Lifetime Dependent upon different Solder Layer Thickness.....	102

III Outlook

6.	Summary.....	105
7.	Zusammenfassung	107

IV Appendix

8.	Material Properties	111
9.	Abbreviation and Symbols	115
10.	Literature	118

Part I

Introduction and Technical Basics

1. Introduction

During the last few years, diode laser systems have become established as a credible photon source for material processing, medical applications, and the pumping of solid-state lasers. These systems typically consist of several diode laser bars, whose beams are coupled in order to achieve powers of up to 10 kW in a single system. The main component of these diode laser systems is a high power diode laser bar. Commercial diode laser bars are available with an optical output power of up to 120W in the near infrared range. The laser bar consists of several individual lasers, which are integrated on one semiconductor chip, the laser bar. The advantages of these lasers are their high efficiency, commonly found to be greater than 50% over a lifetime in excess of 10,000 hours.

The reliability of diode lasers has increased, and typical failures such as catastrophic optical mirror damage (COMD), have become seldom. Around five to ten years ago, typical thresholds of facet load for COMD were in the region of 1-2 MW/cm². The coating process for laser facets has improved during the last few years and today's facets can resist a load of over 20 MW/cm² [63],[67]. Therefore, COMD is no longer a lifetime limiting factor.

The result of the improved facet coatings can be seen in the rising output power data. Several high optical output records for a cm-bar have been reported. The development of these high output records and the power capacity that is commercially available are shown in Figure 1-1.

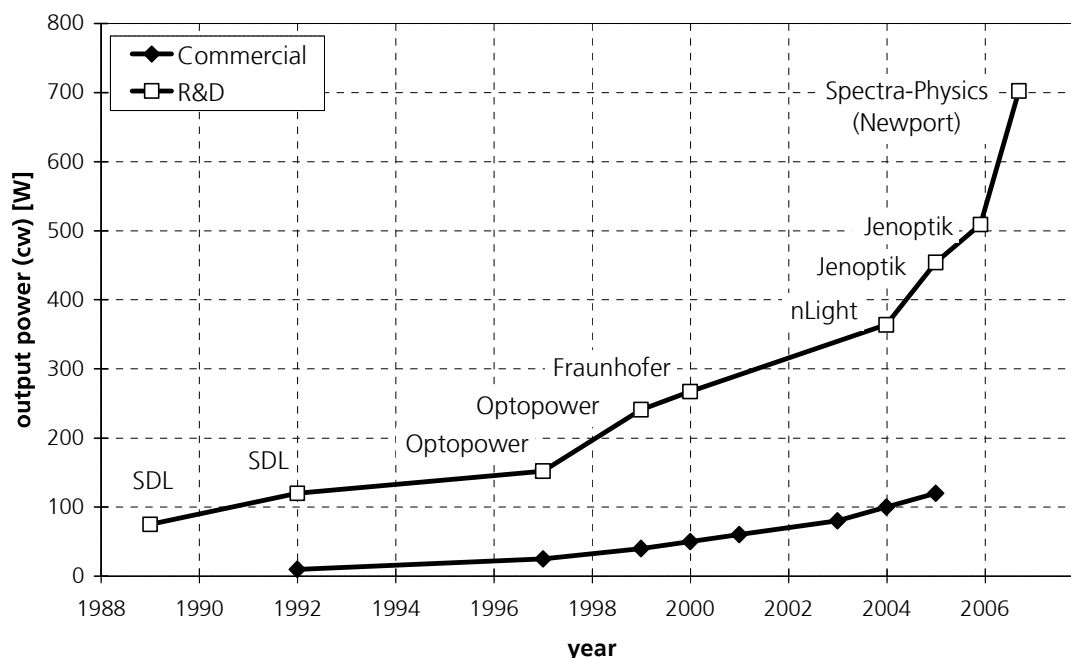


Figure 1-1: Highest reported and commercially available CW (continuous wave) output power delivered by near IR 1cm-bars during the last decade.

Today, the most critical factor when producing high output powers is the increase in temperature experienced during operation. Therefore, the recent increases seen in record output powers over 500W are only possible due to the significantly improved efficiency of laser bars. For example, an output power greater than 500W, demonstrated by Jenoptik at the end of 2005, was achieved using a package which cools both the p- and n-side of the laser bar. Commercial diode laser bars are only cooled on the p-side.

Despite the impressive advancements in laser material technology, the performance and reliability of commercial laser bars continue to be limited by other factors. Thermal management, mechanical stress, and material defects introduced by the mounting/package process are critical issues which need to be resolved in order to achieve reliable laser performance at higher levels of power.

Besides the operating temperature itself, an important factor believed to be responsible for the ageing of diode lasers is thermo-mechanical stress. These high stress levels are caused by the packaging process [73].

Today, laser bars are soldered with indium onto copper heat sinks. The mismatch between the thermal expansion coefficient (CTE) of the heat sink (copper $16.8 \cdot 10^{-6} \text{ K}^{-1}$) and the laser bar (GaAs $6.8 \cdot 10^{-6} \text{ K}^{-1}$) can cause high amounts of mechanical stress. For instance, the change in length of a 10 mm wide laser bar during the cooling process is greater than 10 μm . The ductile properties of indium are used to compensate for the mismatch caused by plastic deformation (creeping). The long term stability due to migration and oxidation of the soft solder indium is an issue. The diffusion that occurs in indium is very strong, leading to change the properties of the solder during the lifetime of the diode laser. These changes can lead to fatigue failures.

If a "hard" solder, such as gold-tin is used, the stress is much higher. These solders typically have a higher melting point, which results in a greater mismatch in length, and are more brittle. Therefore expansion matched submounts, for example those made out of a tungsten copper composite material, are used for gold-tin packages. In this case, the CTE of the submounts must be equal to the CTE of the laser bar material. Slight differences create high stress levels because the brittle solder cannot help reduce the induced strain. Another disadvantage of the brittle solder is the lower thermal conductivity of typical submount materials, which in turn leads to inefficient removal of waste heat. This leads to a higher thermal load during operation, reducing the lifetime. On the other hand, gold-tin solder is more stable over a long period of time due to the high gold ratio, and is also a certified solder for use in the telecommunications market.

It is necessary to investigate the packaging process, particularly the thermo-mechanical behaviour, due to the fact that the packaging process is at the beginning of the value-added chain of a diode laser. The lifetime, dependent on thermal and mechanical influences as well as on operation modes, is very complex. Therefore a precise prediction can not be made. Usually the dependency is determined statistically, using for example the Weibull distribution. Due to the complexity, a large number of lasers are needed for the parameter variation. In the case of diode laser bars it is very cost and equipment intensive. In contrast to this method, this work is a detailed investigation of the key factors of the thermo-mechanical influences and not a large scale overview.

With this gained knowledge, the reliability of diode lasers can be improved and can lower the risk of expensive breakdowns at the end of the value-added chain. An example of this can be seen in the production of a diode laser module (see Figure 1-2).

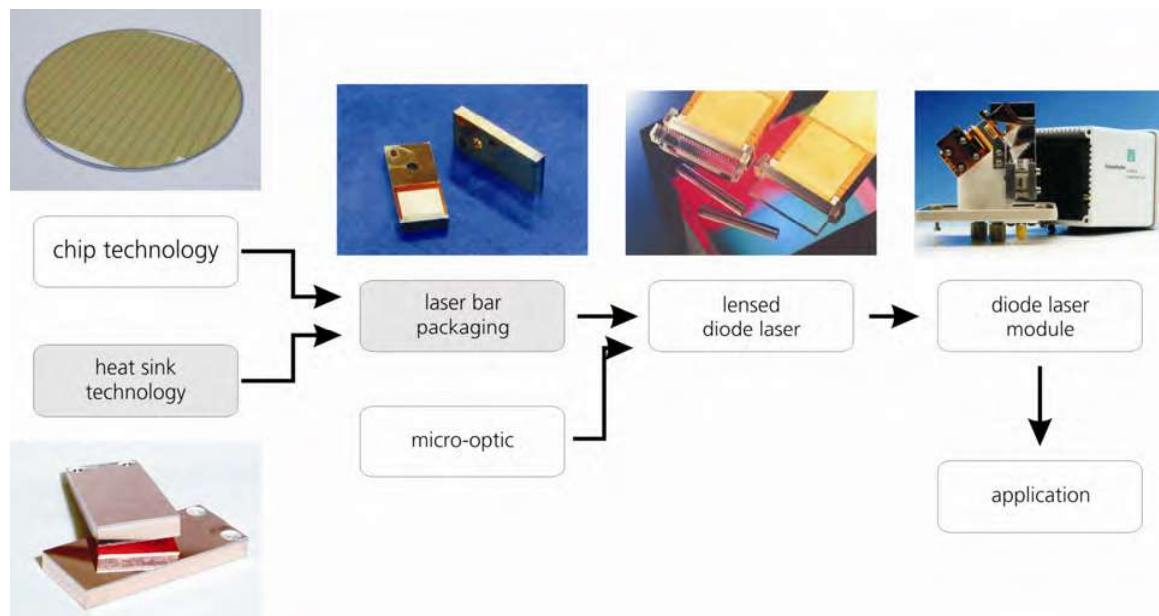


Figure 1-2: Value-added chain for diode laser bars

The thermo-mechanical key factors are the influence of the thermal load, caused by the thermal resistance of the heat sink, insufficient connections and solder layer thickness, as well as the mechanical load, caused by the expansion of the heat sink and the metallurgy of the solder interface.

One method to reduce mechanical strain, is to use expansion matched heat sinks. Typically, submount materials have a lower thermal conductivity than copper, which decreases the thermal load of the laser bar. New actively cooled expansion-matched heat sinks have been developed, in order to reduce the high thermal resistance in expansion matched packages with submounts.

Another method utilised to reduce mechanical stress that is also used in standard packages with copper heat sinks, is to optimise the solder layer. An important aspect of the thermal and mechanical optimisation of the laser bar package is the solder layer thickness. A thicker solder layer should not be as vulnerable to the growth of intermetallic compounds, as the indium ratio is higher. The influence of solder layer thickness on relaxation and thermal load is also investigated here.

Premature failures of diode lasers are often caused by an insufficient mechanical and thermal contact between the heat sink and laser bar. Solder voids can be caused by an insufficient reduction of the solder or by remains left over from the reduction process. Therefore a "protection" method, which prevents oxidation of the indium solder, is investigated. In this case, a reduction method is no longer required.

Chapter 2 outlines the fundamental composition of a typical diode laser bar package. The two main components of the package are the laser bar and heat sink, which are described in depth regarding their thermal and mechanical behaviours. This chapter ends with a short description of the packaging process.

In Chapter 3, the electro-optical properties of diode laser bars and the measurement methods used are described. Measurement methods used to determine the stress level inside of the laser

bar are also described. The chapter ends with the outlining of common metallurgical analysis methods used to determine the properties of the solder composites.

The analysis section is divided into two parts investigating the thermal and mechanical impacts on the laser bar package. Chapter 4 begins with the thermal analysis of newly developed expansion matched heat sinks. Due to poor reduction of the solder, solder voids can negatively influence the performance of the diode laser. The thermal influence of solder voids and a "protection" method to avoid solder oxidation are investigated. The chapter ends with an analysis of the thermal influence of solder layers with varying thicknesses.

In Chapter 5 the mechanical design and fabrication of the expansion matched heat sinks are described. In the first part of the chapter, the expansion matched package is analysed regarding packaging induced stress, and ageing tests are also performed. In the second part of the chapter, the influence of the metallurgical solder composition is investigated, particularly the impact of the solder layer thickness and the influence of diffusion barriers.

The work ends with a summary of the achieved results and conclusions regarding the influence of the investigated key factors.

2. Components of Diode Laser Bar Package and Packaging Process

This chapter describes the main components of the diode laser. The laser bar is of particular interest. Its properties such as wavelength, efficiency, and output power are key factors for use in applications. These properties are temperature and stress dependent, so that they can also be used to analyse and qualify the packaging process.

Different types of heat sinks, which have a great thermal and mechanical influence on the laser bar, are explained regarding their thermal and mechanical behaviour. The solder, which joins the laser bar to the heat sink, is important for insuring that a proper thermal and mechanical connection is made. Therefore the solder properties are also described. The chapter closes with a short description of the packaging process of laser bars.

2.1. Laser Bar

The laser bar is the core of the diode laser. It is an array of diode lasers, which are called emitters. The following elements make up a semiconductor laser. First, a medium is needed that provides an optical gain by stimulated emission. For the near infrared wavelength range (600-1100 nm) gallium arsenide is chosen. The most common material composites for the quantum well structure are InGaAs and AlGaAs. The optical waveguide is the next basic element, which confines the photons in the active region of the semiconductor. In the lateral direction, the injected current, carriers (electrons and holes), and photons are confined as well for an operation in a fundamentally lateral mode. Lastly a resonator creates the optical feedback in order to attain stimulated laser emission.

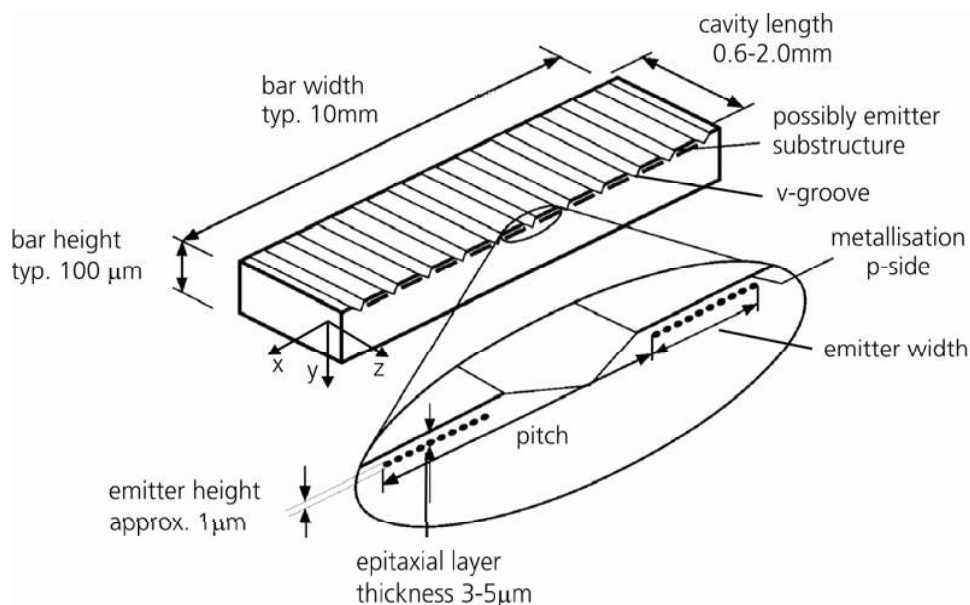


Figure 2-1: Structure of a laser bar and typical dimensions

The laser resonator or the cavity length, is the length of the semiconductor. The front and rear side, also called facet, are the mirrors. Already, the cleaved semiconductor has a reflectivity of

30%, so that the semiconductor can already act as a laser. For high efficiency, the reflectivity is changed by facet coatings. The rear facet gets a highly reflective coating (>95%) and the front facet an antireflective coating (<10%). Nowadays the improved epitaxial processing, especially the facet coating, leads to semiconductor lasers with high output power and very stable facet coatings [61],[77].

The laser bar consists of different emitters, which work individually (no coherent coupling between the emitters). The structure and terms of the laser bar are shown in Figure 2-1. The laser bar is typically 10 mm wide, 0.1 mm high, and has a cavity length (also called resonator length) between 0.6 and 2.0 mm. The width of the emitter is known as emitter width and the distance between two emitters is called the pitch. The quotient of dividing the emitter width by the pitch is called the filling factor.

There are common laser bar structures such as the "x-structure" with a filling factor of 30% and a pitch of 500 μm , the "g-structure" with a filling factor of 50% and a pitch of 400 μm , and for QCW operation the filling factor is approximately 85% with a emitter width of 110 μm and a pitch of 130 μm [55]. The laser bar structure varies from supplier to supplier.

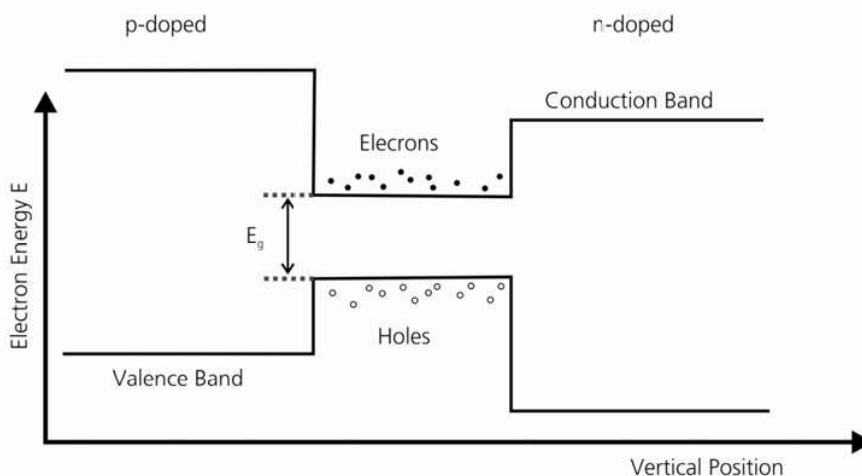


Figure 2-2: Forward biased p-n junction of a diode laser

In Figure 2-2 the principle of a forward-biased p-n structure is shown. Diode lasers are electrically pumped. The electrons recombine with the holes and photons are emitted. The radiating transition has the electrical band gap E_g . The band gap is dependent upon the thermal and mechanical stress. The dependencies are described in the following sub-chapters. The wavelength, which depends on the electrical band gap of the laser, is adjusted by the amount of additional elements such as aluminium or indium. These elements create compressive or tensile strain inside the quantum well, which is called intrinsic strain. In this work (In)AlGaAs and InGaAs quantum well structures are used.

Typical semiconductor and the quantum well materials are shown in Table 2-1.

wavelength range	630-690nm	800-830nm	800-830nm	940-980nm
quantum well (QW)	GaInP	GaAsP	(In)AlGaAs	InGaAs
strain of QW	compressive/tensile	tensile	compressive	compressive

Table 2-1: Typical semiconductor materials and the occurring intrinsic strain of the QW [50]

The laser bars are metallised at the p- and n-contact. The metallisation typically consists of different layers, which vary with different manufactures. All laser bars are gold plated, which is in contact with the solder. Most of the bars used in this work have in between the metallisation a thicker gold layer for current distribution, followed by a diffusion barrier such as platinum and the thin gold contact layer (less than 100 nm).

2.1.1. Temperature Dependent Properties of Laser Bar

The optical output power, or more precisely the threshold current and slope efficiency, is temperature dependent. The temperature dependence of a diode laser can be described using two values, the so called characteristic temperatures T_0 and T_1 . The temperature dependence of the threshold current can be described as follows:

$$\text{threshold current} \quad I_{th}(T) = I_{th}(T_{ref}) \exp\left(\frac{T - T_{ref}}{T_0}\right) \quad \text{Formula 2-1}$$

The slope efficiency can be expressed using the differential quantum efficiency:

$$\text{slope efficiency} \quad \eta_d = \left(\frac{\lambda \cdot e}{h \cdot c}\right) \frac{dP}{dI} \quad \text{for } (I > I_{th}) \quad \text{Formula 2-2}$$

and with this, the temperature dependence of the slope efficiency can be expressed with the second characteristic temperature T_1 :

$$\text{slope efficiency} \quad n_d(T) = n_d(T_{ref}) \exp\left(-\frac{T - T_{ref}}{T_1}\right). \quad \text{Formula 2-3}$$

The larger the characteristic temperatures T_0 and T_1 are, the smaller the temperature dependency of the semiconductor is [10],[79].

T_0 and T_1 differ depending on the laser type and the wavelength. Typical values for broad area lasers are as follow: T_0 is around 150 K and the values for T_1 are between 300 K and 500 K [38],[79].

The optical output power above threshold can be put into the following equations:

$$\begin{aligned}
 P_{opt}(I, T) &= \eta_d(T) \left(\frac{h \cdot c}{\lambda \cdot e} \right) (I - I_{th}(T)) \\
 \text{optical output power} &= \eta_d(T_{ref}) \exp \left(-\frac{T - T_{ref}}{T_1} \right) \left(\frac{h \cdot c}{\lambda \cdot e} \right) \cdot \\
 &\quad \left(I - I_{th}(T_{ref}) \exp \left(\frac{T - T_{ref}}{T_0} \right) \right)
 \end{aligned}
 \tag{Formula 2-4}$$

The temperature used is the sum of the heat sink temperature T_{HS} and the temperature lift due to the thermal resistance of the packaging (Formula 2-5):

$$T(I, T) = T_{HS} + R_{th} \cdot (U(I) \cdot I - P_{opt}(I, T))
 \tag{Formula 2-5}$$

Because the temperature, T , depends on the optical output power, which is also temperature dependent, the optical output power cannot be solved analytically. Only a self-consistent numerical solution is possible.

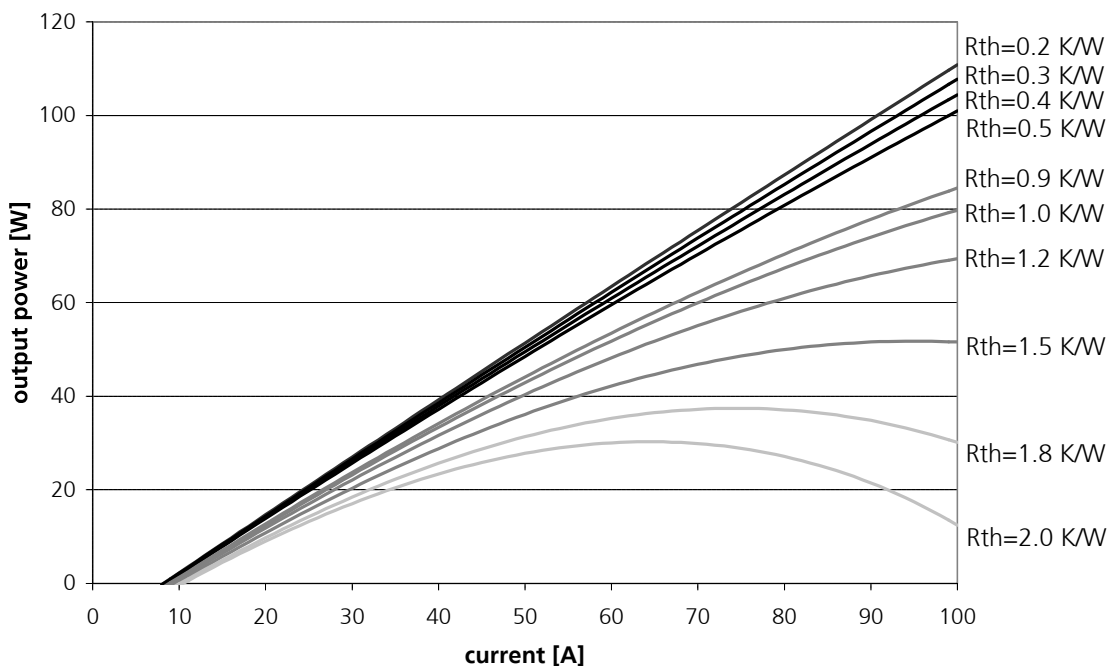


Figure 2-3: Simulated LI-curve dependent upon thermal resistance of the package. ($T_{ref}=293$ K, $T_0=150$ K, $T_1=350$ K, $\eta_d(T_{ref})=1.1$ W/A, $I_{th}(T_{ref})=8$ A)

Theoretical LI-curves are shown in Figure 2-3. Typical thermal resistance for active cooled heat sinks is in the range of 0.2 to 0.5 K/W and typical values for conductively cooled heat sinks are in the range of 0.8 to 1.4 K/W.

The wavelength is also temperature dependent. The energy gap in the semiconductor varies with the temperature according to the following equation:

$$\text{energy gap} \quad E_g(T) = E_o - \frac{\alpha \cdot T^2}{T + \beta} \quad \text{Formula 2-6}$$

E_o is the energy gap at 0 K and α and β are material constants. There are two effects, which cause the change of the energy gap. Firstly, there is a temperature dependent dilatation of the lattice. Second, the temperature dependent electron lattice interaction effects the energy gap. For gallium arsenide the wavelength-shift is about 0.3 nm/K [74].

Also, the packaging induced stress influences the wavelength shift. The mechanical pressure tuning contribution is about 15% of the wavelength shift [69]. Therefore high mechanical stress can significantly change the wavelength of the diode laser.

The refractive index of the semiconductor material is temperature dependent as well. The refraction index rises with rising temperature in small increments. For example, the change in the refraction index is around 1% for a wavelength of 880 nm and a temperature deviation of 100 K [43]. This change in the refraction index leads to thermal lensing, but this has no major effect on the optical path, especially for multimode lasers [83].

2.1.2. Influence of Mechanical Stress

There are different sources of mechanical stress in a high-power diode laser. The semiconductor itself is under the intrinsic strain caused by the different lattice constants of the substrate and quantum well. This strain is known as built-in strain.

A typical material composite for the quantum well structure is InGaAs. By changing the indium content of the semiconductor, the band gap and the wavelength can be adjusted. The band gap, E_g , at a temperature of 300 K, can be calculated using the following equation for $\text{In}_x\text{Ga}_{1-x}\text{As}$ [57].

$$\begin{array}{ll} \text{energy gap for} & E_g(x) = 1.424 - 1.615 \cdot x + 0.555 \cdot x^2 \\ \text{In}_x\text{Ga}_{1-x}\text{As} & \text{for } (0 \leq x \leq 1) \end{array} \quad \text{Formula 2-7}$$

Therefore, InGaAs quantum films are compressively strained, due to their material composition. Other materials compositions can cause tensile strain in their crystal structure (see Table 2-1). The laser is deliberately under intrinsic strain because it defines the output wavelength. Therefore, in all semiconductor lasers, including the unpackaged ones, a certain level of stress already exists.

Extrinsic strain is the processing-induced strain created by the metallisation and v-grooves of the laser bar, the defect-induced strain created by point defects, and the packaging-induced strain created by the solder and heat sink.

It is difficult to determine the quantitative influence of each source of strain, due to the fact that all processes act parallel to one another. By using bars from the same wafer with the same quantum well structure, nearly the same intrinsic, processing-induced, and defect-induced strains occur. Therefore, the differences seen in the measured strain or stress are most likely due to the packaging induced strain, which is examined further in Chapter 5.

In the following, the influence of strain on the band structure of the semiconductor is explained in detail.

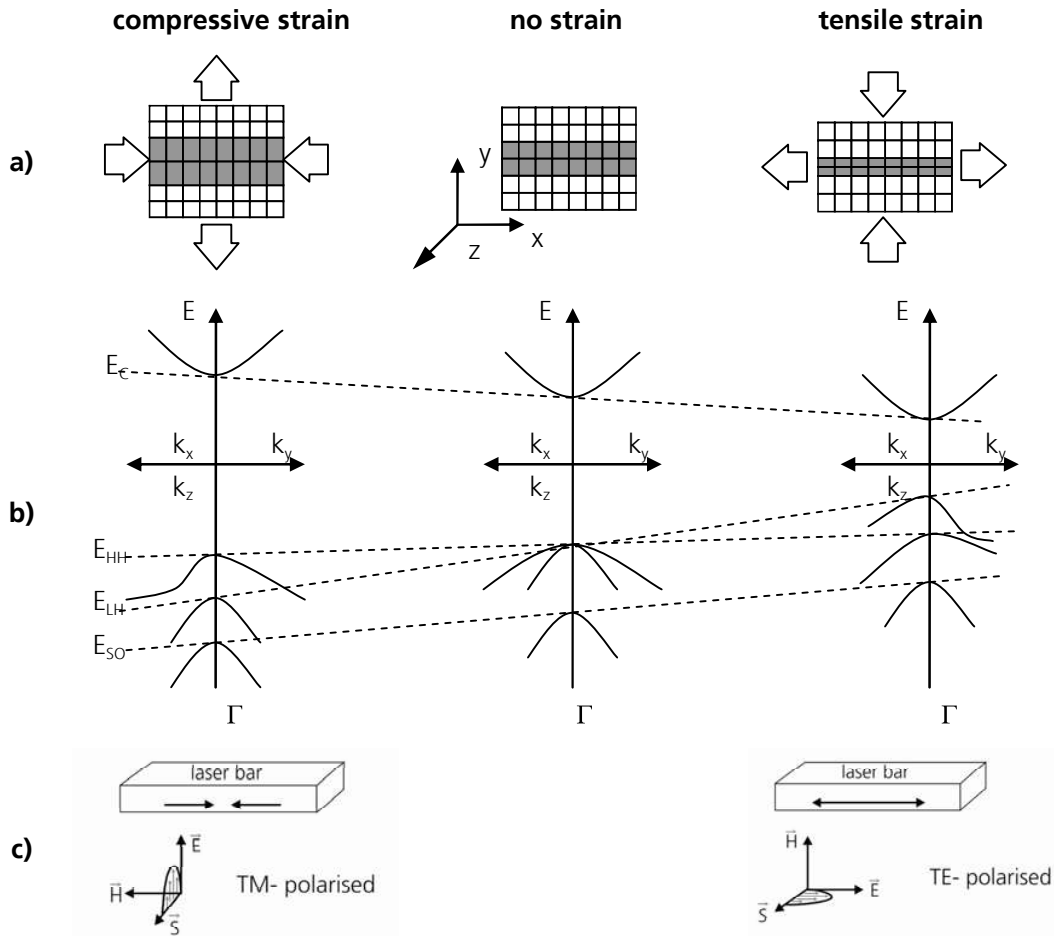


Figure 2-4: a) Schematic view of the lattice mismatch. b) Schematic representation of the change in band structure caused by tensile and compressive strain [18]. c) Polarisation in dependence of the strain.

In Figure 2-4, the strain influence of a zinc blende type semiconductor is shown. The strain splits the degeneracy at the valence band edge maximum, and separates the heavy-hole E_{HH} and light-hole E_{LH} sub-bands. The bands are named by the effective mass, m^* , of their holes and the higher bands with less bending have heavier holes (Formula 2-8).

effective mass $m^* = \hbar^2 \frac{\partial k^2}{\partial E^2}$ Formula 2-8

E_{SO} is the split-off band while E_C is the lowest conduction band. The electrons of the valence-bands are distributed according to the Fermi-Dirac-statistic. Under compressive strain, the heavy-hole valence band receives less electrons because it has a higher energy level than the light hole valence band (Figure 2-4, left side). Therefore, the transition feasibility of the heavy-hole band is higher. If the crystal is tensile strained, the electrons from the conductive band will be more likely to move to the light-hole valence band than to the heavy-hole valence band.

The energy shift of the light and heavy-hole band can be estimated using the kp-perturbation theory at the Γ -point. (for fcc-crystals and a strain tensor generated by [001] epitaxy)

energy shift
heavy-hole band $\Delta E_{hh} = H - S$ Formula 2-9

energy shift
light-hole band $\Delta E_{lh} = H + S$ Formula 2-10

S is the uniaxial strain part and H is the isotrop strain part. For fcc-crystals, this strain can be described as follows:

uniaxial strain part $S = 2 \cdot (-b) \frac{C_{11} + 2C_{12}}{C_{11}} \cdot \varepsilon$ Formula 2-11

isotrop strain part $H = 2 \cdot a \frac{C_{11} - C_{12}}{C_{11}} \cdot \varepsilon$ Formula 2-12

strain coefficient $\varepsilon = \frac{a_{epi} - a_{sub}}{a_{epi}}$ Formula 2-13

C_{11} and C_{12} are components of the elastic modulus tensor, where a and b are deformation potentials. The strain coefficient can be calculated from the different lattice parameters of the substrate a_{sub} and the epitaxial layers a_{epi} [65].

Additionally, the polarisation of the emitted light depends on which valence band is involved in the transition. A compressively strained quantum well takes part in the transition between

electrons and heavy holes, which leads to a polarisation perpendicular to the quantum well plane (TE mode). Quantum wells under tensile strain undergo a transition between electrons and light holes, which leads to a polarisation in the quantum well plane (TM mode) [18],[79]. The different transitions according to the Bloch theorem and the polarisations states are described by Singh [65].

Therefore, the wavelength shift (energy gap) and the polarisation can be used as a stress indicator. Methods to measure these values are explained in Chapter 3.5.

2.2. Heat Sink

The heat generated during operation of commercially available diode lasers is in the range of 60 to 100 W. In order to handle this heat, special heat sinks for diode lasers bars have been developed and are in use. For high power applications such as pumping of solid state lasers and direct material processing, actively cooled heat sinks are used. Cooled water flows through heat sink structures especially designed for heat exchange. An actively cooled heat sink is, itself, a heat exchanger. For lower power applications such as in the medical field (PDT, surgical), conductively cooled heat sinks are used. The heat sink's function is heat distribution and is cooled for example, using a thermoelectric cooler (TEC).

In general, the thermal expansion coefficients (CTE) of the semiconductor and the heat sink material mismatches. Due to temperature changes that occur during packaging and operation, mechanical stress is induced in the diode laser bar. In the following, conductively and actively cooled in addition to expansion matched heat sinks, are introduced.

The heat sinks can be classified by their thermal resistance and the observed thermal expansion coefficient on their mounting surface. To gauge the thermal performance of diode laser packaging, the thermal resistance, R_{th} , is commonly used. It is defined as

$$\text{thermal resistance} \quad R_{th} = \frac{dT_{laser}}{dP_{loss}} \quad [R_{th}] = \frac{K}{W}, \quad \text{Formula 2-14}$$

where T_{laser} is the operating temperature of the mounted diode laser bar and P_{loss} is the lost power at a given operating point.

For an interpretation of the thermal resistance values, it is important to consider its dependence on the heat generation area. Using the same heat sink, but a larger laser bar with the same power loss, the thermal resistance will be lower because the heat flow is spread out over a larger contact area. In order to get more comparable values for the thermal performance of a heat sink, the thermal impedance, $I_{thermal}$, is used.

$$\text{thermal impedance} \quad I_{thermal} = R_{th} \cdot A = \frac{dT_{laser}}{dP_{loss}} \cdot A \quad \text{Formula 2-15}$$

$$[I_{thermal}] = \frac{K \cdot mm^2}{W} \quad \text{and} \quad A = w \times l$$

where w is the bar width, l the resonator length, and A the resulting chip size.

This gives more fitting values, but a large difference is still seen when laser bars with different fill-factors are used. Due to the three-dimensional heat flow (heat spreading) inside the heat sink, no simple equation can be given in order to compare the thermal behaviour of different heat sinks packaged with different laser bar geometries.

Even with this knowledge, typical values for heat sinks given by manufactures are thermal resistances. Due to the dependence of the thermal resistance on the laser bar structure, the values can not be compared.

2.2.1. Conductively Cooled Heat Sink

A conductively cooled heat sink is a monolithic block of a material with high thermal conductivity that must meet high requirements of surface quality. The flatness of the mounting area ($10 \times 3 \text{ mm}^2$) must be below $1 \text{ }\mu\text{m}$ and the edge radius must also be below $2 \text{ }\mu\text{m}$ for mounting and cooling purposes. A sharp edge is needed for the positioning of the laser bar. A sharp edge will also cool the front facet of the laser bar better because the heat sink is closer to the heat source. The flatness is necessary in order to avoid bending of the laser bar during packaging when it is pressed onto the heat sink. The bending is also influenced by other parameters, but flatness is a major factor. The bending that occurs should be below $1 \text{ }\mu\text{m}$ in order to form a straight focal line of all the emitters, which is required for micro-optics. These surface requirements can be easily achieved with the diamond turning of copper. The flatness of diamond turned copper is below $0.1 \text{ }\mu\text{m}$ and the roughness R_a is less than 3 nm [24],[44].

Another important aspect is the connection between the heat sink and cooling device for instance a TEC. The surfaces of these components must be smooth and planar and if needed, additional deformable materials can be added in-between to ensure a solid contact. The additional layer should be thin if its thermal conductivity is below that of the heat sink. A heat-conductive paste with lower thermal conductivity and small grain size is better than a highly conductive paste with a larger grain size. [14]. Also, the heat transfer coefficient is influenced by the thermal conductivity and the thickness of the heat transfer layer. Typical heat transfer coefficients for different conditions are shown in Table 2-2.

contact condition	heat transfer coefficient [kW/m ² ·K]
metal surface with roughness $R_z \approx 6.4 \text{ }\mu\text{m}$	10
carbon foil (0.125 mm thick, 16 W/mK thermal conductivity)	18
heat-conductive paste (3.0 W/mK thermal conductivity)	15-20
Indium foil (0.1 mm thick)	25

Table 2-2: Heat transfer coefficients for different contact conditions. A higher value leads to a better heat flux. All measurements are done with the same pressing force [32].

Another important factor is the thickness of such conductively cooled heat sinks. The heat sink has the task of spreading the heat over a larger area. If the heat sink is too thin, the heat is spreaded only on a small area and gets accumulated on the bottom side, because the heat transfer layer is not able to handle the heat density efficiently. Therefore there is a minimum heat sink thickness for a set of the transfer coefficient and the dissipation power of the laser bar. The simulated dependency of the operating temperature versus the heat sink is shown in Figure 2-5.

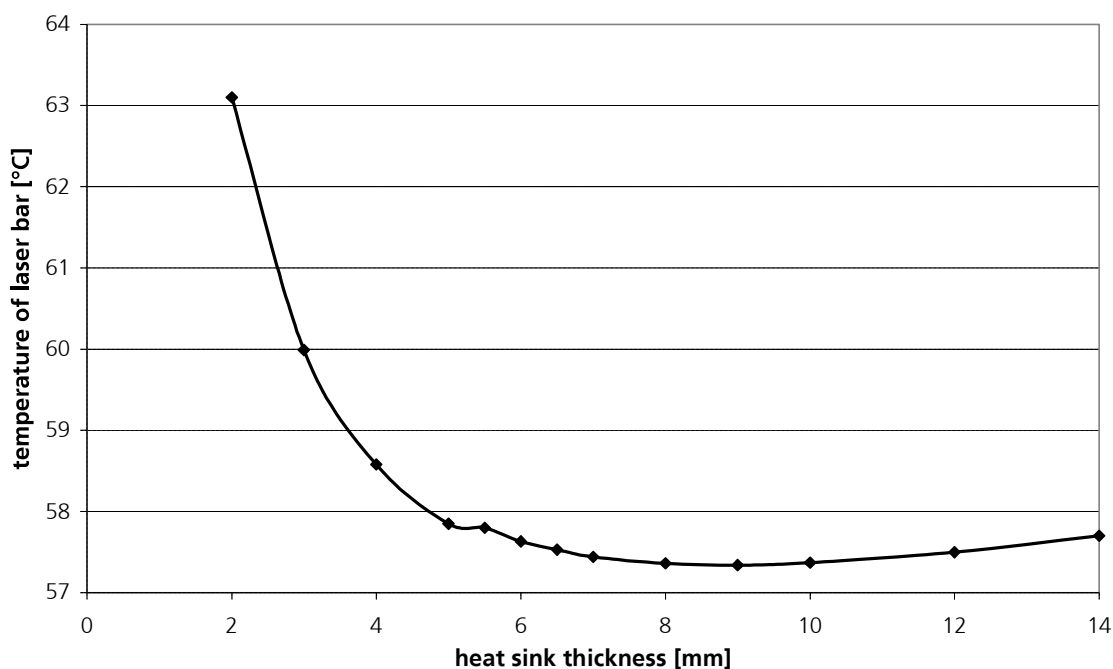


Figure 2-5: Laser bar temperature in dependence of heat sink thickness. Heat sink geometry is 27x27 mm² and the heat transfer coefficient is 15 kW/m²K [32].

All conductively cooled heat sinks used in this work are made of E-Cu57 copper. The properties of E-Cu57 are shown in Chapter 8. A typical heat sink with the dimensions of 20 x 20 mm is shown in Figure 2-6. Typically, laser bars with a 30% fill-factor and a bar width of 6 mm are mounted on these heat sinks. The thermal resistance of this 12-emitter bar package is around 1.2 to 1.4 K/W.

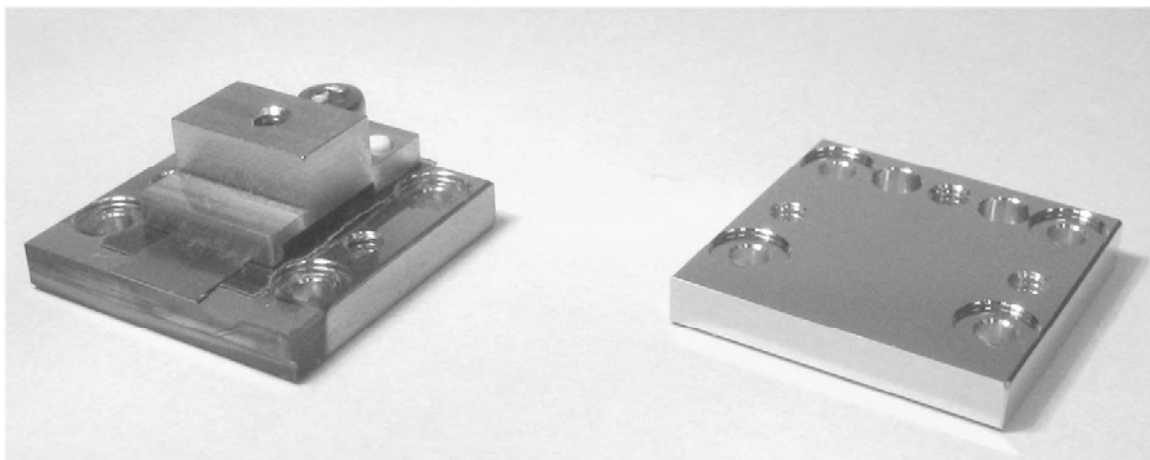


Figure 2-6: Typical conductively cooled heat sink. On the left is a packaged diode laser and on the right side a gold plated heat sink (ILT-Design).

2.2.2. Actively Cooled Heat Sink

Actively cooled heat sinks made of copper are commonly used in high power applications. There are micro channels in the heat exchange area that allow the contact surface to expand between the copper and cooling water. Therefore, these types of heat sinks are also known as micro-channel heat sinks.

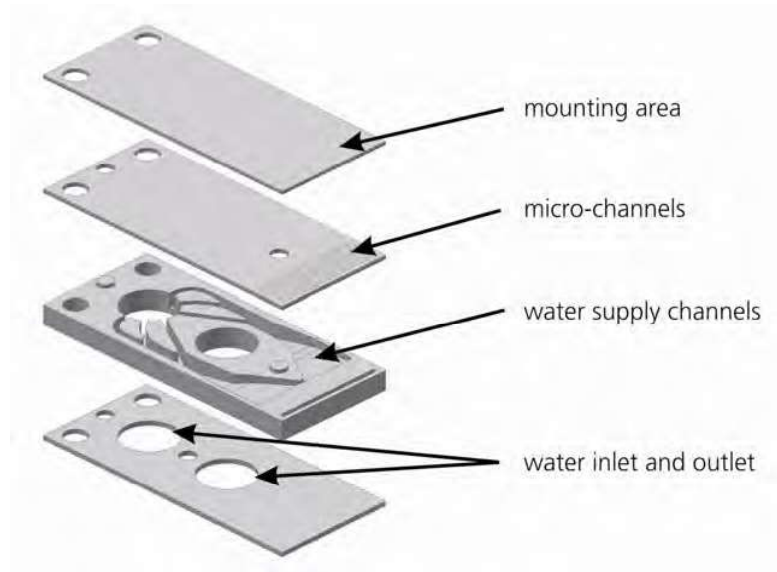


Figure 2-7: Schematic view of heat sink assembly. The different sheets are joined together by diffusion soldering.

In order to produce the inner structure of this heat sink, while maintaining the typical outer dimensions of $12 \times 2 \times 25 \text{ mm}^3$, the heat sink consists of different layers that are joined together. To achieve this a silver solder is used in a diffusion bonding process. The area of greatest concern is the heat exchange area located underneath the mounting area where the micro channels are located. The arrangement of the micro channels differ from supplier to supplier, but they all use a similar structure to create a large contact surface between copper and water. The layout of the water flow is important for long term stability because corrosion and erosion can reduce the lifetime of heat sinks. Deionised water is used to counter the effects of a galvanic cell, especially if a diode laser stack is used. A schematic view of this assembly is shown in Figure 2-7 [21].

Typical thermal resistance values of actively cooled heat sinks are between 0.2 and 0.5 K/W [13],[21],[58].

2.2.3. Expansion Matched Heat Sink

Expansion matched heat sinks are a further development of the actively cooled or conductively cooled heat sinks, which are typically made of copper.

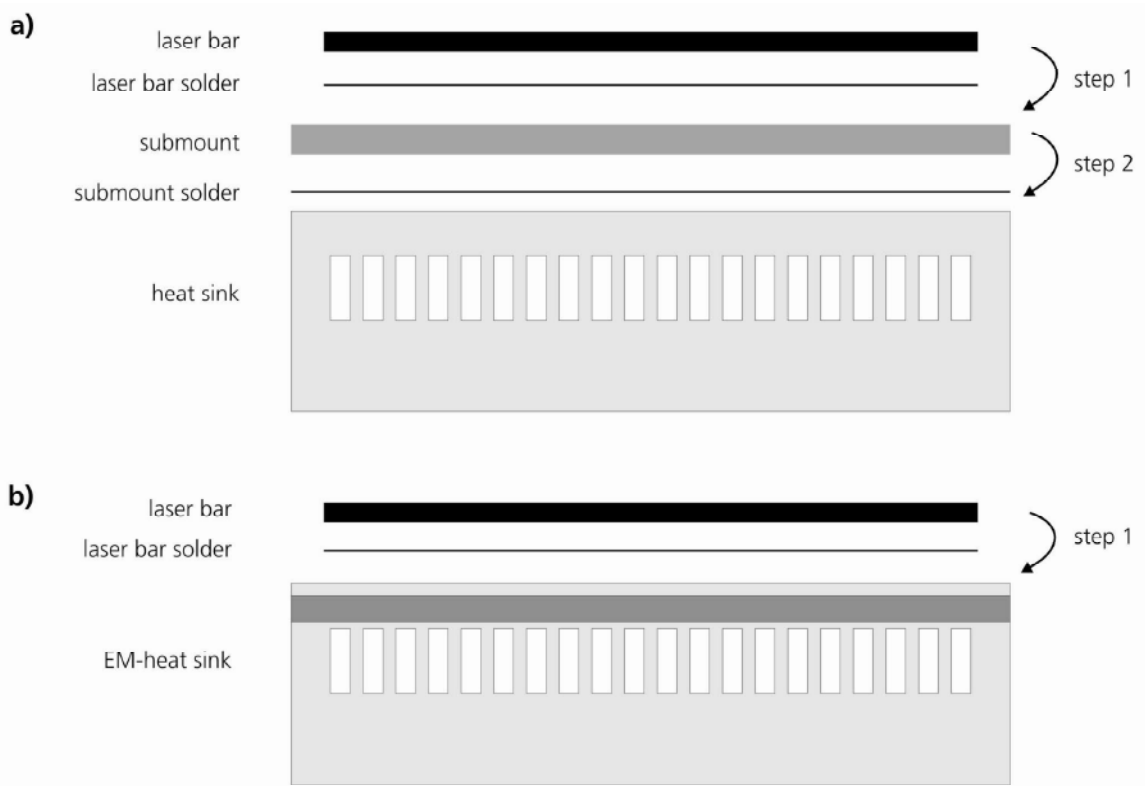


Figure 2-8: Schematic view (cross section) of heat sink assembly a) with submount and b) on expansion matched heat sink

There are two ways for an expansion matching package to be manufactured. The first, and currently more commonly used method, is to use an expansion matched submount such as diamond, ceramic, or tungsten-copper composites. The first step is to solder the laser bar onto the submount using a laser bar solder. In the second step, this package is mounted on the heat sink with a submount solder. The melting temperature of the laser bar solder has to be lower than the melting temperature of submount solder in order to avoid melting, causing a disconnection between the laser bar and submount. An alternative method is to directly use an expansion matched heat sink. At the moment this type of heat sink is only available as a prototype. The advantage of using an expansion matched heat sink is that only one solder step is needed. Also, it results in a lower thermal resistance because there are fewer thermal transfer surfaces compared to the submount package (see Figure 2-8).

Two different actively cooled expansion matched heat sinks have been developed and fabricated within this work.

The first type of expansion matched heat sink uses an expansion matched material as the top layer. This type is called a "top-layer" heat sinks. By using such materials, e.g. composite materials, the expansion matching is solved, but because typical thermal conductivities of these materials are low, so that the thermal load is high. Due to the hardness and layer thickness of such material, the bending of the heat sink is small, so that no bending compensation is necessary.

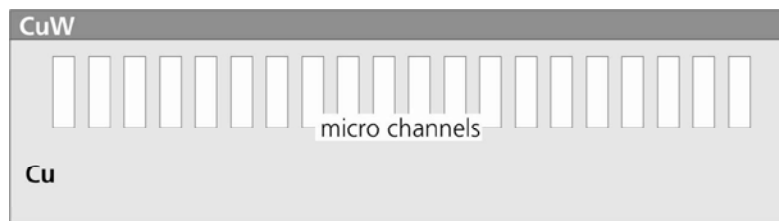


Figure 2-9: Schematic view (cross section) of an expansion matched "top-layer" heat sink, not bending compensated

The second type has a copper surface, but underneath a material with a lower CTE than GaAs, which reduces the CTE of the thin top copper layer, is used. This type of heat sink is called "sandwich" heat sink. The thin copper layer acts as a heat spreader, so that the thermal resistance is lowered. Due to machining tolerances, the thickness of the top layer and with that the thermal expansion coefficient of the mounting surface varies. In order to avoid bending during temperature changes, the heat sink is built symmetrically.

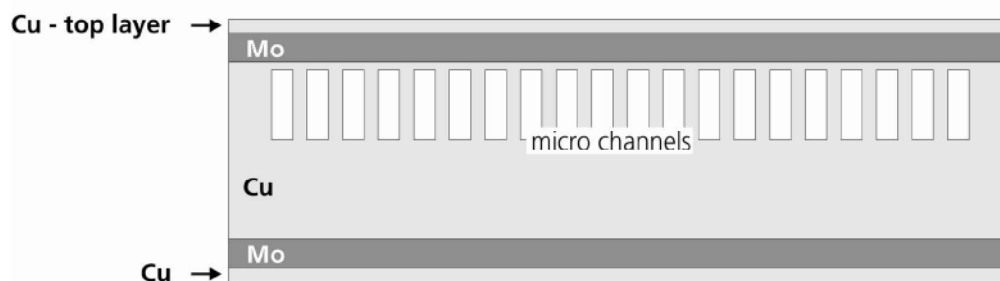


Figure 2-10: Schematic view (cross section) of "sandwich" heat sink design. Mo is used to influence the CTE of the top copper layer. To avoid bending the heat sink is symmetrical.

The thermal design and investigation is shown in Chapter 4.1 and the mechanical design is developed and investigated in Chapter 5.2.

2.3. Solder

The connections of the laser bar need to have high thermal and electrical conductivity. For this reason, typically metal solders are used. The connection must be able to withstand currents of up to 150 A and thermal loads of 100 W/mm². Electrically conductive glue, for example, is not nearly strong enough to fulfil these requirements.

To connect the heat sink and the laser bar, a thin layer of solder is needed. A common ductile solder is indium, and gold-tin as a brittle solder. Both solders are classified as soft solders, because their melting points are below 450 °C. In telecom applications, gold-tin is used because its properties remain constant even over a period of several years. Indium diffuses easily with nearly all materials, allowing the properties of the solder layer to change as a result of any changes in the metallurgical composition. To minimize this effect, diffusion barriers are used to stop the diffusion.

2.3.1. Indium

Indium is a very soft, ductile, malleable, silvery-white metal with a brilliant lustre. It was discovered by Ferdinand Reich and H. Richter in 1863 in Freiberg, Germany using spectroscopic analysis. The metal was named for a brilliant indigo line in its spectrum.

It was first found in zinc ore, but can be also found in iron, lead, and copper ores and is produced commercially as a by-product of the smelting of zinc. The Earth is estimated to contain about 0.1 ppm of indium, making it approximately as abundant as silver.

Its current applications are in low-melting alloys, such as the eutectic alloy 75.5Ga/24.5In which has a melting point of 15.7 °C, or for the bonding of non-metallic materials such as glass and ceramics. Due to the good wetting properties of glass, it is used to form a mirror surface that is more corrosion-resistant than, and reflects as well as silver. Since the late 1980's it has also been used in semiconductors as a primary component and as a dopant. Nowadays, the most common use of indium is in the thin-film applications such as liquid crystal displays (LCD) [23],[34],[80].

Indium is chosen as a soft solder for the laser bar due to its softness and ductile properties. The activation energy of indium for diffusion and creeping is very low, allowing a connection between other metals and indium to be established quickly at low temperatures. Also, indium can be applied onto the heat sink using physical vapour deposition (PVD) in order to get very thin solder layers. Thin solder preforms are available with thicknesses, ranging in between 25 and 50 µm.

The material properties of indium are listed in the appendix (Table 8-4).

Upon solidification, indium contracts leading to a volume reduction of about 2.5%. If indium or indium alloys are used to join copper or copper alloys, a diffusion barrier, such as nickel, is recommended. A solid state diffusion occurs between indium and copper, which forms an intermetallic compound. These intermetallics are brittle and can lead to joint failure [35].

Indium, which is generated during rapid cooling, has a small grain size and a high elongation after fracture. This property decreases with increasing grain size, while hardening is more or less independent of grain size [8]. Indium is already "relaxed" at room temperature, and it is also important to note that separate annealing steps are not necessary [35].

In air, three known oxides of indium, In_2O_3 , In_2O , and InO can form. Under normal conditions, the sesquioxide In_2O_3 is the oxide that forms. On freshly etched indium metal, the sesquioxide quickly forms with a thickness of 30-40 angstroms. After ageing a few days, the oxide layer stops growing at a thickness of 80-100 angstroms [35].

Indium is a very soft material and smears easily during polishing. Therefore traditional metallographic methods for surface analysis are not recommended. The best approach, in this case, would be to use surface analysis techniques such as Auger or EDX [35].

The creep behaviour, which plays an important role in the indium laser bar package, can be described using the power law, which is an empirical law [29].

power-law

$$\dot{\epsilon} = A \left(\frac{\sigma}{G} \right)^n \cdot e^{\frac{-Q}{kT}}$$

Formula 2-16

The stress exponent for creeping, n , and the activation energy, Q , are $n=5$ and $Q=78$ kJ/mol for pure indium [51]. The activation energy is very low compared to SnPb or other solders, which results in strong creep behaviour, even at low temperatures.

The shear behaviour of indium solder joints are investigated in detail by R. Darveaux and I. Turlik [15]. They used solder joints with a thickness of around 500 μm and a 100mm² contact area. Intermetallic compounds like the η -phase $\text{In}_{25}\text{Ni}_{10}$ and Au/In intermetallics are found. Therefore they used a 500 μm thick solder layers to neglect the influence of the intermetallics. These are different conditions than for the solder layer of laser bars. The thickness is 50 to 100 times smaller and the contact area is around 12 mm². The factors for the deformation properties are the same. The samples are investigated regarding work hardening and stress relaxation. The work hardening increases with an increasing strain rate in the range of 10^{-4} to 10^{-2} s^{-1} and also increases with the volume fraction of intermetallic compounds in the solder bulk. At lower strain levels the work hardening rate is much greater. For relaxation times of 2-13h, nearly complete recovery occurs, if the plastic strain was less than about 0.02. For shorter relaxation times and larger strains, the solder was left in a work hardened state.

2.3.2. Indium-Tin

A common indium alloy is the eutectic solder In52Sn48 with a melting point of 118 °C and thermal conductivity of about 33 W/mK. The thermal expansion coefficient is 31 ppm/K [81]. The phase diagram of indium-tin is shown in Figure 2-11.

This solder is used for the n-contact sheet solder because its melting point is below the melting point of indium. The n-contact sheet can then be joined in a second step after the bar soldering process.

By using the In52Sn48 alloy on elements, which are gold plated, Au-Sn intermetallic compounds and Au-In can be formed. The Au-Sn intermetallic compounds will form first, but these intermetallic compounds are very brittle and will weaken the joint. Some Au-In intermetallic compounds will form, but about 13 to 14 times less than the amount of the Au-Sn formation observed. Au-In intermetallic compounds are more flexible than the Au-Sn and are therefore better. If the gold plate is thick, long term reliability problems can occur. A larger amount of Au-Sn intermetallic compounds, which form with this thicker gold plate, will adversely affect the strength of the joint [35].

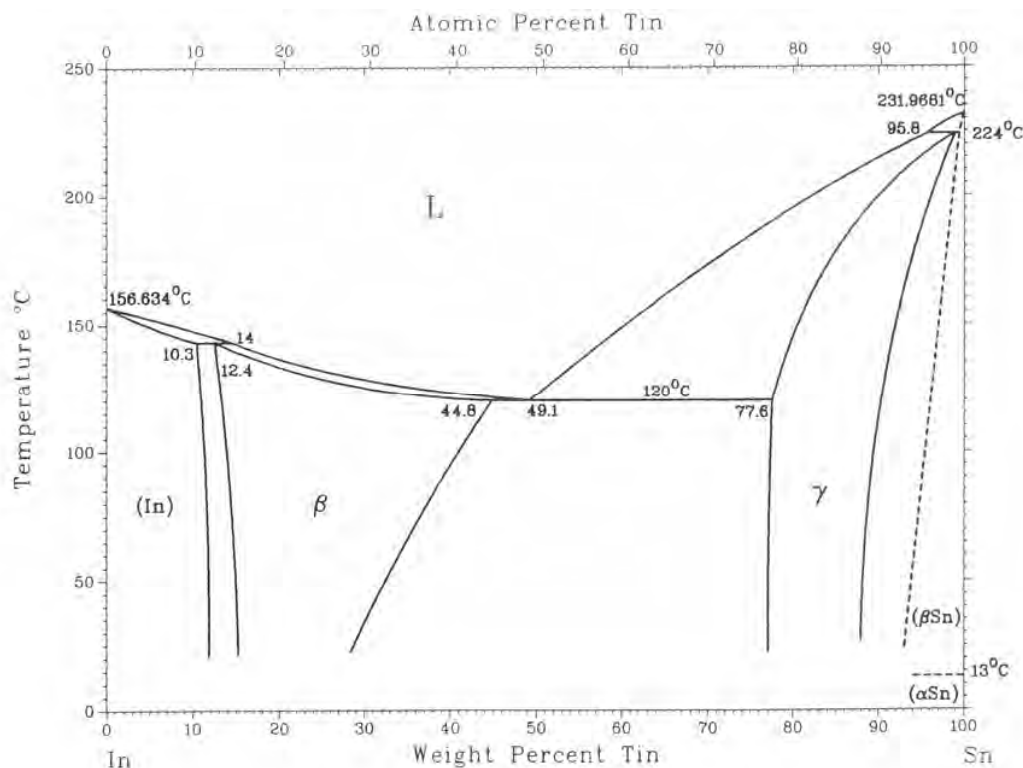


Figure 2-11: Phase diagram of indium / tin. The eutectic alloy is at 48wt% of tin with a melting temperature of 118 °C [54].

2.3.3. Gold-Tin

As a robust solder, the eutectic gold-tin composite is commonly used. The composite consists of 80wt% gold and 20wt% tin, and has a melting temperature of 278 °C. The phase diagram of this binary alloy can be seen in Figure 2-12. The mechanical and physical properties of Au80Sn20 are shown in Table 8-3. The advantage of this composite is its very low degree of oxidation, due to the high gold content. The alloy is available as solder preform with the thinnest thickness used being 25 μm . It can also be deposited using PVD with an eutectic material, or in parallel with two sources (gold and tin). The gold-tin solder can also be pulsed electroplated from a single galvanic solution [31].

Interdiffusion between gold and tin readily takes place at room temperature. The gold diffuses into tin using the interstitial mechanism, whereas tin diffuses into gold by way of the slower substitutional (vacancy) mechanism [75].

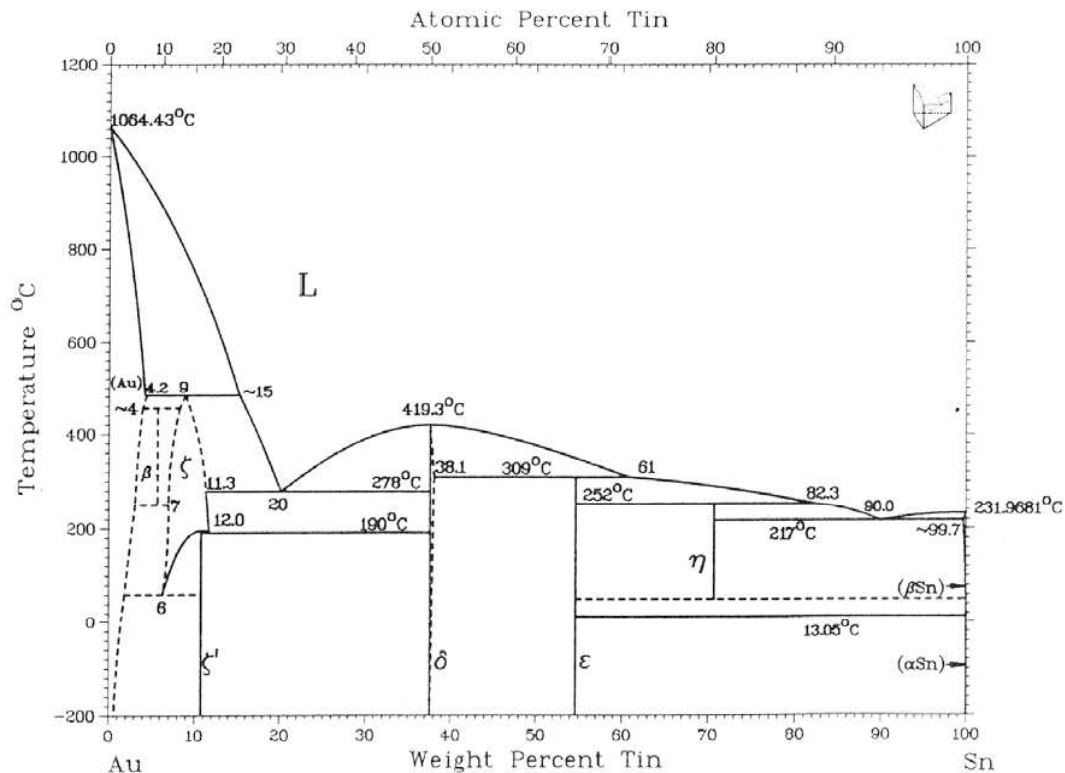


Figure 2-12: Phase diagram of gold / tin. The eutectic alloy is at 20wt% of tin with a melting temperature of 279 °C [54].

Studies show that the ζ -phase of gold-tin has a lower micro hardness than the eutectic AuSn composition. Therefore, the solder and contact layers need to be arranged so that a higher amount of gold can create the ζ -phase during the packaging process [59].

In general the eutectic gold-tin solder is brittle, especially if compared to the ductile solder indium.

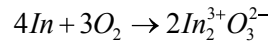
2.3.4. Oxidation and Reduction of Solder

All metals oxidise. The ratio of oxidation depends on the preciousness. Therefore, solders containing a high amount of gold or other precious metals have either no oxidation layer, or only a very thin one.

Oxidation can passivate the metal surface, stopping chemical reactions such as alloy growth. Therefore, oxidation films are to be avoided in order to form a good bond between the gold contact surface and the indium solder.

Oxidation is any electrochemical process which involves the formal oxidation state of an atom or atoms (within a molecule) being increased by the removal of electrons. In the case of indium, the following reaction takes place:

indium oxidation



Formula 2-17

The oxidation takes place immediately and a 3 to 10 nm thick oxide layer grows. The oxide layer passivates the surface so that it grows no further. A detailed investigation on the oxide layer is done in Chapter 4.2.1.

The solid oxide film has a very high melting point and therefore acts as a barrier, preventing the molten solder from making contact with the parts to be joined. Even the thin oxide film of indium makes it impossible to join the parts directly. Therefore the oxide film has to be removed. This can be achieved using several different methods such as wet chemical reduction, the vacuum solder process or using a formier gas. A common reduction method for diode laser bars is to use a formic acid aerosol.

To reduce the indium oxide layer, nitrogen gas is enriched with formic acid. The resulting concentration should be below 1%. A schematic view of the production of formic acid aerosol is shown in Figure 2-13.

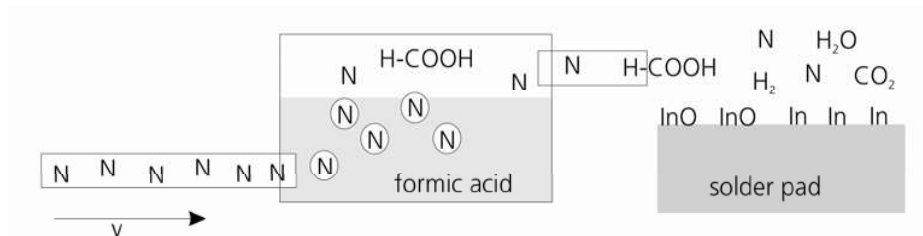
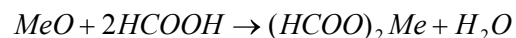


Figure 2-13: Schematic view of nitrogen enriched with formic acid used for reduction. The nitrogen is blown through liquid formic acid, during which it becomes enriched.

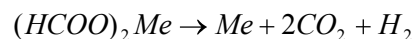
The formic acid aerosol can then be used to reduce the oxide on the solder surface. The chemical reaction of oxide with formic acid is shown below. At temperatures above 150 °C, the metal oxide (MeO) is transformed into an unstable metal compound (Formula 2-18). At temperatures above 200 °C, the metal compound splits into pure metal, carbon dioxide and hydrogen (Formula 2-19). At higher temperatures, the formic acid disintegrates and can no longer reduce the metal oxide [5].

reaction oxide and
formic acid
($T > 150^\circ\text{C}$)



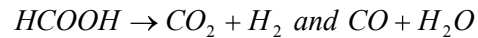
Formula 2-18

thermal splitting
($T > 200^\circ\text{C}$)



Formula 2-19

thermal
disintegration of
formic acid
($T > 350^{\circ}\text{C}$)



Formula 2-20

If the concentration of the formic acid is too high, salts of the acid (formate) start to grow. The formate disturbs the soldering process and can lead to unconnected spots in the solder layer. In Figure 2-13, formate remains are shown, and their effects are investigated in Chapter 4.2.

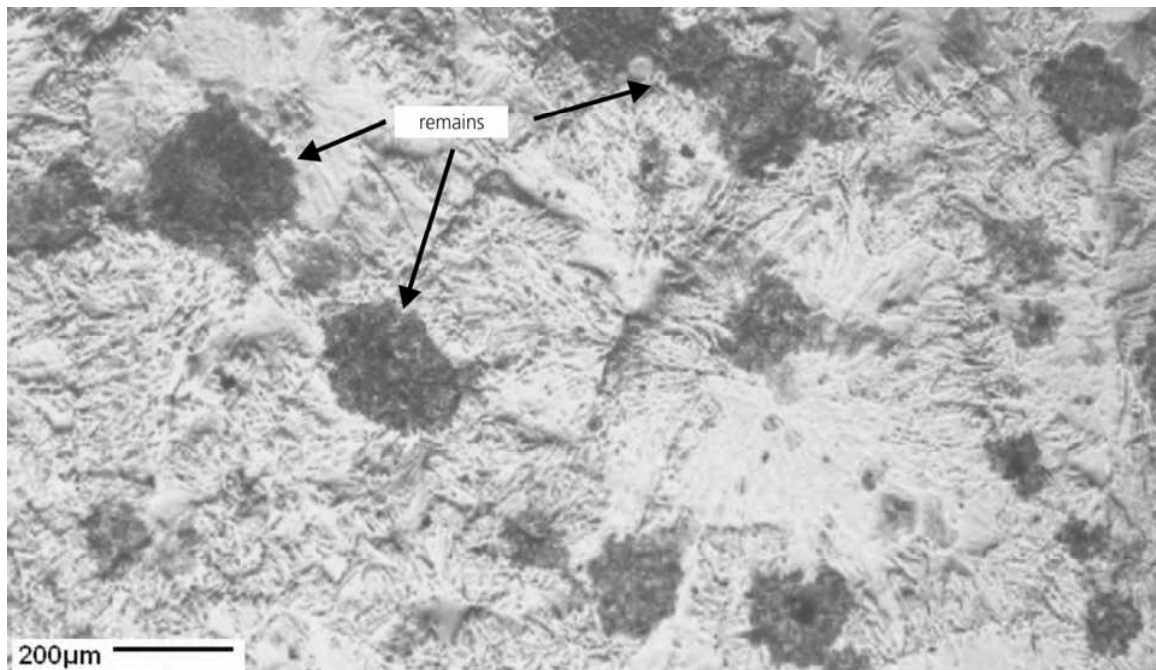


Figure 2-14: Remains of reduction with formic acid. If the concentration is too high, formate grows.

Generally, formic acid aerosol method is a good reduction method but the concentration has to be carefully controlled in order to avoid formate generation.

In order to avoid oxide layers, solders with high quantities of precious metals can be used. These solders typically build no or only partial oxide layers, which need no reduction. A typical solder is gold-tin (Au80Sn20), which is widely used for single emitters and also for laser bar packaging.

2.3.5. Plating and Diffusion Barrier

For reproducible packaging, the contact surfaces of the laser bar and heat sink must be clean and protected against oxidation. This can be achieved with appropriate plating. The laser bars are metallised on the p- and n-side with different elements. The metallisation differs from supplier to supplier, but all metallisation ends with a diffusion barrier and a thin gold contact layer. The diffusion barrier protects the semiconductor material against diffusion with solder or heat sink material, which would destroy the semiconductor. Gold is chosen as the contact partner for the

solder because it diffuses easily with other metals and does not oxidise. The interdiffusion of the contact gold layer and solder is important in order to establish a connection.

The interdiffusion of gold and indium takes also place at room temperature. Within a few days the gold colour of sequentially deposited gold and indium films with a gold content of around 60% disappears [64]. Also the degradation of gold bond wire coming in contact with indium is investigated. It forms a brittle gold-indium intermetallic compounds and the volume of this intermetallic compounds occupies approximately four times the volume the originally consumed gold. In this case the bond wire failed after a number of thermal excursions [30].

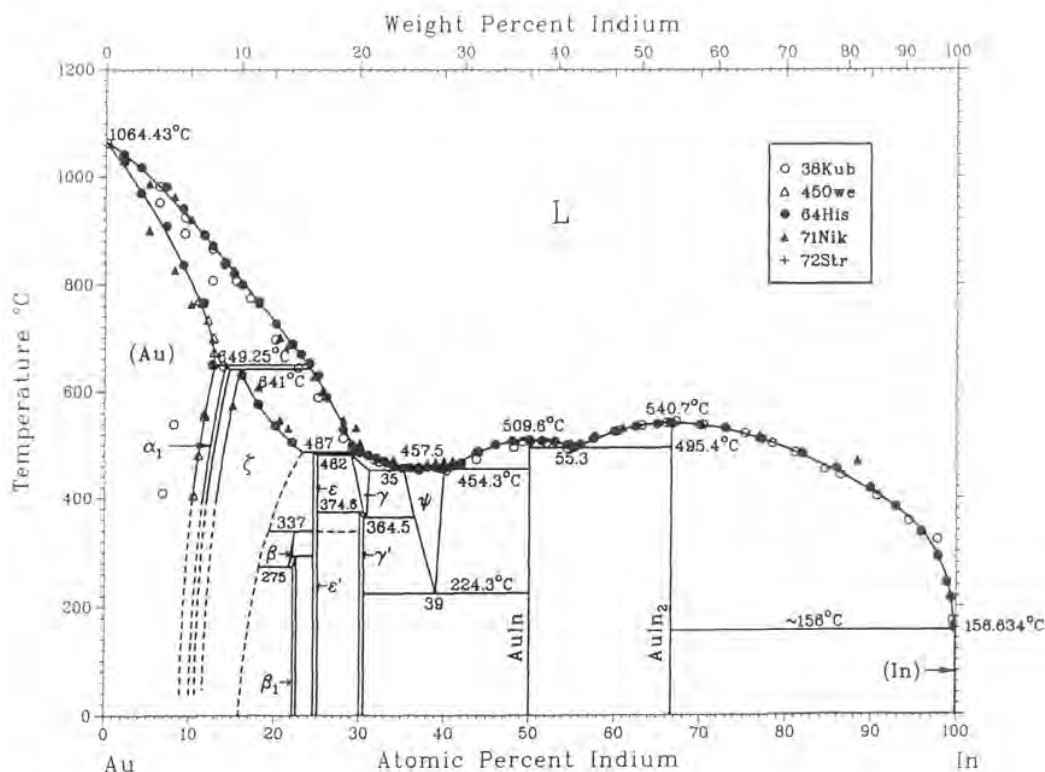


Figure 2-15: Phase diagram of gold / indium [78]

The heat sink is normally plated with gold in order to protect the surface from oxidation and to have a willing partner for diffusion with the solder. The phase diagram of indium and gold is shown in Figure 2-15.

The indium solder layer is thermally evaporated in a vacuum chamber onto the heat sinks. Typical solder layer thicknesses are between 5 and 10 μm . Immediately during the evaporation process, the indium and the gold from the heat sink interdiffuse and start to form AuIn₂. The growth of AuIn₂ is non-uniform. It grows in various sizes; smaller and columnar near the gold source and larger and blocky further out. At temperatures above 100 °C, the growth is more non-uniform than it is at temperatures of 80 °C or lower. Also, the grain size increases with increasing temperature. If the gold fraction increases, the AuIn alloy is produced [7],[15],[49].

The reaction rate of AuIn_2 was found out to be

$$\text{AuIn}_2 \text{ reaction rate} \quad \beta = 6,88 \cdot 10^8 \frac{\mu\text{m}}{\text{h}} e^{-\frac{0,72\text{eV}}{k_n T}} \quad \text{Formula 2-21}$$

where k_B is the Boltzmann constant and T the absolute temperature. The activation energy is expressed as 0.72 eV [39].

The intermetallic compound AuIn_2 is stable over a period of 14 years at room temperature. If the indium concentration is too low, also AuIn is formed. The micro-hardness of AuIn is five times higher than the micro-hardness of AuIn_2 [39],[49].

In contrast to the diffusion of gold and the solder, which is wanted to establish a connection, the diffusion of the heat sink material into the solder is unwanted. Typically intermetallic compounds are more brittle and make the solder layer harder. Also, there is enough heat sink material available to change the complete solder layer into a different metallic compound layer. These changes of the solder properties can lead to joint failures. The phase diagram of copper and indium, which are typical heat sink and solder materials is shown in Figure 2-16.

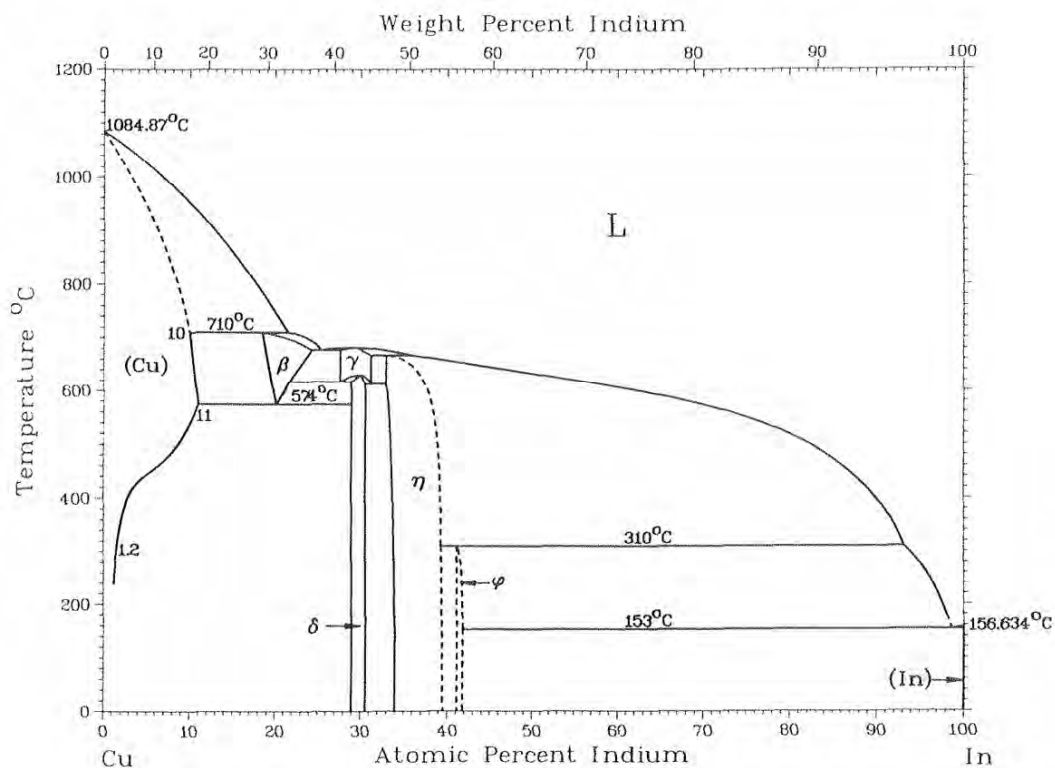


Figure 2-16: Phase diagram of copper and indium [78]

The CuIn intermetallic compound forms even at room temperature. During soldering the copper diffuses into the liquid indium and at temperatures below 300 °C the scallop-shaped $\text{Cu}_{11}\text{In}_9$

intermetallic is formed. At temperatures above 300 °C the scallop-shaped $\text{Cu}_{16}\text{In}_9$ intermetallic compound is formed. Also the indium diffuses into the copper and forms the CuIn intermetallic compound [84].

Therefore the solder layer has to be protected against the heat sink material. Diffusion barriers are used, in order to avoid diffusion of the heat sink material into the solder. Typical diffusion barriers are thin nickel, titanium nitride, or chrome layers. These barriers also act as adhesive layers. The thickness depends on the plating method used, such as sputtering or galvanising. In order to characterise the different diffusion barriers, long term tests have to be carried out. The metal compounds should be stable after the packaging process and no further changing of the composites should occur. Therefore, diffusion barriers are needed to prevent an overgrowth of intermetallic compounds, which results in a brittle fracture at the interface.

2.4. N-Contact Sheet and Isolation Foil

The n-contact can be a metal sheet which is soldered to the n-contact of the laser bar, or the n-contact of the laser bar is wire bonded to a electrical contact plate. The function of the n-contact is to provide currents of up to 100 A and to avoid stress onto the laser bar, caused by clamping the diode laser. This can be achieved by wire bonding or a special design of the n-contact.

In order to separate the n-contact from the heat sink, an isolation foil or ceramic sheet is used. The cheapest option is a polyamide foil, which is also used in the electronics industry to separate the layers of a multi-layer circuit board.

These components only have a small role in the thermal and mechanical properties of the package. Therefore, they are not described in more detail.

2.5. Packaging of Diode Laser Bars

A diode laser consists of the laser bar, which is connected to the heat sink and the n-contact sheet. The packaging process, described in the following, is a two step packaging process. First the laser bar is soldered onto the heat sink. Second, the n-contact sheet is soldered on top of the laser bar. In the analytic part, the effects of an insufficient connection between the components are investigated.

The process starts with a gold plated heat sink. The laser bar solder is typically applied onto the heat sink by evaporation in a vacuum chamber. A mask is used so that solder is only deposited in the laser bar contact area. The evaporated solder thickness is between 5 and 10 μm and the thickness of the solder layer varies by approximately 1 μm .

Next, the laser bar is positioned p-side down onto the heat sink inside a soldering furnace. Because the laser bar is an edge emitting device, the emitting area cannot be obstructed. In order to achieve this, the front edge of the laser bar hangs over the edge of the heat sink. This overhang has to be as small as possible, otherwise the thermal load is too high and the facet can be damaged. If the edge of the laser bar is positioned behind the edge of the heat sink, the laser light shines onto the heat sink. This heats the heat sink and the reflection acts as a second light source for optical elements in front of the laser bar, in turn making the diode laser ineffective.

Before the laser bar can be soldered onto the heat sink, the solder has to be deoxidised. This can be done using different methods such as wet chemical reduction with acid or gas reduction with hydrogen or aerosols. Since solder reduction is important, it is described in greater detail in

section 2.3.4. Otherwise, different solders can be used, which are nearly not oxidised, such as gold-tin solder. In the electronic field, solder wetting of 95% are excellent [16], but for laser bar packaging the solder wetting ratio has to be nearly 100%. Voids in the solder lead to thermal hot spots, which reduce the lifetime of the diode laser.

In the second soldering step, at a lower solder melting temperature than the laser bar solder, the n-contact sheet is mounted on top of the laser bar (n-side). The typical n-contact sheet solder is indium-tin with a melting temperature of 128 °C. The necessary positional accuracy of the n-contact sheet onto the laser bar is around 50 μm , because it must almost only rely on the electrical function to supply the needed current. Thermally there is nearly no heat flux, which cools the laser bar.

For isolation between the n-contact and the p-contact (heat sink), an isolation foil is inserted between the n-contact sheet and the heat sink [2],[37].

An exploded view of the diode laser with its components is shown in Figure 2-17.

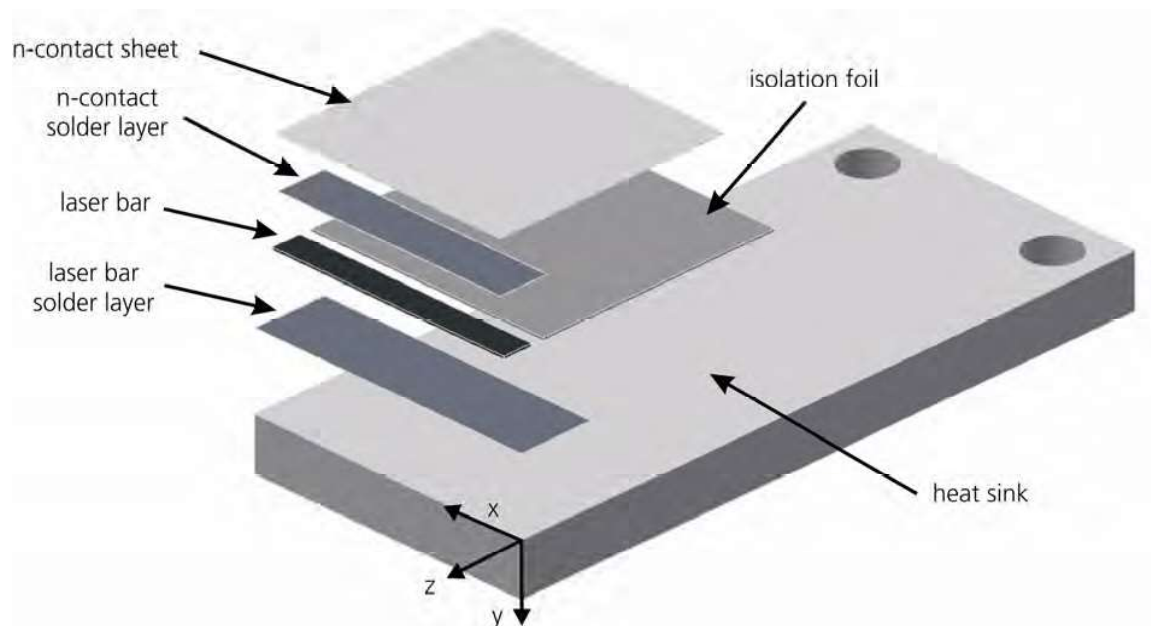


Figure 2-17: Assembly of diode laser. The laser bar is mounted onto the heat sink using a laser bar solder and the n-contact sheet with the n-contact solder. An isolation foil isolates the n-contact from the p-contact (heat sink).

3. Properties of Diode Laser Bars and Measurement Methods

In this chapter an overview of the measurement methods for the electro-optical and thermal properties of packaged diode lasers is given. Sub-Chapter 3.5 describes the measurement methods for stress, which are used for analysing the packaged laser bars.

3.1. Electro-Optical Properties

The electro-optical characteristics of a diode laser are obtained by measuring the optical output power, voltage drop, and emission spectrum at different currents and temperatures. A typical test is the light-current-voltage (LIV) measurement. Typically, the voltage drop versus current is also measured, so that the total efficiency can be calculated. (see Figure 3-1)

Typical state-of-the-art diode lasers have a lifetime of at least 10000 h and an output power of 80W. The total efficiency of actual designs reaches 70%. [40],[77]

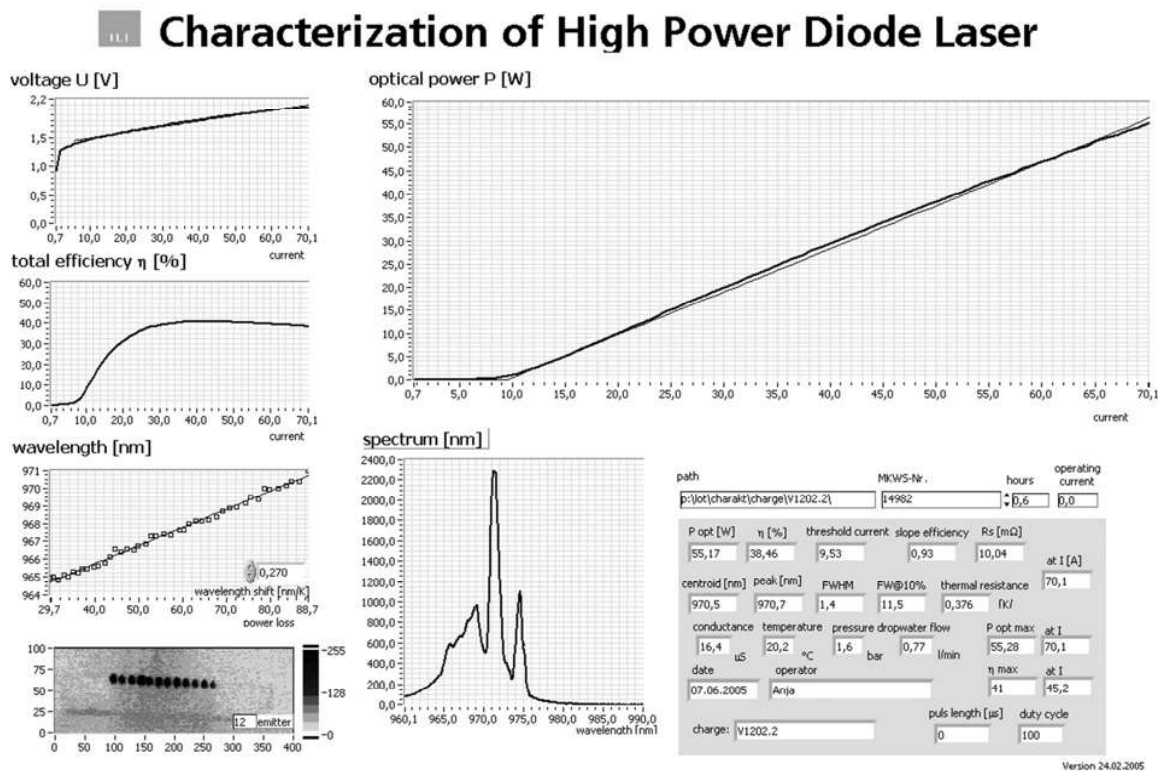


Figure 3-1: LIV-curve and the characteristic values of a tapered laser mini bar. Standard characterisation sheet, measured at Fraunhofer ILT. The laser bar is provided by Fraunhofer IAF.

There is no official standard available on how to measure the characteristics of a diode laser bars. An unofficial standard is the Telcordia specification, "Generic Reliability Assurance Requirements for Optoelectronic Devices Used in Telecommunications Equipment", which is used in the telecommunication industry [68].

The following enumerates the more critical requirements, which are necessary for the telecommunication market. Requirements are features and functions that must be satisfied. Features and properties for modulated output (e.g. signal transmission) are omitted, because diode laser bars are not used in these application fields.

All of these criteria will be mentioned in the following for the qualification and reliability of diode lasers. While requirements also exist for laser modules, they are not addressed here.

A typical set of parameters, which shall be included in characterisation are as follows: optical spectrum, light-current curve, voltage-current curve, and far-field pattern. These parameters shall be measured at room temperature, in addition to minimum, and maximum operational temperatures. The far-field pattern will only be measured at room temperature.

- **Central (λ_c) or Peak (λ_p) Wavelength:**

The peak wavelength is the wavelength achieved at the maximum power. The central wavelength λ_c is the statistically weighted centre of the optical spectrum. $P(\lambda)$ is the intensity at the wavelength λ and P_0 is the intensity of the whole spectrum.

$$\text{central wavelength} \quad \lambda_c = \left(\frac{1}{P_0} \right) \int p(\lambda) \lambda \, d\lambda \quad \text{Formula 3-1}$$

- **Spectral Width ($\Delta\lambda$):**

The spectral width $\Delta\lambda$ is the root-mean-square (RMS) width of the spectrum.

$$\text{spectral width} \quad \lambda_c = \sqrt{\left(\frac{1}{P_0} \right) \int (\lambda - \lambda_c)^2 \, d\lambda} \quad \text{Formula 3-2}$$

Secondary spectral peaks shall be mentioned.

- **Threshold Current (I_{TH}):**

Three methods are defined that should give approximately the same results. The current increments should be set to small values (less than 0.25 mA) and the temperature should be controlled to within ± 0.2 °C.

Method I (Two-Segment fit): Fit a straight line using the linear regression portion of the LI-curve just below the knee and another line above. The threshold current is the current at the point of intersection of the two lines.

Method II (First Derivative): Calculate the first derivative of the LI-curve (i.e., dL/dI). The threshold current is the current at which the derivative reaches half of its peak value (along the steep leading edge).

Method III (Second Derivative): Calculate the second derivative of the LI-curve (i.e., d^2L/dI^2). The threshold current is the current corresponding to the peak in the second derivative curve. This is the preferred method.

- **Characteristic Temperature (T_0):**

The characteristic temperature can be calculated using the following formula:

$$T_0 = \frac{T_a - T_b}{\ln(I_{TH}(T_a)) - \ln(I_{TH}(T_b))} \quad \text{Formula 3-3}$$

characteristic
temperature T_0

Recommended values for T_a and T_b are 343 K (70 °C) and 293 K (20 °C) and typical values for T_0 fall within the range of 45-90 K for the measurements. To avoid self-heating effects, these measurements can be made during pulsed rather than continuous operation.

- **L-I Linearity:**

At no point from just above the threshold to 120% of maximum-rated power should the LI-curve deviate from a straight line by more than 20%.

The overall linearity can be measured using three accepted methods.

Method I (dL/dI): By calculating the derivative of the L-I curve, the changes must be within specified limits. This method is preferred and can be performed in conjunction with the kink test.

Method II (Harmonics): Nonlinear behaviour can be identified by converting the LI-curve into a frequency spectrum. Therefore, the output power must change sinusoidally over the full operating range by biasing the laser at 50% of the maximum output power. The electrical output of a linear detector is fed into a spectrum analyzer. Second order (or higher) harmonics are evidence of nonlinearities.

Method III (Graphical Analysis): Mark the points on the LI-curve which correspond to 10% and 90% of the optical output power. Draw a straight line through these points and measure the largest deviation.

- **Kink:**

Kinks are defined as small bumps in the LI-curve as well as abrupt discontinuous changes in the curve's slope. No kink in the LI-curve should exceed $\pm 10\%$ of the maximum dL/dI value from just above the threshold up to the optical power at 120% of the maximum rated drive current.

- **L-I Saturation/Slope Efficiency (η_d):**

The saturation is the (normal) drop-off of the light output from a ideal linear response. The optical output of a laser is considered saturated and an excessive curvature in the LI-curve (also referred to as "rollover") is unacceptable. This is measured as a drop in dL/dI with respect to its (initial) maximum value.

- **Front/Rear Tracking ratio (r_{fr}):**

The front/rear tracking should not deviate from a straight line by more than 5%.

- **Forward Voltage (V_F):**

In conjunction with the LI-curve, the voltage-current (V-I) curve will be measured. Any unusual behaviour of the curve should be cause for investigation. Specifically, the forward voltage (V_F) at threshold shall be recorded for all measurements of the LI/VI-curves. By examining the curve for any degradation at reverse biases, leakage problems can become obvious.

- **Far-Field Pattern (FWHM θ_{\parallel} , θ_{\perp}):**

The optical power versus angle will be measured for the parallel plane (slow axis) and for the perpendicular plane (fast axis) of the laser's active layer. The measurements can be carried out several Rayleigh lengths away or in the focus. The full width of the spectrum at half of the maximum power has to be reported for both directions.

- **Thermal Impedance:**

This issue was eliminated from the device base because it was too costly. However it is still required at the module assembly level. The measurement methods are as follows:

Method I (Threshold Current): The temperature of the laser is lowered until the threshold current of the CW measurement becomes the same as that measured in pulsed conditions. The power difference, P, is the difference between the electrical input power at the thresholds. The thermal impedance can be calculated by dividing the temperature difference between CW and pulse operation by P.

Method II (Rollover L-I Method): A pulsed LI-curve and a LI-curve at CW until rollover are measured. The crossover point corresponds to the same light output powers, but different electrical input power as well as different temperatures for CW and pulsed measurements. The thermal impedance is the ratio of the temperature difference and the electrical power difference at the crossover point.

Method III (Forward Voltage Method)[33]: This method is based on the fact that the voltage of a constant forward current is linearly proportional to the junction temperature. The proportional factor K can be determined by measuring the forward voltage at room temperature and at maximum operating temperature as the laser is driven by very low constant power. The forward voltage is then measured again before and after the device is heated by a pulsed drive current (with heating power P_{heat}). The thermal impedance is calculated as follows:

$$\text{thermal impedance} \quad I_{\text{thermal}} = K \left[\frac{\Delta U}{P_{\text{heat}}} \right] \quad \text{Formula 3-4}$$

Two other values are also of interest. The total efficiency, also known as conversions efficiency, is the quotient of the optical output power divided by the electrical power that is put into the diode laser. The higher the value the less dissipation heat is produced, allowing the diode to be operated at a higher power level.

$$\text{total efficiency} \quad \eta = \frac{P_{\text{opt}}}{U \cdot I} \quad \text{Formula 3-5}$$

The series resistance can be calculated from the voltage - current curve. The slope is the series resistance. An insufficient contact of the laser bar increases the resistance.

3.2. Measurement Methods of Electro-Optical Properties

To measure the electro-optical characteristics of a laser bar an integrating sphere is used. The diode laser is emitted through the sample port into the sphere. The inside of the sphere consists of a diffused high reflection coating, so that the optical power and the wavelength spectrum are the same at each detector port. At the detector ports, the spectrometer and power meter are connected. The forward current of the diode laser is controlled by a computer, which measures other values such as voltage, optical power, and wavelength dependent upon the current. A typical result is shown in Figure 3-1, and a schematic view of the set-up in Figure 3-2. In addition to the water flow rate, water temperature and the conductivity of the water is also determined [37].

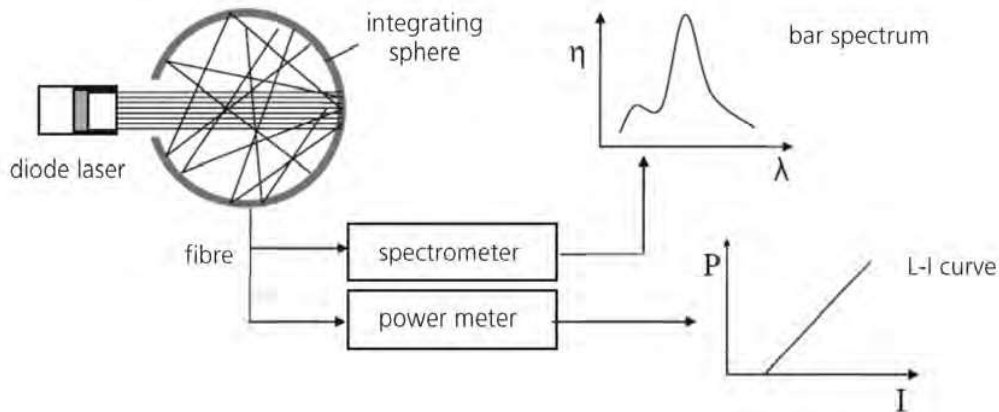


Figure 3-2: Schematic view of the measurement set-up using an integrating sphere

In order to measure the maximum wavelength or spectrum of each emitter, a fibre scanning set-up is used. A single mode fibre with a 9 μm core collects the light off the emitters. By positioning the fibre near the output facet and moving it in the lateral direction, the wavelength spectrum of each emitter can be obtained (see Figure 3-3).

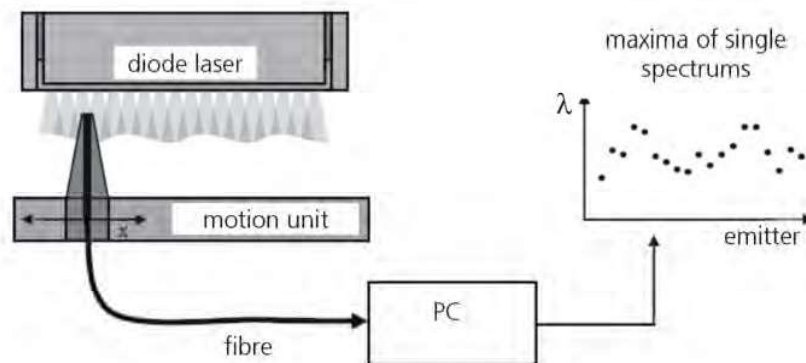


Figure 3-3: Schematic view of fibre sensor for emitter resolved wavelength measurements

The following measurement set-up is used to measure the transversal position of each emitter, the so called "smile" of the diode laser. The output facet of all emitters is simultaneously displayed on a camera. By putting a polariser into the optical path, the polarisation of each emitter can be determined.

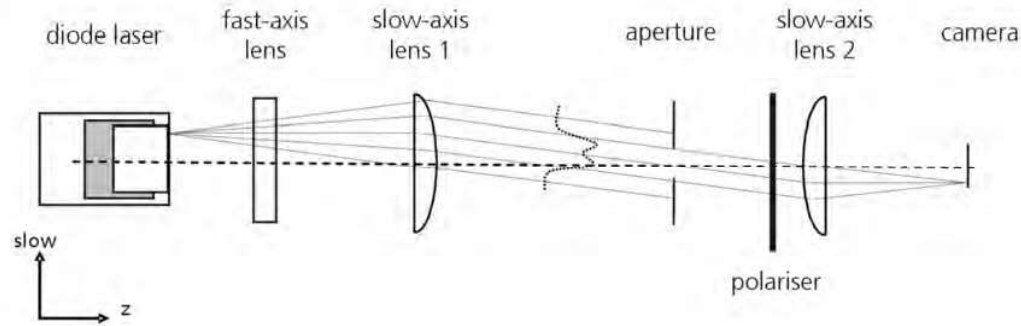


Figure 3-4: Schematic view of emitter resolved polarisation measurements

3.3. Lifetime of Diode Laser Bars

Diode lasers are operated in constant current or constant power mode. The mode is application dependent. If the optical output power decreases below 80% of the specified output power or if the current increases by 20%, the end of the lifetime of this device has been reached. Burn-in and ageing tests are typically done in constant current mode, due to the fact that it is easier and cheaper to keep the current constant instead of the optical output power.

The degradation of diode lasers differs from other electronic devices due to the radiant recombination process of electron-hole pairs and the presence of high optical densities within the active region and at the output facet [26]. Primary degradation modes are defect growth, facet degradation due to oxidation, solder degradation, and heat sink degradation. The degradation can be enhanced by increased current, temperature, and output power.

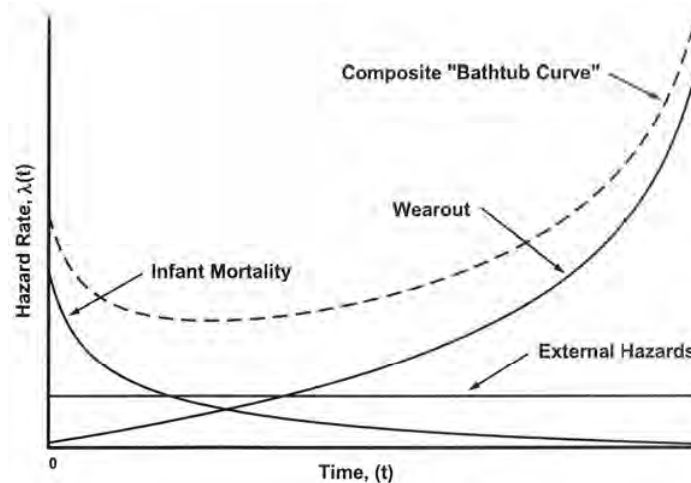


Figure 3-5: Hazard rate characteristic curve for diode lasers [41]

Typical failure types are random or wear-out failure. Wear-out failure is generally the result of defect growth in the inner active region and can be detected by a slow degradation of the performance of the laser. Random failures are usually caused by catastrophic optical damage, heat sink, or bond failures. Random failures are characterized by rapid degradation of laser performance.

In Figure 3-5 the hazard rate is plotted versus the lifetime of the device. The composite curve is a typical bathtub curve. This curve contains the wear-out curve as well as the infant mortality curve, which describes the occurring of early failure due to the manufacturing process or intrinsic semiconductor defects. External hazards can be current surges or ESD events. The wear-out failures are described above.

After packaging and first characterization, the device is burned. This means that the device is operated under normal or accelerated conditions. Burn-in times of less than 100 hours are common. If the characteristic values such as threshold current, slope efficiency, and optical output power vary significantly before and after burn-in, the device can be rejected because it is a clear candidate for early failure during its lifetime (Infant mortality) [41].

The lifetime or mean time to failure (MTTF) can be described with statistics. Usually the Weibull distribution is used for failure description [60].

A standard for reliability is the ISO 17526:2003, IEC 61751:1998 and Telcordia GRU 486.

The influence of mounting induced strain on the degradation of diode laser bars has been investigated by R. Xia. It was found that a mounting induced strain threshold exists from which point the degradation begins [82].

- **Accelerated Ageing**

Accelerated ageing tests are carried out by operating the device under stressed conditions. When operating under such conditions the physical mechanisms involved in the degradation process are accelerated, allowing the evolution of the laser parameters to take place faster than under normal operation conditions. The ageing tests must be designed to produce the same degradation process as expected from normal operation of the device. On the other hand, these enhancement factors are among the main agents on degradation during normal operation. In such a case, it makes sense to establish a relationship between the degradation processes and one or more enhancement factors such as temperature, injection current, or output power. This relation is found using statistics. This method is simple for single emitters, but very cost intensive for laser bars. Due to the fact that a laser bar consists of several individual emitters, the failure mechanisms are more complicated. If one emitter fails, the other emitters have to run at a higher current level in order to keep the output power constant. This leads to a faster degradation of the remaining emitters. Therefore accelerated ageing is not a standard process for diode laser bars.

The lifetime of the device can be plotted as a function of the temperature using the Arrhenius equation, with the assumption that the gradual degradation process is thermally activated [42].

Arrhenius equation

$$\tau = \tau_0 \cdot e^{\frac{E}{k \cdot T}}$$

Formula 3-6

E is the characteristic activation energy, k the Boltzmann constant, T the ambient temperature, and τ_0 the pre-exponential factor.

Typical values for the activation energy are in the range of 0.2 to 0.7 eV. Laser ageing can be accelerated significantly by higher temperatures. For example, a diode laser with a lifetime of 100.000 h and an activation energy of 0.7 eV at ambient temperature, only has a lifetime of 2.300 h at 70 °C. Increasing the temperature to accelerate ageing is a method commonly used in accelerated life tests [41].

3.4. Thermal Properties of Heat Sinks

As a measure of the thermal performance of diode laser packages, the total thermal resistance, R_{th} , is commonly used. It is defined as

$$\text{thermal resistance} \quad R_{th} = \frac{dT_{laser}}{dP_{loss}}. \quad \text{Formula 3-7}$$

The lost power P_{loss} can be calculated from the characteristic curves of the diode laser bar,

$$\text{power loss} \quad P_{loss}(I) = U(I) \cdot I - P_{opt}(I) \quad \text{Formula 3-8}$$

where $P_{opt}(I)$ is the optical output power and $U(I)$ is the voltage, as a function of the driving current I .

The operating temperature of the bar can be calculated from the emission wavelength:

$$\text{temperature laser} \quad T_{laser}(I) = T_{without} + \left[\frac{d\lambda}{dT} \right]^{-1} (\lambda(I) - \lambda_{without}) \quad \text{Formula 3-9}$$

$$\text{coolant temp.} \quad T_{without} = T(I = 0) = T_{coolant} \quad \text{Formula 3-10}$$

$$\text{wavelength at coolant temp.} \quad \lambda_{without} = \lambda(I = 0) = \lambda_{pulse}(T_{without}). \quad \text{Formula 3-11}$$

In this calculation, $T_{without}$ is the temperature without thermal load, which is the coolant temperature, $T_{coolant}$. $\lambda_{without}$ is the short pulse wavelength at the temperature $T_{without}$ and $d\lambda/dT$ is the thermal wavelength shift. Both $\lambda_{without}$ and $d\lambda/dT$ are nearly constant for each fabrication batch. The thermal wavelength shift can be measured using a short pulse and a low duty cycle. The generated heat inside the laser bar can be neglected so that the laser bar has the same temperature as the coolant.

With this, the thermal resistance can be calculated with the wavelength, λ_{laser} , thermal wavelength shift, $\frac{d\lambda}{dT}$, and power loss, P_{loss} .

thermal resistance

$$R_{th} = \frac{d\lambda_{laser}}{dP_{loss}} \cdot \left[\frac{d\lambda}{dT} \right]^{-1}$$

Formula 3-12

The thermal resistance measured in accordance to this method depends on the geometry of the laser bar. For example, a packaged heat sink with a 50% fill-factor bar and with the same dissipation power has, in reality, a lower thermal resistance than a packaged heat sink with a 30% fill-factor bar. The heat is generated inside the emitters, which are located on the p-side of the laser bar. The emitters are a nearly two-dimensional structure located only a few micrometers away from the bar solder layer. Therefore, the emitters size is the size of the area where the heat is coupled into the heat sink. If the same heat is coupled into a larger area, the thermal resistance decreases.

A better value for comparison is the thermal impedance, $I_{thermal}$:

thermal impedance

$$I_{thermal} = A \cdot R_{th} = A \cdot \frac{dT_{laser}}{dP_{loss}}$$

Formula 3-13

The thermal impedance takes into account the different size heat generation areas, A. The area A is the laser bar size (length x cavity length) multiplied by the fill-factor.

Also, this value does not take into account the three dimensional heat flux inside the heat sink. For the comparison of different heat sinks, it is necessary to use nearly the same bar geometry.

- **Measurement of thermal resistance:**

In order to measure the thermal resistance of a packaged diode laser, the thermal wavelength shift of the laser bar batch and the wavelength behaviour dependent upon the power loss of the packaged diode laser has to be measured.

The short pulse wavelength is measured with a low duty-cycle, pulse length, and injection current. The overall power loss generated in the laser bar should be only a few mW. This small power loss has no significant effect on the laser bar temperature, therefore it is defined by the cooling water temperature.

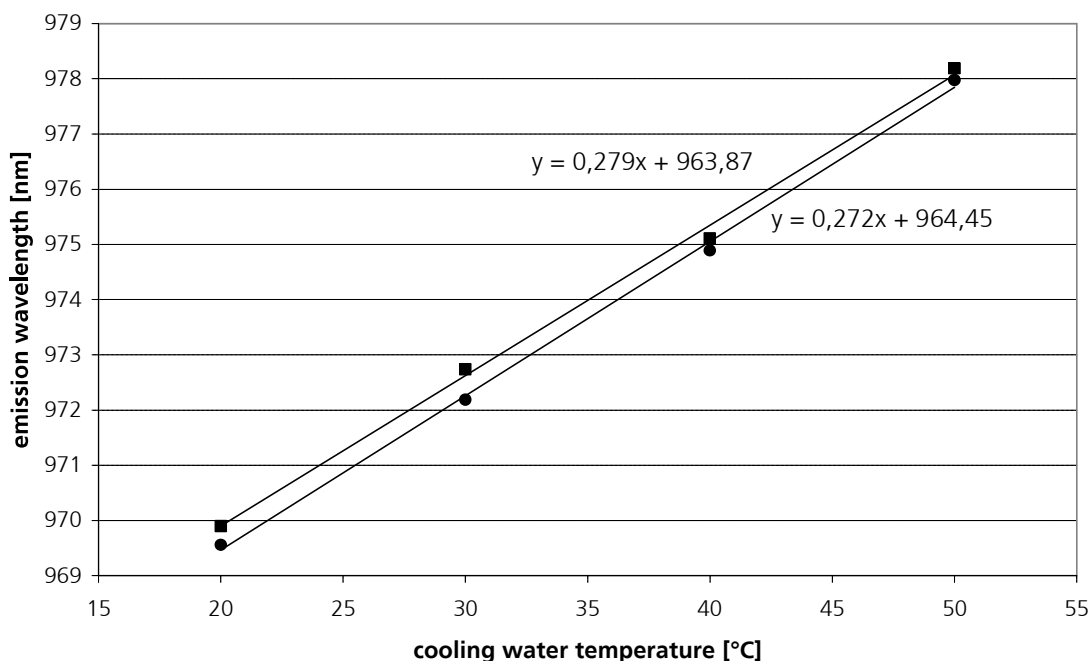


Figure 3-6: Measured wavelength dependent upon the cooling water temperature. The slope is the short pulse wavelength. Measured with 0.05% duty cycle, 2 μ m pulse length, and 30 A injection current.

The slope of the graph of the emission peak wavelength versus the cooling water temperature is the thermal wavelength shift (Figure 3-6). This wavelength shift is in the range of 0.2 and 0.3 nm/K. Also the packaging induced stress influences the wavelength. The mechanical pressure tuning contribution can be 15% of the thermal wavelength shift [69].

In order to calculate the thermal resistance the wavelength, dependent upon the power loss, is measured. By calculating the power loss (optical output power minus the driving current, times voltage drop) and the corresponding wavelength, a graph of wavelength versus power loss can be plotted (see Figure 3-7).

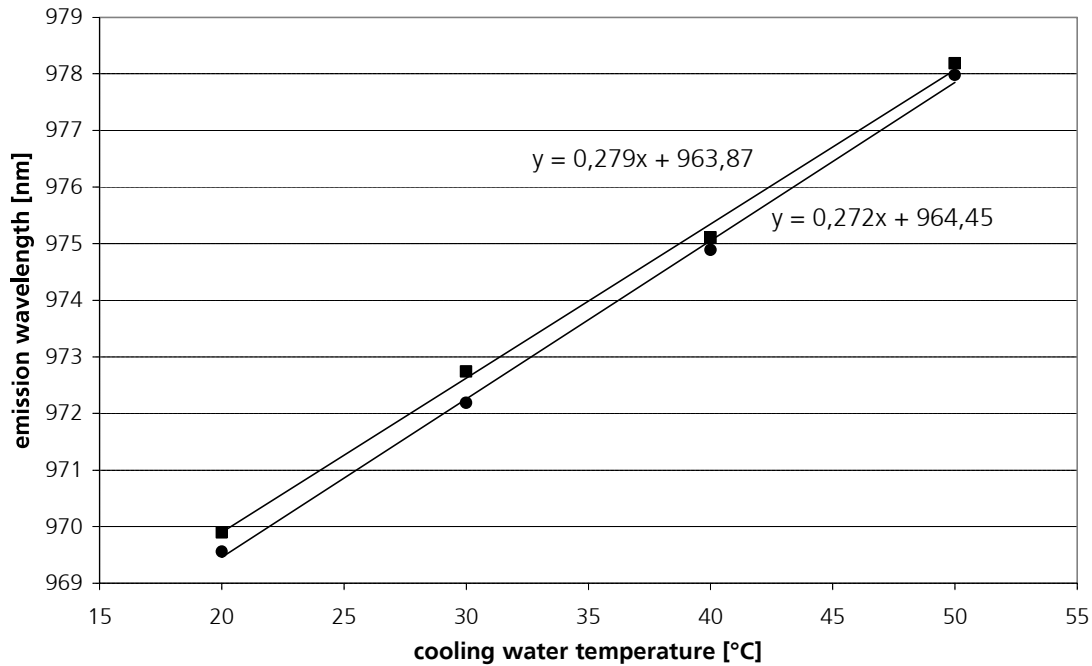


Figure 3-7: Measured wavelength versus power loss. The slope divided by the thermal wavelength shift is the thermal resistance.

The thermal resistance is the wavelength shift in dependence of the power loss divided by the thermal wavelength shift. For the shown example, the thermal resistance is 0.56 K/W.

$$\text{thermal resistance} \quad R_{th} = \frac{d\lambda_{laser}}{dP_{loss}} \cdot \left[\frac{d\lambda}{dT} \right]^{-1} = \frac{0.157 \frac{nm}{W}}{0.276 \frac{nm}{K}} = 0.56 \frac{K}{W} \quad \text{Formula 3-14}$$

3.5. Measurement Methods for Packaging Induced Stress

As described in Chapter 2.1, the electron band structure is temperature and strain dependant. The following measurement methods use this behaviour to measure the stress in the laser bar indirectly. Spatially resolved x-ray [85] or electron-beam-diffraction techniques can directly measure the deformation of the crystal, but these methods are expensive, complicated, and cannot be directly applied to packaged devices.

The relationship between stress, deformation, and strain is described by Hooke's law. For one dimension, the strain, ϵ , is proportional to the created stress, σ . For three-dimensional stress, a 4th order tensor, c_{ijkl} , has to be defined to link the stress tensor, σ_{ij} , and the strain tensor, ϵ_{kl} . As stress

is measured in units of pressure and strain is dimensionless, the tensor values, c_{ijkl} , are also in units of pressure.(Formula 3-15)

Hooke's law
$$\sigma_{ij} = \sum_{kl} c_{ijkl} \cdot \varepsilon_{kl}$$
 Formula 3-15

Indirect methods, such as micro Photoluminescence spectroscopy, photocurrent spectroscopy, and the degree of polarisation photoluminescence use the change in the electronic band structure. The energy modification, E_{ij} , is also linked by a 4th order tensor to the strain. Bardeen and Shockley introduced the concept of electron-phonon coupling in semiconductors [2]:

Bardeen-Shockley theorem
$$E_{ij} = \sum_{kl} \xi_{ijkl} \cdot \varepsilon_{kl}$$
 Formula 3-16

By using a perturbation-method this theorem has been developed further [6],[71]. By measuring the energy modification of the band gap, qualitative information about the strain and stress can be obtained. Further information about the device structure and calculating the band-structure using the k·p perturbation theory can lead to a quantitative strain analysis of AlGaAs-based devices [70].

The measured values of micro-PL, PCS, and DoP, which are described in the following chapters, are scalar information, which do not allow full determination of all the stress or strain tensor components.

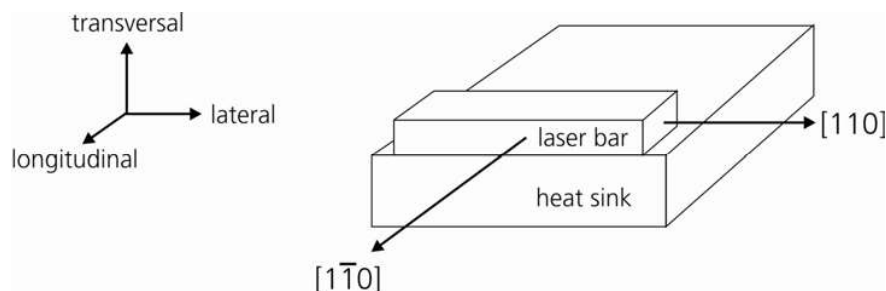


Figure 3-8: Schematic view of a packaged laser bar on a heat sink

During cm-bar packaging, the main stress of the packaging process occurs in the lateral direction. Thus the stress field can be considered uniaxial in the [110]-direction.

All the methods described in the following measure stress indirectly. Normally, only a qualitative distribution is obtained. The methods differ in their spatial resolution, information depth, and measuring time. Some methods are passive, while other measurements can only be made while the device is being operated [71],[73].

3.5.1. Photo-Current Spectroscopy (PCS)

Photocurrent measurement is a non-invasive technique that analyses the band structure of the waveguide. For PC spectroscopy, the diode laser is operated in a manner similar to a photodiode without any bias because the diode laser is photosensitive. The front facet of the diode laser is illuminated and certain parts of the light are absorbed inside the diode laser and the reflection is fed into a Fourier-transform spectrometer. Such a spectrum is shown in Figure 3-9. The optical transitions are attained using the first derivation of the PC spectrum. With this, the different transitions, such as heavy hole and light hole to the conductive band, can be studied.

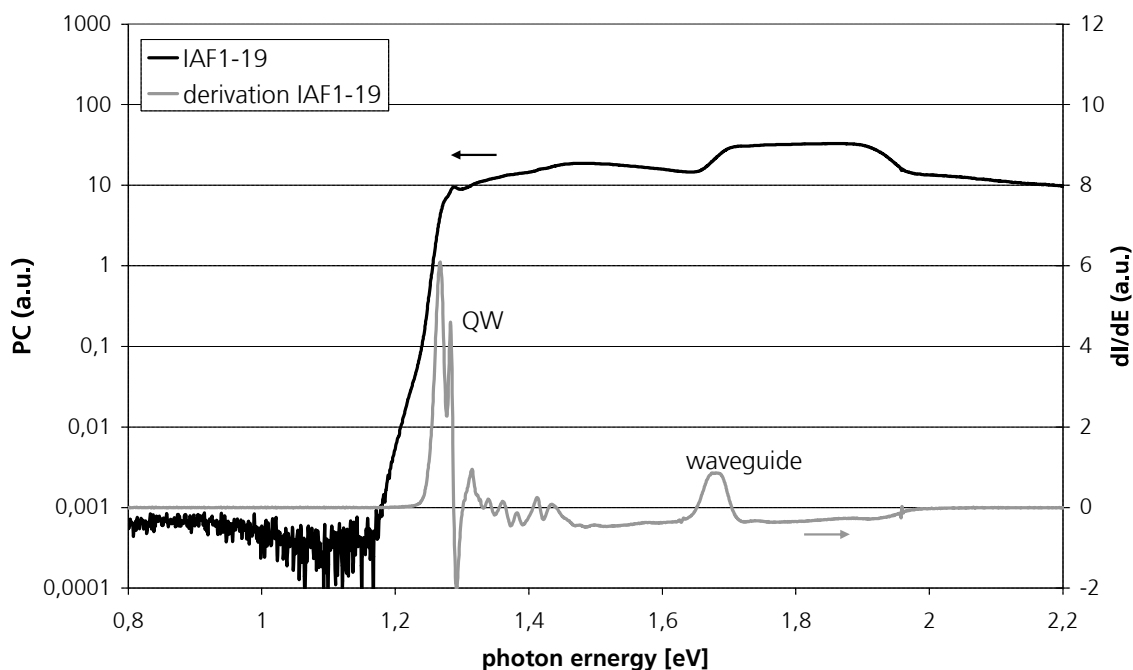


Figure 3-9: PC spectrum and its first derivation for a diode laser [Measurement performed at MBI].

By measuring these values for each emitter, the deformation of the band structure can be analyzed. By plotting the photon energy of the transition heavy hole to the conductive band (1hh-1e) versus the local position of each emitter, the strain distribution of the device is shown. A shift towards higher transition energies indicates compressive strain (see Figure 3-10).

The spatial resolution is larger than 30 μm and the measuring time per data point is around 10 minutes. The received information of the strain is the strain inside the quantum well and waveguide, because only this is sensitive to the PCS. The information depth is 20-50 μm in the QW and 2-5 μm in the waveguide, which is limited by absorption [4],[71].

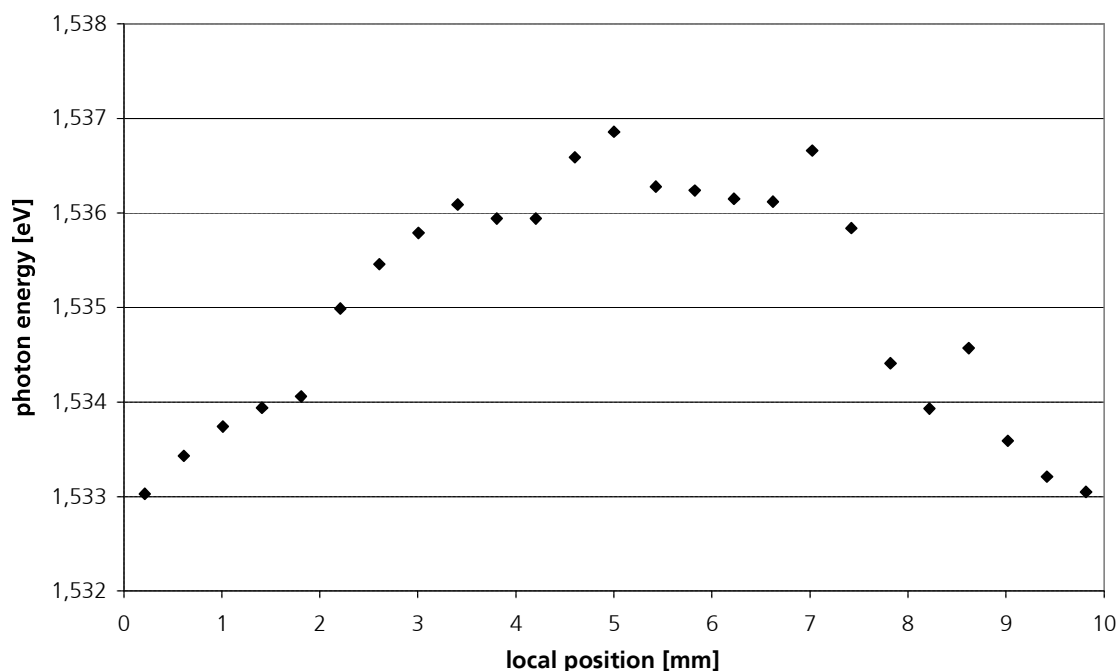


Figure 3-10: Spectral position of the 1hh-1e transition of each emitter versus the local position. The diode laser is mounted on a copper heat sink and therefore a compressive induced strain appears [Measurement performed at MBI]

PCS measurements done in this work are performed at Max-Born-Institute in Berlin (MBI).

3.5.2. Micro-Photoluminescence Spectroscopy

Micro-photoluminescence spectroscopy is similar to the photo-current spectroscopy and also works for the semiconductor substrate. The semiconductor material is excited by light and the photoluminescence spectrum is then analysed using a spectrometer.

In order to get a small spatial resolution, the excitation light is focused using a microscope optic onto the front side of the laser bar. The produced photoluminescence spectrum is analysed through the same optic. By moving the optic, the whole front side of the laser bar can be scanned. For each position a spectrum is recorded and analysed. The spatial resolution is $0.7 \mu\text{m}^2$ and the information depth is around $3 \mu\text{m}$.

The micro-PL measurements done in this work, are performed in the middle, $50 \mu\text{m}$ above the active region of the laser bar on the substrate. Typically, every $10 \mu\text{m}$ a spectrum is measured over the whole width of the laser bar. Crystal defects influence the photoluminescence as well so that not only the strain is investigated.

In Figure 3-11, the spectral position of the PL-peak wavelength versus the local position along the laser bar is shown. The bending of the curve, not the absolute position, is related to the strain distribution. In order to compare different measurements, the wavelength shift $\Delta\lambda$ is important. This indicates the degree of strain. The peaks of the curve represent defects.

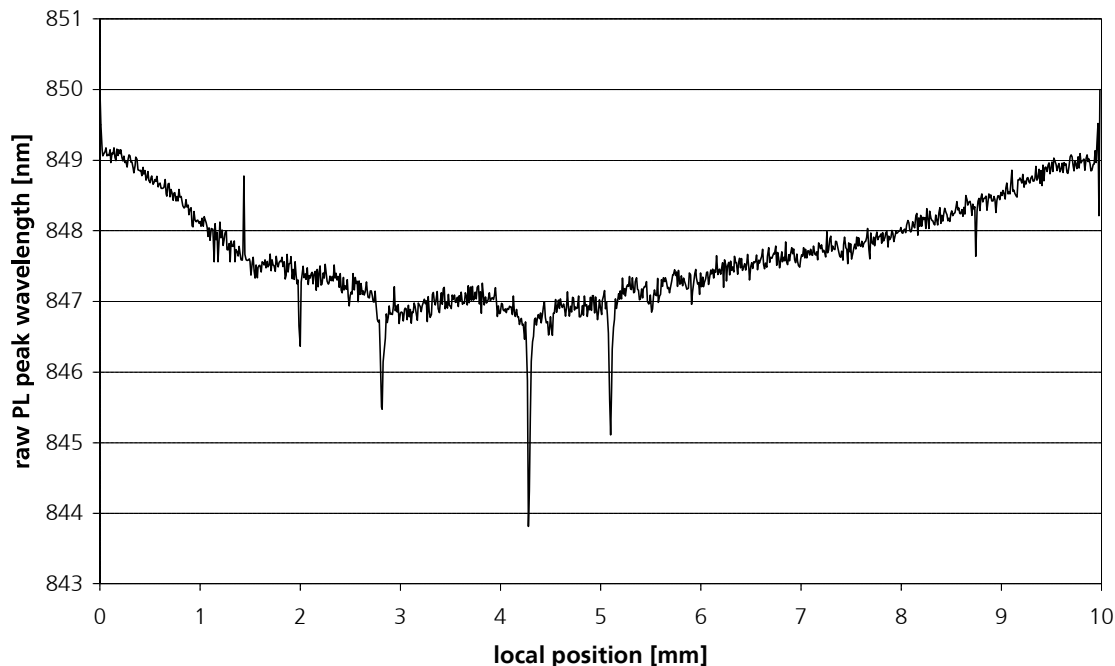


Figure 3-11: PL-peak position versus local position. A bending towards the bottom indicates compressive strain [Measurement performed at MBI].

The spatial resolution of μ -PL is $\sim 1 \mu\text{m}$ and the information depth is $\sim 1 \mu\text{m}$, limited by the diffusion length of the excitation light [53],[71].

Micro-PL measurements done in this work are performed at Thales Research & Technology (TRT).

3.5.3. DoP-Electroluminescence

In this case, the polarisation of the electroluminescent radiation is determined. As described in Chapter 2.1.2, the polarisation depends on the stress inside the quantum well. Measuring the intensity, I , of the TE and TM polarisation, the degree of polarisation, DoP, can be calculated.

Degree of Polarisation (DoP)	$DoP = \frac{I_{TE} - I_{TM}}{I_{TE} + I_{TM}} = K_{\sigma} (\sigma_{xx} - \sigma_{yy})$	Formula 3-17
---------------------------------	--	--------------

By using photoluminescence instead of electroluminescence, the information depth is limited to the facet. In this case, the DoP can be traced back to the strain distribution in the facet plane (σ_{xx} , σ_{yy}) and K_{σ} is proportional constant (Formula 3-17)[25]. The higher the DoP value is, the greater the compressive strain on the device. A DoP of zero signifies that the device is not strained. The DoP value can vary from -1 (tensile strain) to 1 (compressive strain). The dependency of polarisation and strain are described in Chapter 2.1.2.

By using electroluminescence, the information depth is the whole cavity length of the laser bar. Photons, which are emitted in a certain angle inside the waveguide are directed by the waveguide to the output facet. The 3-dimensional band structure can be very complicated, making it difficult to assign a higher value to a higher compressive state. Therefore the strain distribution can only be measured qualitative. A straight line indicated a homogeneous strain distribution, which indicates a low packaging induced strain. Shifts are an indicator of packaging induced strain.

The measurements are done with current below the threshold current. Due to the operating device, the device heats up locally, which induces operating induced stress. Therefore, this method measures the packaging and parts for operating induced stress [71],[76].

The intensity measurements are done for all emitters simultaneously using a camera. Therefore, the lateral resolution is around 10 μm and the information depth is the cavity length.

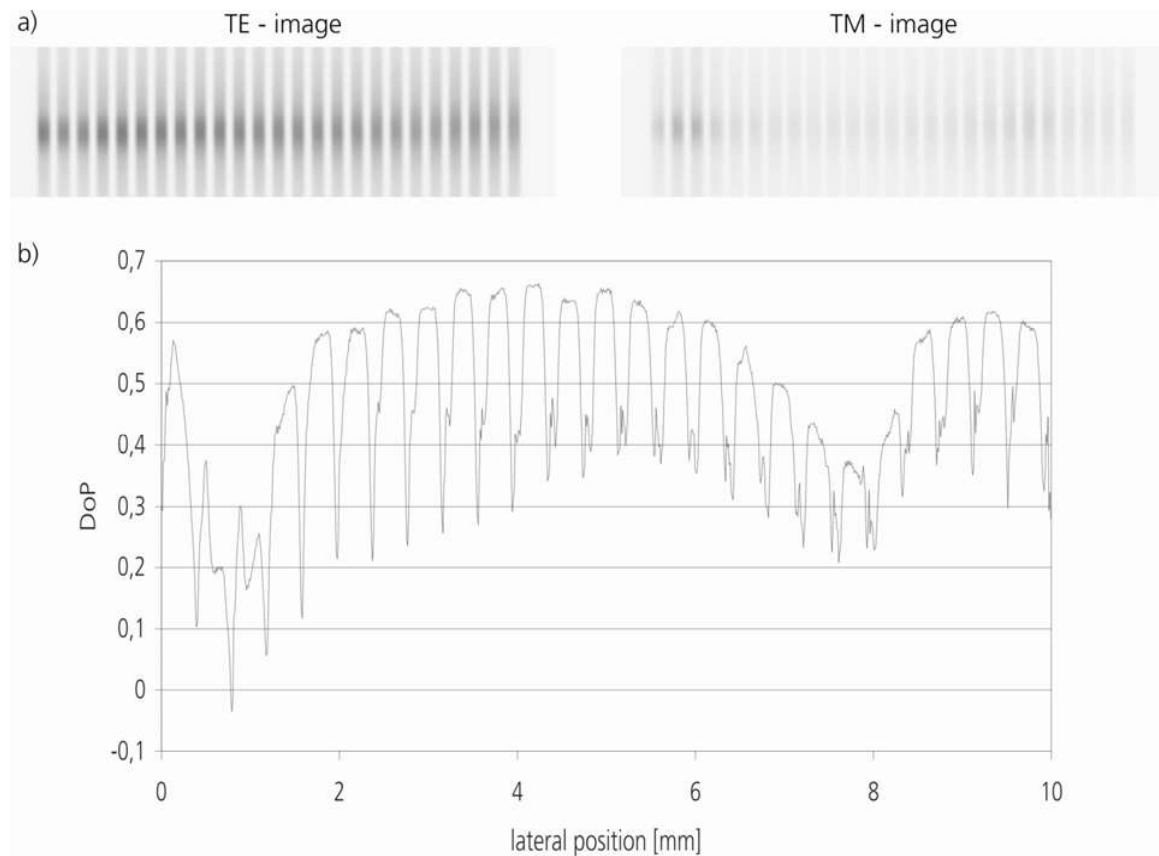


Figure 3-12: a) TE and TM image of the camera. The stripes represent one emitter. b) Calculated DoP value based on the images

The polarisation is not only dependent on the transition feasibility of the band structure, but also on defects and the facet of the emitter. These can significantly change the DoP curve [72].

3.6. Metallurgical Analysis

During the packaging process and life of the diode laser, the metallurgical composite of the solder layer changes. Properties of the solder such as elasticity and hardness, depend on the metallurgical composition. Therefore the metallurgical composition of the solder layer is of great interest, because it can change the properties significantly.

3.6.1. Analysis of Solder Cross Section

The solder layer is too thin to do a cross-sectional analysis. Typical solder layer thicknesses are in the range of 1 to 10 μm . In order to see differences in the solder interface, a spot size less than 200 nm in diameter is required. Typical spot sizes are around 2 μm . Lower spot sizes significantly lower the signal strength and increase the measurement time. Typical measurement methods and their information depth for chemical analysis are shown in Table 3-1. In order to scale up the solder interface, an angle polish can be done or a dimple grinding technique can be used.

abbreviation	analysis technique	information depth
XPS (ESCA)	X -ray photoelectron spectroscopy (Electron spectroscopy for chemical analysis) is a quantitative spectroscopic technique that measures the elemental composition, chemical state, and electronic state of the elements that exist within a material.	1-10 nm
AES	A uger electron spectroscopy examines the chemistry of a surface by measuring the energy of electrons emitted from that surface when it is irradiated with electron with energy in the range 2–50 keV. It is more sensitive for lighter elements.	few nm
SEM	The s canning electron microscope (SEM) is a type of electron microscope capable of producing high resolution images of a sample surface	1-5 nm spot size
EDX	E nergy dispersive X -ray spectroscopy (EDX or EDS) is a method used to determine the energy spectrum of X-ray radiation. It is mainly used in chemical analysis, in an electron microprobe (e.g. inside an scanning electron microscope)	2-20 μm

Table 3-1: Techniques for chemical analysis [80]

The dimple grinding technique has the advantage of measuring the depth by measuring the diameter of the dimple. See Figure 3-13 and Figure 3-14. The diameter can easily be measured by using a SEM image or a measuring microscope. By using the Formula 3-18, the depth (d) of each position (x) can be calculated with the radius of the ball (R) and the radius of the dimple (a).

depth of dimple

$$d = \sqrt{R^2 - a^2} - \sqrt{R^2 - (a - x)^2}$$

Formula 3-18

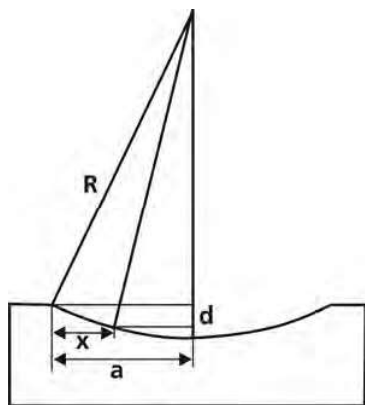


Figure 3-13: Scheme of the dimple

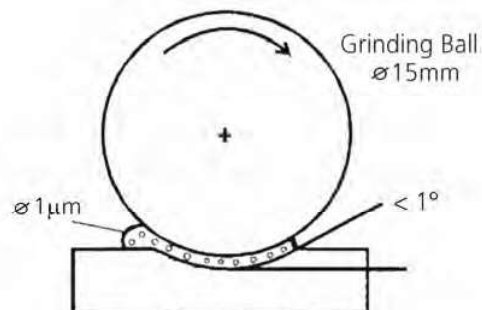


Figure 3-14: Dimple grinding technique

As a grinding liquid, a suspension of 1 or 0.25 μm diamond particles is used. Indium is a very soft metal that is difficult to grind and even more difficult to polish. Therefore the diamond particles are likely to get stuck in pure indium layers.

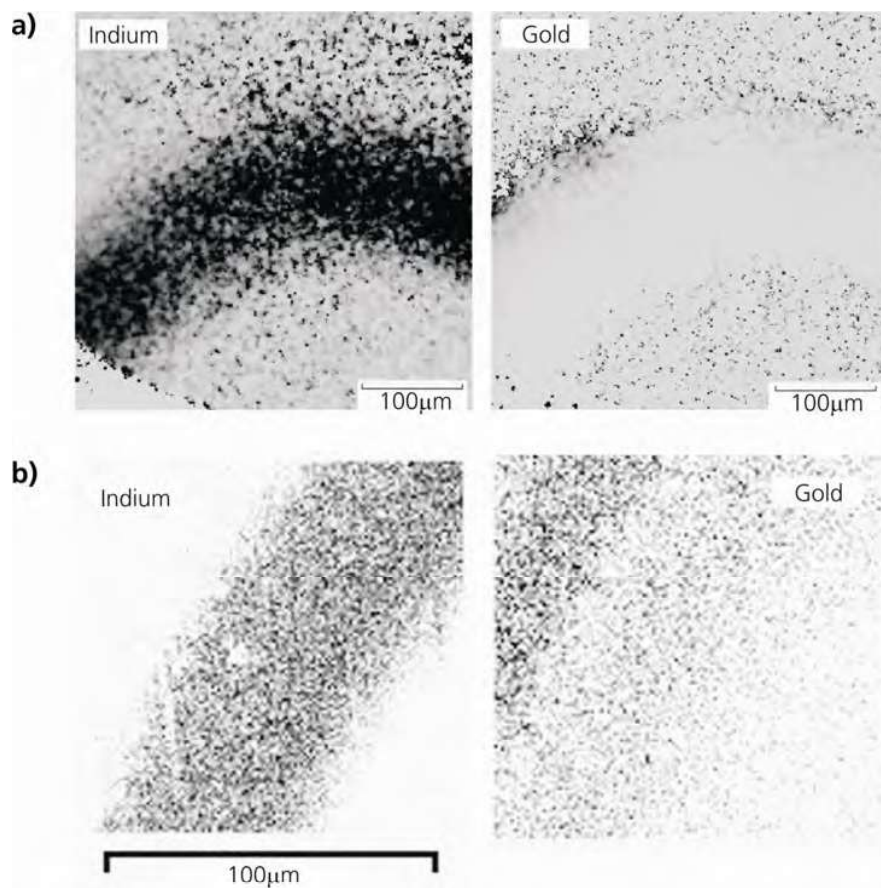


Figure 3-15: a) EDX mapping result. Darker points represent a larger amount of the element b) XPS mapping of an indium solder layer. Dark points represent a larger amount of the investigated element [measurement performed at the Deutsches Wollforschungsinstitut].

The prepared samples are then analysed with EDX or XPS. The XPS has a low information depth but the local resolution is poor. EDX has a much greater information depth, but the local position is much smaller, and with that the resolution is higher.

In Figure 3-15 the same sample is investigated using XPS-mapping and EDX-mapping. The spatial resolution is lower for the XPS measurement. The high resolution resulted from a long measurement over an extended period of time (several hours).

In both images the same sample is shown at nearly the same location. It is a laser bar solder layer with a thickness of 3 μm . The laser bar is at the top of the images. At the bottom, the nickel plating of the heat sink can be seen.

EDX is fast (several minutes) and point measurements analysing the metallurgical composition at exact chosen locations can also be carried out. (Figure 3-16)

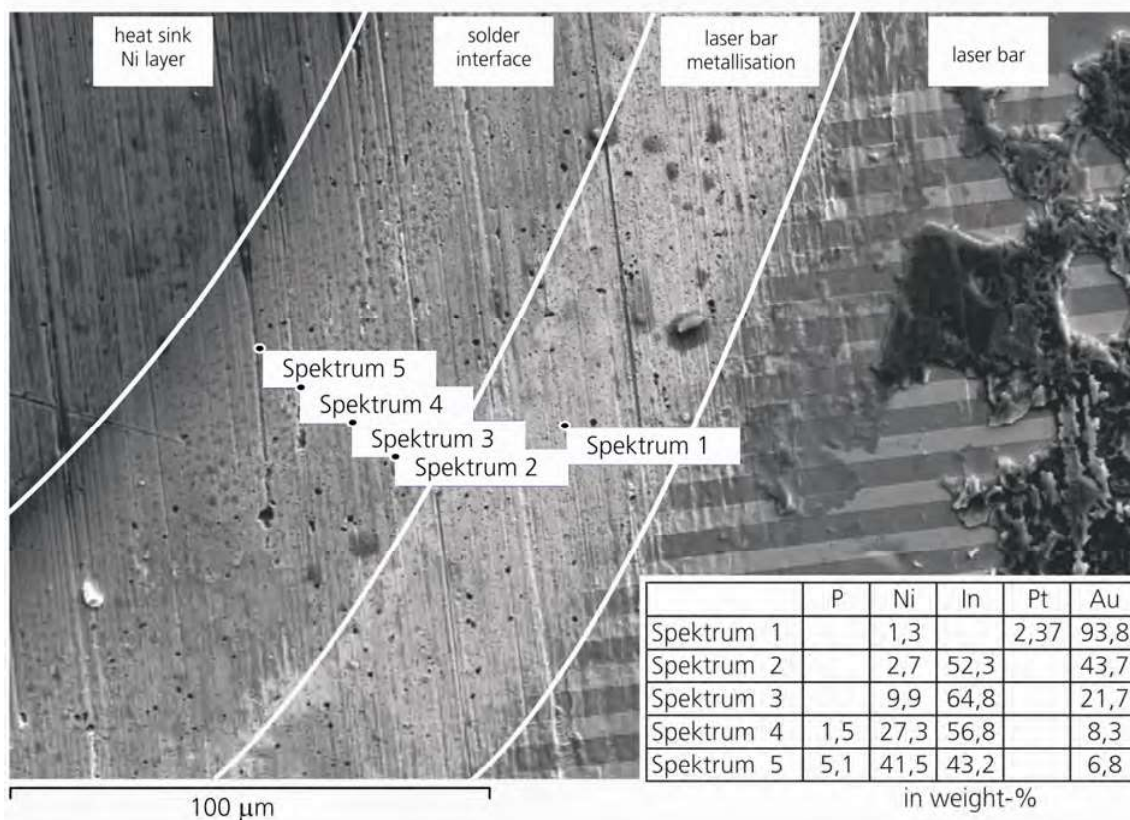


Figure 3-16: Point EDX analyses. The background is the SEM-image of a laser bar solder layer, which helps to chose the analysis points. The heat sink is on the left and the laser bar on the right. The point analysis is carried out where the black dots are located.

For metallurgical analysis of the solder layers EDX is chosen. It has the advantage that a SEM image shows the exact measurement point and it is a relatively fast method. Therefore, it must be pointed out that lower layers such as the nickel plating of the heat sink, influence the analysis. For example, in Figure 3-16, the nickel layer which is underneath the gold indium layer becomes visible at spectrum 3. At spectrum 4 and 5 the nickel is detected even more, even though it is only underneath and not mixed with the gold indium layer.

3.6.2. Shear Tests

The shear test machine is used to remove the laser bar from the heat sink. The set-up allows the measurement of the shear force to be dependent upon the displacement. The footprint of the laser bar shows how homogeneously the laser bar was soldered onto the heat sink. Grey areas indicate a connection between laser bar and solder, dark areas or imprint free areas indicates less or no connection (Figure 3-17). Also, the shear force gives information of the properties of the solder layer. The harder the solder layer is, the higher the shear force.

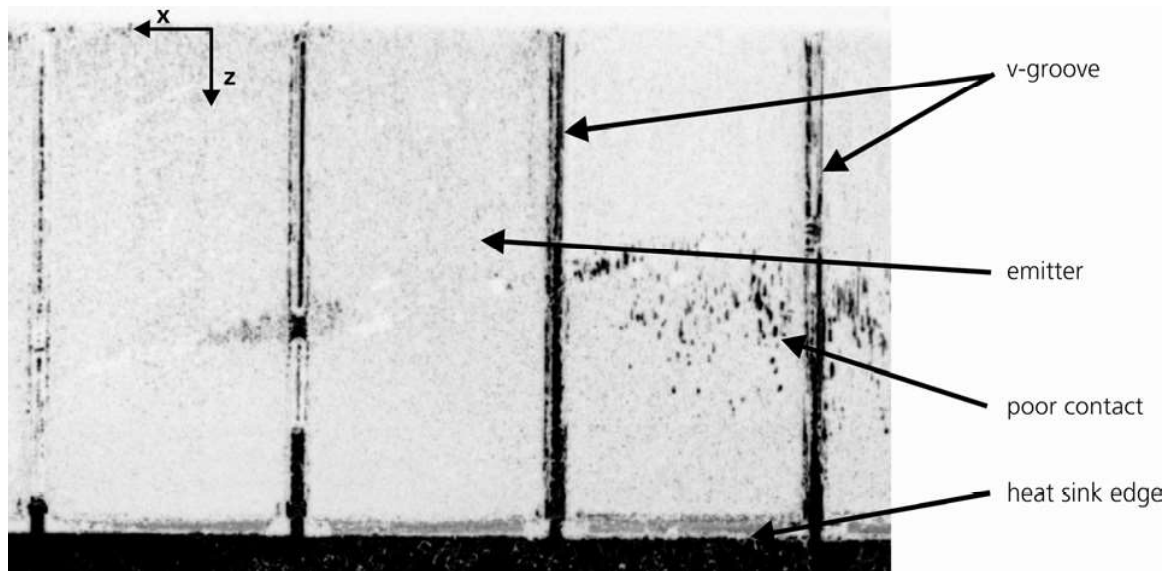


Figure 3-17: Footprint of a part of a laser bar. Grey areas indicate the imprint of the emitters, dark lines are the v-grooves, which have no contact to the solder. Dark dots in the emitter region indicate a poor contact.

Part II

Analysis

4. Thermal Influence of the Packaging

During operation, the dissipation power generates heat inside the laser bar. State of the art diode lasers have an efficiency of up to 70% in laboratory [12] and commercial products have an typical efficiency between 50 and 55% [9],[56]. Most and also aged diode lasers have a conversion efficiency of 50%. This means 50% of the electrical power which is put into the diode laser is transformed into optical power. The other half generates heat that has to be removed from the semiconductor. Most of the heat is generated in the active region of the emitters due to non-radiating transitions. A small part of the power loss is created due to the ohmic resistance of the semiconductor material. The resistance of the diode laser bar, including the contacts is around 5 m Ω .

The laser bars used in this thesis have 200 μm wide emitters, are 1200 μm long (cavity length), and have a fill-factor of 50%. The emitter height is 1 to 2 μm , allowing an emitter to be seen as a 2-dimensional structure. The typical optical output power of one emitter is 2.5 W. With an efficiency of 50%, the heat density is about 10 W/mm². For comparison, a AMD Athlon 1000 MHz processor has a die heat density of 0.64 W/mm² [36].

These enormous heat densities are handled with micro-channel heat sinks (actively water cooled) or with conductively cooled heat sinks made out of copper at lower power. A description of the heat sink types can be found in Chapter 2.2.

There are also packaging induced thermal properties. The thermal connection between heat sink and laser bar consists of several layers such as the heat sink plating and solder. Therefore the thermal resistance depends on the design and quality of these layers.

The output power and characteristic values of a laser bar such as threshold, slope efficiency, wavelength, and lifetime are temperature dependent (see Chapter 2.1). In order to optimize these parameters, the thermal load has to be minimized.

In the following, the thermal properties of the packaging regarding heat sink and solder will be investigated in detail.

4.1. Thermal Resistance

Altogether three different kinds of heat sinks are investigated. A standard heat sink made of copper, which is used in commercial products, is examined as reference. For expansion matching two different types of heat sink are designed, the "top-layer" heat sink and the "sandwich" heat sink, which are described in Chapter 2.2.3.

4.1.1. Simulation

The heat sink and laser bar geometry is transferred to a finite element software that is able to calculate temperature distributions for a given set of material parameters and boundary conditions.

For the simulation, a bar with a fill-factor of 50% and a power loss of 80 W is used. This is a power loss of 3.2 W per emitter.

The heat-transfer coefficient used inside the micro-channels is 100.000 W/m²·K and 10 W/m²·K for the supply channels. The location of the micro-channels and supply channels can be seen in

Figure 2-7. These values are found to be realistic and are used for the following thermal simulations. The values are similar to the values published by others such as a heat transfer coefficient of 8 to 15 W/m²·K inside the supply channels [50] and 87.000 W/m²·K inside the micro-channels [21]. These values are used for the boundary conditions for the thermal simulations.

The heat generated in the active region flows directly from the emitter through the bar solder layer into the heat sink. There is also an indirect route from the laser bar through the n-contact sheet, then through the isolation foil into the heat sink. The following simulations are carried out to see, if the indirect method can be neglected in order to simplify the simulation.

A complete packaged diode laser is thermally simulated. The isolation foil is made of polyimide (properties are shown in Table 8-7). Typically the n-contact sheet lays only on the isolation foil and is not fixed with glue or other similar adhesive materials.

The simulations are carried out with a 100% thermal contact between the n-contact sheet and the isolation foil and shows a heat flow of 0.5 W of the complete dissipation power of the laser bar being 80 W. This part of the power loss is less than 1%. In reality it will be even less due to the fact that the contact between the n-contact sheet and the isolation foil is loose.

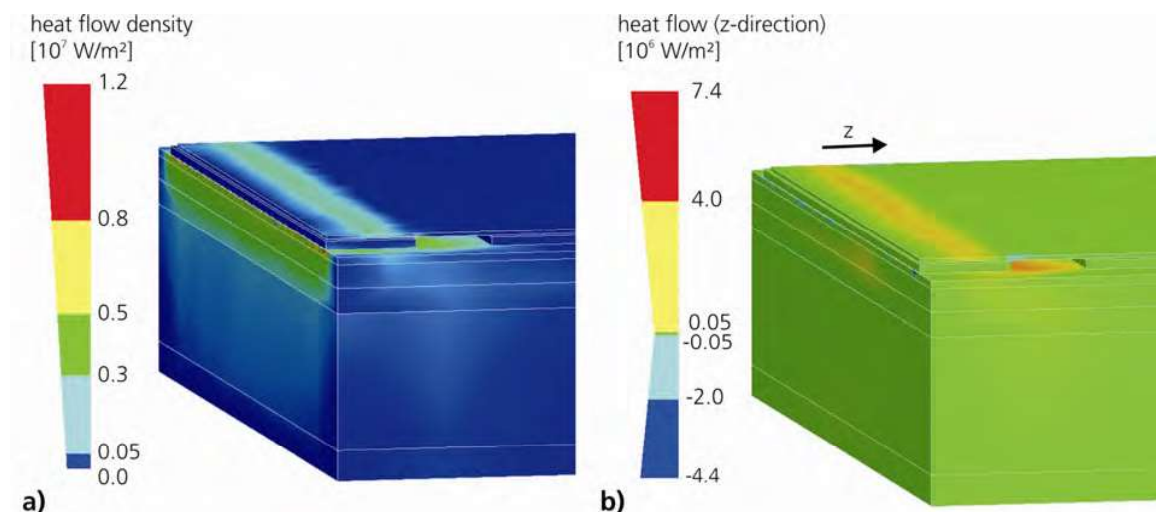


Figure 4-1: a) heat flow density of a packaged laser bar with a power loss of 80W. b) Heat flow in z-direction of a packaged laser bar with a power loss of 80W. Nearly all power loss is transferred directly into the heat sink and only 1% through the n-contact sheet.

On the left in Figure 4-1 the heat flow density of the packaged diode laser is shown, and on the right the part of the heat flow in the z-direction. The part of interest is the heat flow over the n-contact sheet between the laser bar and the isolation foil, which is less than 0,05 W. This shows that there is nearly no heat flow to the isolation foil.

The heat flow through the n-contact sheet is neglected. Lorenzen [50] has shown that the heat flow through a 50 μm thick copper n-contact sheet and the isolation foil reduced the thermal resistance by 0.02 K/W. Also the heat emission by thermal convection to the surrounding air is only 10 mW for a 50 W laser. This is also neglected in the following simulations.

The first type of expansion matched heat sink, called a "top-layer" heat sink, uses an expansion matched material as the top layer. The second type, called a "sandwich" heat sink, has a copper

surface, but underneath a material with a lower thermal expansion coefficient as GaAs, which reduces the thermal expansion of the thin top copper layer, is used. Details of these two types of expansion matched heat sinks are described in Chapter 5.2. As a reference for all the simulations, a standard copper heat sink with the same geometry and inner structure is used.

The results of the thermal simulation of the three types of heat sinks are shown in Figure 4-2. The maximum temperature of the laser bar on a copper heat sink is 54.5 °C, on the "sandwich" heat sink 66.0 °C, and on the "top-layer" heat sink 70.5 °C.

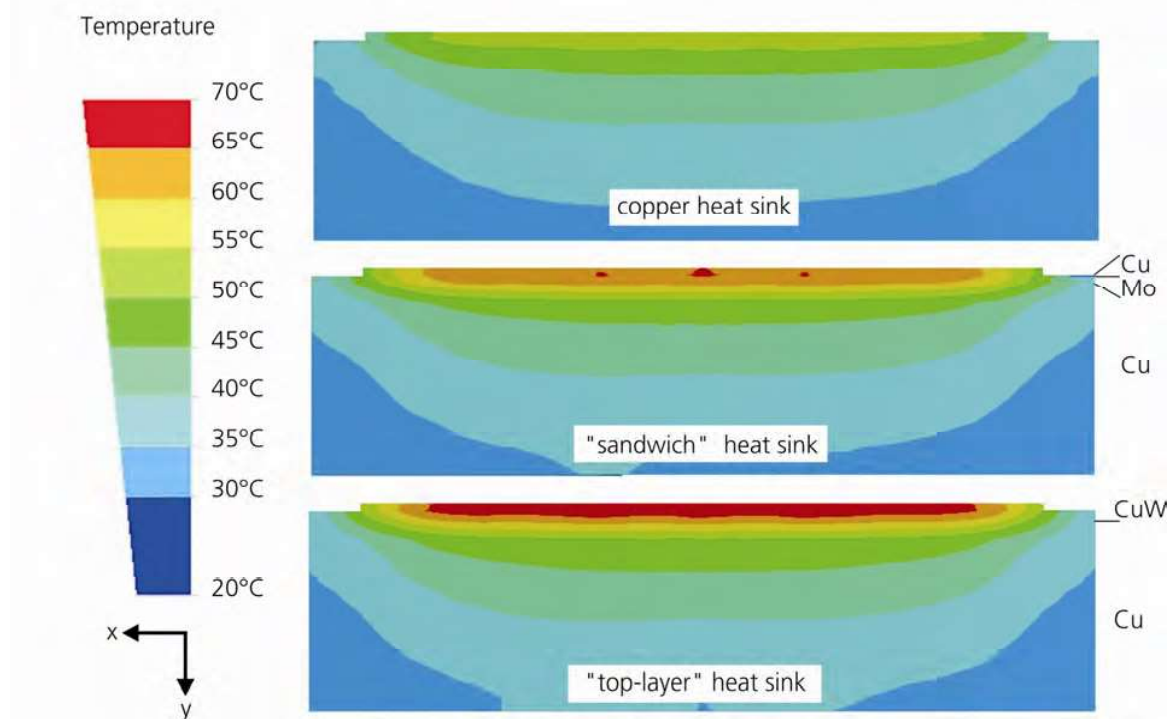


Figure 4-2: Temperature distribution of the three simulated heat sink designs. Top the standard copper heat sink, in the middle the "sandwich" and at the bottom the "top-layer" heat sink.

The high temperature of the packaged "top-layer" heat sink is due to the low thermal conductivity of the CuW material. It is two times smaller than the thermal conductivity of copper. The thermal conductivity of molybdenum, used in the "sandwich" heat sink, is also more than two times smaller, but the thin top copper layer helps to spread the heat. The thin thickness of the copper layer (0.1 mm) results in a lower thermal resistance than the "top-layer" heat sink. The simulated thermal resistances are 0,43 K/W for the standard copper heat sinks, 0,58 K/W for the "sandwich" heat sink, and 0,63 K/W for the top-layer heat sink.

4.1.2. Experiment

The two types of expansion matched heat sinks and the standard copper heat sink are investigated. All heat sinks are packaged with similar laser bars. The fill-factor is always 30% (150 μm emitter width and 500 μm pitch) and the resonator length is 0.9 and 1mm. The thermal resistance is measured with the wavelength shift method as described in Chapter 3.4.

The measured thermal resistance of the copper, "sandwich", and "top-layer" heat sink are shown in Figure 4-3. The line in the diagram is the average thermal resistance of each heat sink type. Due to fabrication problems such as the joining of different materials such as molybdenum or tungsten, the influence of improperly joined heat sink layers is responsible for the large range of measured thermal resistance.

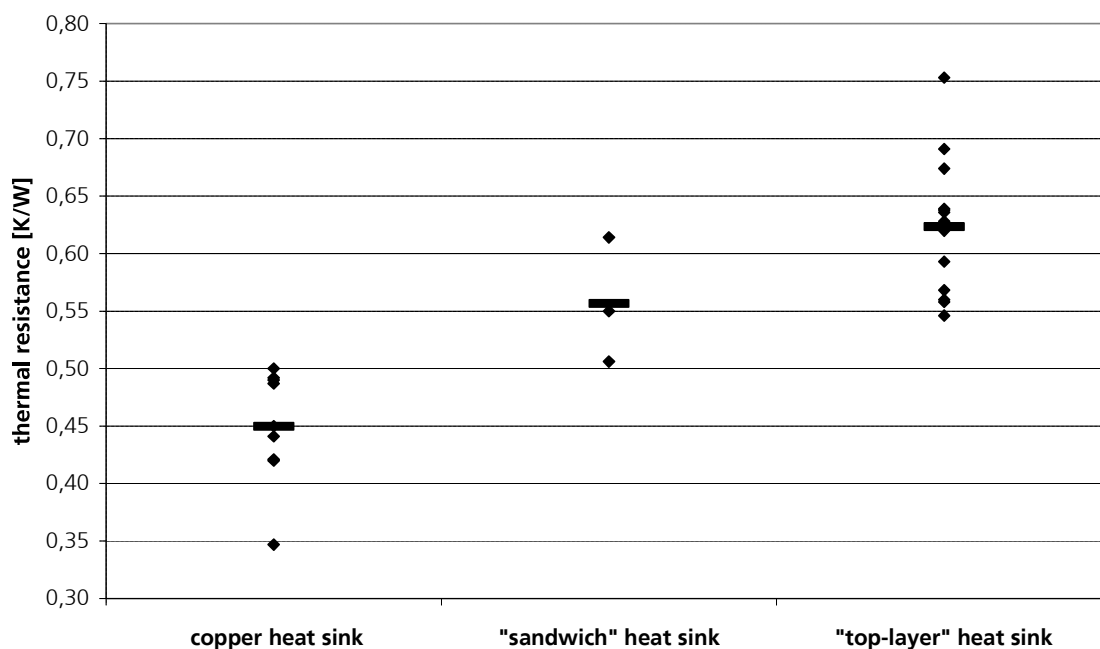


Figure 4-3: Thermal resistance of the "top-layer", "sandwich", and standard copper heat sink package. The small dots represent one device and the thicker line is the average of each type.

The comparison of the simulated and measured values is shown in Table 4-1. The simulated values are done for a 30% and 50% fill-factor laser bar, and the experimental data is determined from 30% fill-factor laser bars. Typically the thermal resistance of a 50% fill-factor laser bar is 20 to 30% higher compared to a 30% fill-factor laser bar. The better values of the simulation are due to the assumption of having 100% thermal contacts between the different layers, which in reality are not the case. Especially with large heat fluxes and small layers thicknesses, the influence becomes measurable, but it is nearly impossible to determine the real heat transfer coefficients of the different layer connections.

heat sink type	R_{th} (simulation) 30% fill-factor	R_{th} (simulation) 50% fill-factor	R_{th} (experiment) 30% fill-factor
"copper"	0.32 K/W	0.43 K/W	0.45 K/W
"sandwich"	0.45 K/W	0.58 K/W	0.56 K/W
"top-layer"	0.51 K/W	0.63 K/W	0.62 K/W

Table 4-1: Simulated and measured thermal resistance of a standard copper, the "sandwich", and "top-layer" heat sink. The simulated values are calculated from the maximum temperature of a simulation with 3.2 W power loss per emitter of a 50% fill-factor laser bar. The experimental data are from 30% fill-factor laser bars.

The experimental data and the simulated data show the same order and difference between the different heat sink types. Even if the simulated values are better, the assumptions for the thermal simulation are in the correct range and the simulation model can be used for thermal designing of heat sink.

The "top-layer" heat sink, which is similar to the submount packaging, has the highest thermal resistance. By using the "sandwich" heat sink, the thermal resistance for expansion matched packaging can be lowered by more than 10%. There is in reality also the same factor between the "sandwich" and a standard copper heat sink compared to the simulations.

4.2. Thermal Contact between Heat Sink and Laser Bar

The bar solder layer is responsible for the mechanical and thermal connection of the laser bar. The demand on the mechanical stability is low, because it does not need to resist external forces. By clamping the diode laser, the force goes directly on the heat sink and not on the laser bar. The force is needed for water proof connections for active cooled heat sinks or for a sufficient thermal contact for conductively cooled heat sinks. By connecting the n-contact, only a small vertical force is applied onto the n-contact sheet, which has nearly no mechanical influence on the bar solder layer.

An important issue is the thermal contact provided by the solder layer. With a power loss of 3W per emitter and an emitter area of 0.2 mm by 1.2 mm, the heat density is 12.5 W/mm². If there is a disconnection of 0.1 mm², which is equal to a cross sectional area of a human hair, more than 4% of the heat has to flow an indirect way. This leads to a hot spot, which can damages the semiconductor material. The damage can reach from a higher defect growth rate to catastrophic damage and will reduce the lifetime of the device.

The connection can be disturbed by contamination (Figure 4-4) such as remains from the reduction process, solder oxide, lack of solder, and organic films.

Larger voids are often the cause of broken diode lasers after the first "power on". Failures of this kind are usually very obvious and can be avoided with conventional methods. A lack of solder can be seen by visual inspection of the evaporated solder before soldering. Dust can be avoided by packaging in a clean environment. Particles larger than 10 μ m lead to a loose connection because there is not enough solder to close such a large gap. This failure mechanism can be reduced by working in a clean environment and a well thought out process.

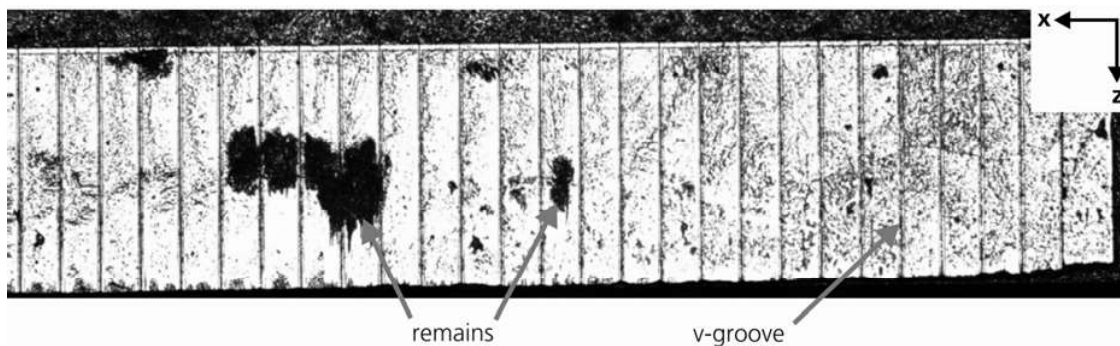


Figure 4-4: Footprint of laser bar left in the solder layer after shearing off the laser bar. Dark areas are contamination of the bar solder layer, white areas indicate connected/soldered areas.

Organic films disrupt the connection between solder and metallisation of the laser bar or heat sink. If an organic film develops, then no diffusion of the solder into the contact partners is possible, therefore no connection forms. After heating up the solder above melting temperature, the solder contracts (Figure 4-5). Before heating up, it is difficult to recognise the organic film. A typical source of organic film is insufficient cleaning or a polluted cleaning solution.

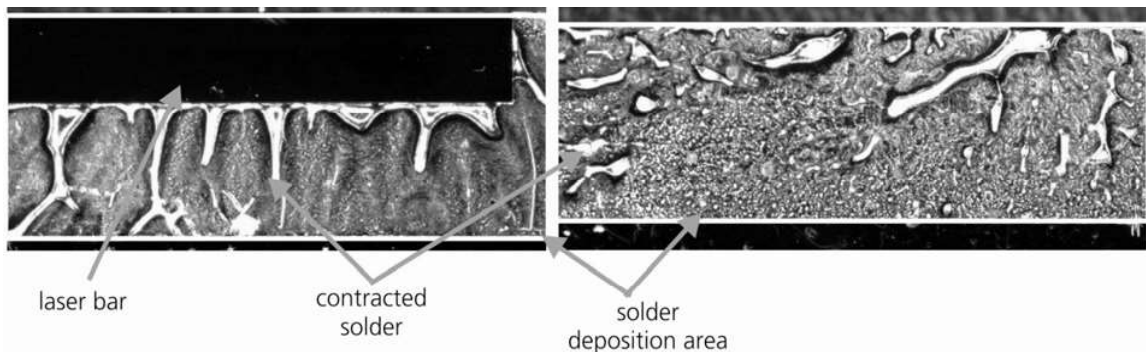


Figure 4-5: Influence of an organic film on the heat sink after heating up above the melting point of the solder (left: top view of solder layer with laser bar, right: without laser bar).

The evaporated solder itself is typically free of contamination if the source material is clean as well. After solder deposition, the solder layer oxidises. If the reduction is not performed correctly, the solder surface can become contaminated. In order to avoid the risk of contamination during reduction, a method to avoid oxidation is described in the following chapter. The influence of insufficient thermal and electrical connections caused by solder voids or remains is investigated in Chapters 4.2.2 and 4.2.3.

4.2.1. Avoiding Oxidation of Solder

If the oxidation of the solder layer can be avoided, no reduction is necessary, which is preferable as this process raises the risk of contamination.

In order to get an idea of the indium oxidation film development, two samples have been investigated. The first sample is only 3 hours old and protected by n-pentane (alcohol) to avoid oxidation in the atmosphere. It was exposed to air only temporarily, when the sample was taken

out of the vaporization holder. The second sample is more than 9 months old and has not been protected against air.

The analysis of the indium layer is done with XPS (X-ray Photoelectron Spectroscopy). The x-ray photoemission gathers the spectrum of the valence electron, which determines the physical and chemical properties of the element and the inner-shell electron. Since the local chemical and electronic environment can contribute to so-called "chemical shifts", further information about the chemical state of an atomic species on the surface can be obtained. That is the reason that XPS is also called ESCA – Electron Spectroscopy for Chemical Analysis. The reason for the chemical shifts is the influence of the binding energy due to ligands. By attracting the valence electrons with electronegative ligands, the potential of the atom is changed, which provides the electrons. Also the binding energy of the inner-shell electrons increases [3].

The information depth of XPS is about 8 nm. The whole thickness of the investigated indium layer is about 4 μm .

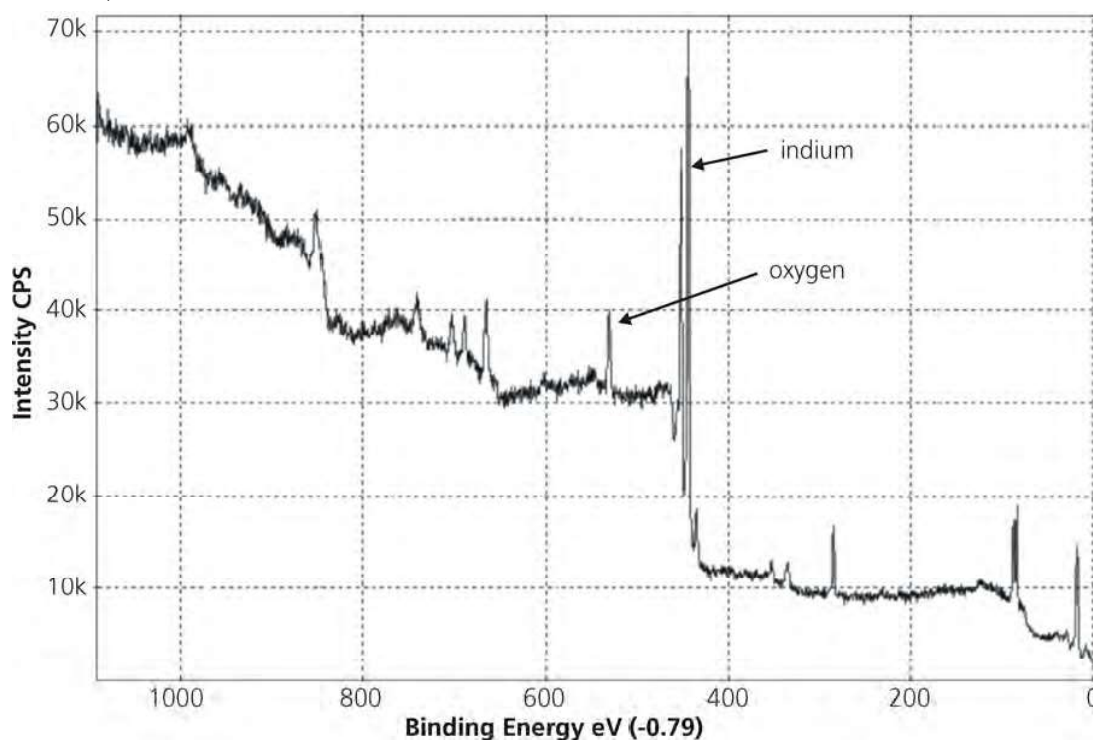


Figure 4-6: Spectrum measured by XPS of 3 hours old sample before sputtering. Indium and oxygen peak visible

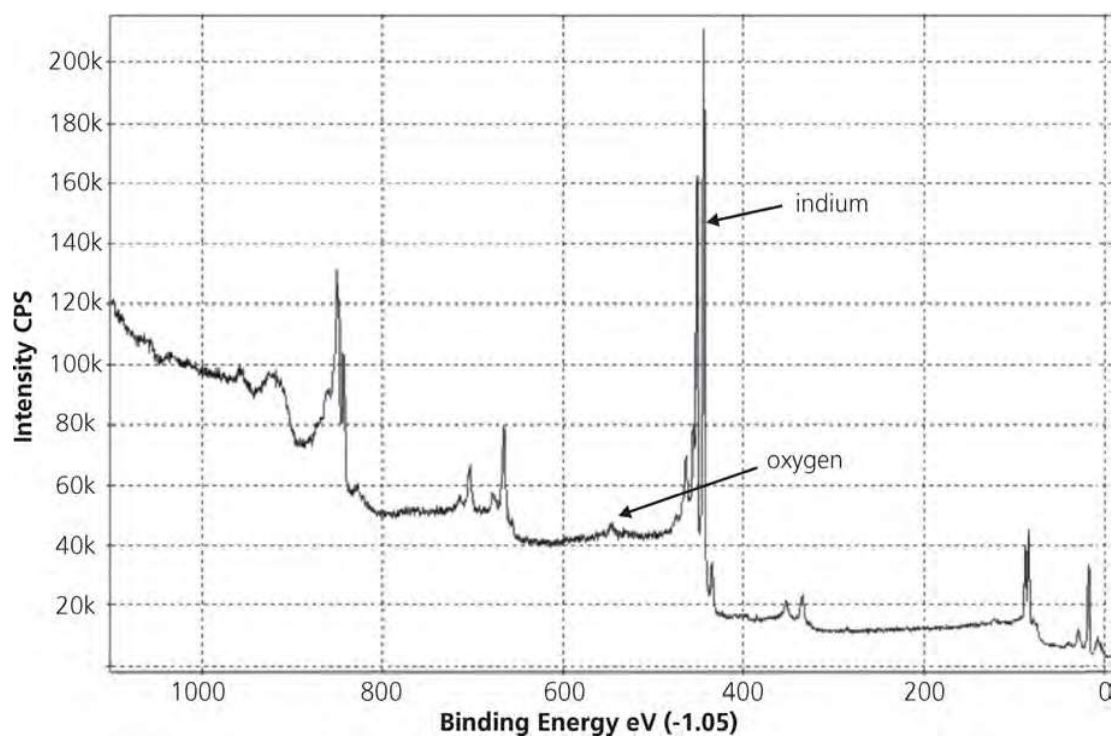


Figure 4-7: Spectrum measured by XPS of 3 hours old sample after sputtering approximately 2 nm of the surface. Oxygen peak nearly disappeared.

After identifying and fitting the peaks of the possible molecules, the concentration results are given by the program. The fittings of the molecules have a certain error margin, which is evident upon closer examination of the peaks. The indium peak (Figure 4-8) consists of three peaks: indium, indium oxide, and indium hydroxide peak. The sum of these peaks is the grey peak, which closely fits the measured data.

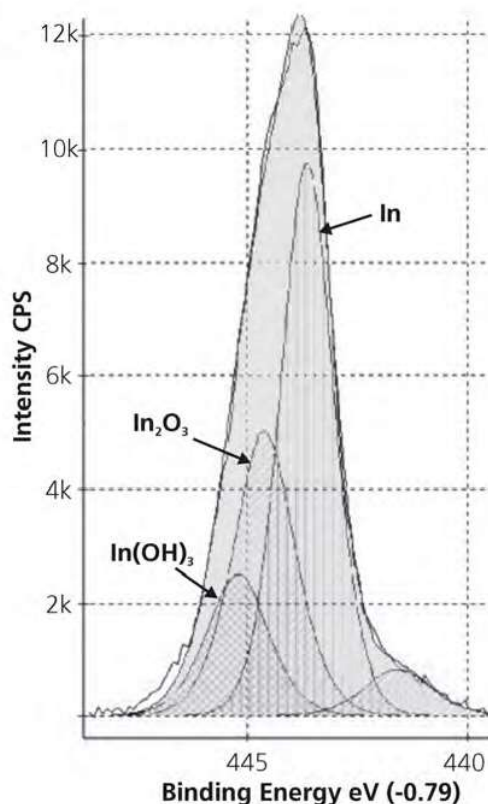


Figure 4-8: Indium XPS-peaks of the 3 h old sample before sputtering

The oxide film is very thin, only several atoms thick, because it is completely removed after a short sputtering time. In Figure 4-6 the oxygen peak is very obvious before sputtering and after removing approximately 2 nm by sputtering, the oxygen peak nearly disappeared (see Figure 4-7). The analyses of the peaks shows, that after sputtering only indium and carbon are still available (see Table 4-2).

This sample contains carbon contaminants that are formed due to the alcohol used during transportation to prevent further oxidation. The used solder metal is 99.99% pure indium, but this figure is only relative to other metals in the compound, therefore there could be carbon present in the metal, which will also evaporate.

Similar investigations were carried out by Adolphi and Blassek. A 20% or higher carbon concentration was observed in samples, which came in contact with flux or dissolver. The thickness of the oxide layers are 3 nm for evaporated indium layers and 10 nm for bulk material. The oxide films arise immediately, independent of pre-treatment, and 70% of the indium is oxidised [1].

Peak name		Concentration [%]	
		before sputtering	after sputtering (approximate 2nm)
C1s	(C)	37,2	10,0
C1s	(CO)	1,9	1,4
In3d5/2	(In)	16,1	88,6
In3d5/2	(In ₂ O ₃)	9,8	0
In3d5/2	(In(OH) ₃)	4,9	0
O1s	(In ₂ O ₃)	12,9	0
O1s	(In(OH) ₃)	13,3	0
O1s	(crystal water)	3,7	0
O1s	(CO)	0,3	0

Table 4-2: Concentrations of the oxide film and other contamination before and after sputtering of the 3 hour old sample. The oxide is removed after 1 sputter cycle.

Peak name		3h old conc. %	> 9 month old conc. %
C1s	(C)	39,2	34,0
C1s	(CO)	1,9	0,0
In3d5/2	(In)	16,1	13,9
In3d5/2	(In ₂ O ₃)	9,8	13,3
In3d5/2	(In(OH) ₃)	4,9	5,1
O1s	(In ₂ O ₃)	12,9	16,0
O1s	(In(OH) ₃)	13,3	10,9
O1s	(crystal water)	0,7	6,7
O1s	(CO)	0,3	0,0

Table 4-3: Comparison of 3 hour and 9 month old probe before sputtering: The concentrations of In₂O₃ and In(OH)₃ are nearly the same, only the crystal water concentration rises significant.

The oxide layers of In₂O₃ and In(OH)₃ are created very quickly (within minutes) and then increase in thickness very slowly. The 3 hour sample was exposed to air for only a few minutes during handling, followed by 3 hours in n-pentane, producing an oxide film about 1.0 nm thick. After 9 months, the indium layer is about 1.5 nm in thickness, which is only 0.5 nm thicker than before (see Table 4-3).

Only the crystal water rises significantly over time. A test with indium evaporated heat sinks, one set stored in a dry chamber and the other in humid conditions, was performed. No differences between devices with a high or low amount of crystal water could be found. The solder was reduced by the wet chemical reduction method and the devices were aged for several hundred hours.

In order to avoid the growing of the oxide, the layer has to be protected after evaporation without coming in contact with oxygen.

A way to protect the indium is to use a gold protective layer. The evaporation of indium is carried out in a vacuum chamber with a vacuum of about 10⁻⁵ to 10⁻⁶ mbar so that the indium does not oxidise. After the indium deposition, a protective layer of a gold is vaporised on top of it in the same vacuum cycle. The gold diffuses immediately with the indium and creates the intermetallic phase AuIn₂. The AuIn₂ layer also protects the indium solder against oxidation [45],[46].

The vaporised layers are shown in Figure 4-9. During the soldering process the liquid indium diffuses through the AuIn_2 protective layer to the gold contact layer of the laser bar. During this process a stable connection is established.

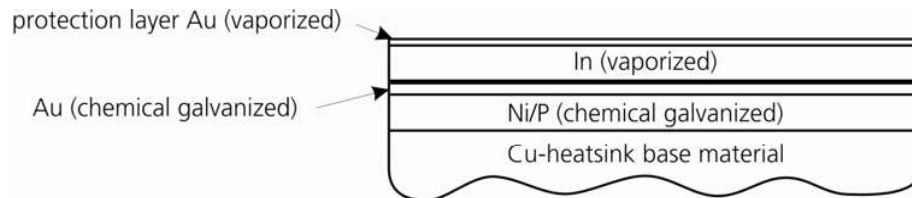


Figure 4-9: Layer structure of the plated heat sink with indium solder before melting

The thickness of the AuIn_2 film is less than 10 nm after the evaporated gold flash. Taking a closer look using a Scanning-Electron-Microscope (SEM), it can be seen that the whole surface is covered with a very thin AuIn_2 layer. No holes or in homogeneities can be found.

In Figure 4-10, a soldered laser bar, prepared according to the process explained above, is shown. The laser bar is mounted with a small overhang on the top of the heat sink. The image shows the overhang of the contact surface of the laser bar from the p-side. It can be seen that the solder wets the gold contact layer of the laser bar and forms a meniscus. This meniscus is the result of the surface tension between the solder and the golden contact surface. The meniscus is a sign of good wetting behaviour, which means that the surfaces are nearly free of oxidation. The temperature cycles do not have to be elongated. Also, no voids could be found using a scanning acoustic microscope (SAM).

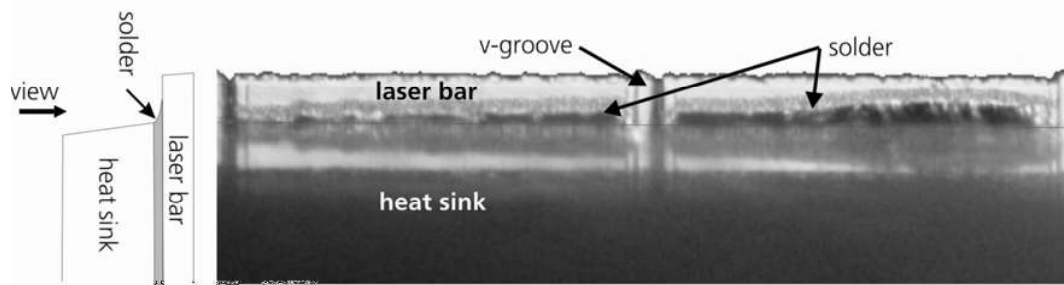


Figure 4-10: View on p-side (overhang) of a mounted laser bar. The wetting of the solder can clearly be seen.

If the gold protective layer is too thick, the metallurgical compound of the solder layer changes. The gold diffuses too deep into the solder layer and changes the properties. The dependence of the solder metallurgy, regarding the stress, is investigated in Chapter 5.3.

4.2.2. Solder Voids Experiment

In order to examine the influence of solder voids, several diode lasers have been prepared in a special way. Small pieces of foil were glued on to the heat sink before solder deposition. By removing the foil after solder deposition, parts of the laser bar contact area were not coated with solder. Laser bars were then packaged onto these prepared heat sinks.

First, electro-optical characterisations were performed on these bars. Due to the expected thermal problems of the diode laser with solder voids, a reduced current was used so that the diode laser would survive the electro-optical characterisation. The optical output power, slope efficiency, and conversion efficiency are nearly the same for the diode laser with and without solder voids. The power loss is roughly 35 W. Therefore the electro-optical data gives no evidence of the solder voids. However a closer look at the emission spectrum (Figure 4-11) shows an unusual spectrum shape with side-peaks for the diode laser with voids. In this case it seems that some emitters operate at a higher wavelength, which is the result of a higher operation temperature.

Strong strain distributions can also lead to an inhomogeneous emission spectrum, so that side peaks cannot be clearly allocated to solder voids and with it the higher temperature.

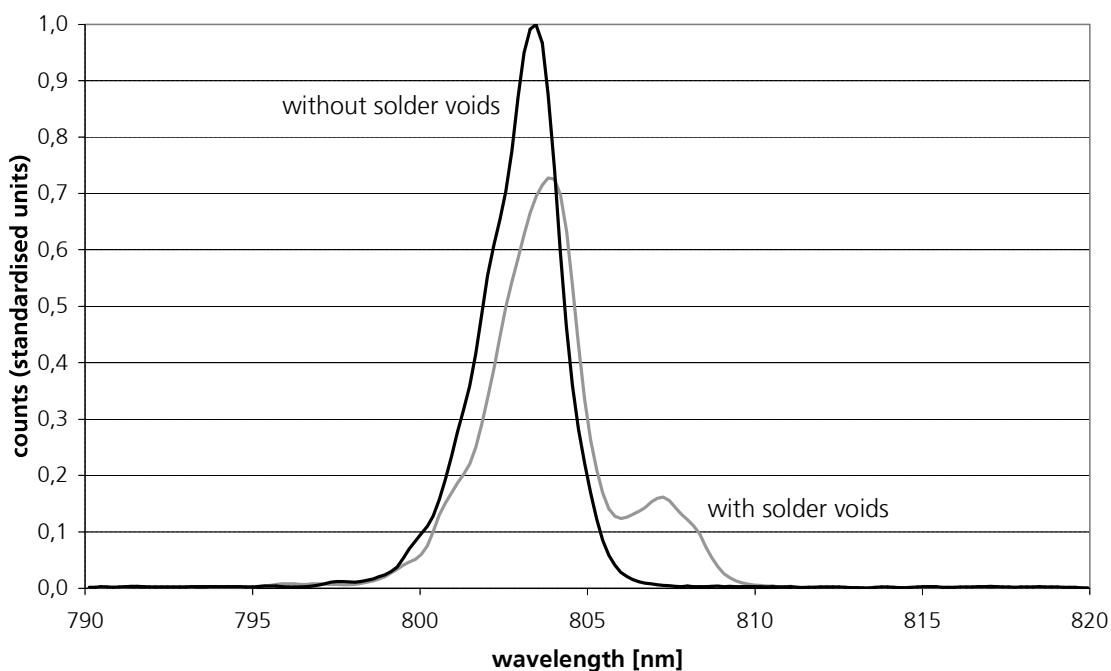


Figure 4-11: Emission spectra of a diode laser with and without solder voids. The diode laser with solder voids shows a side-peak towards higher wavelength.

By looking at the emission spectra of each emitter separately, the warmer emitters could be localised (see Figure 4-13). The spectra are measured with a fibre-scanning-spectrometer (Chapter 3.2). After determining the central wavelength of each emitter, the wavelength is converted into the emitter temperature. For conversion, the theoretical value of 0.3 nm/K is used. After all measurements, the laser bar is removed from the heat sink by using a shear test machine in order to analyse the shape of the solder voids. The footprint of the laser bar is shown in Figure 4-12.



Figure 4-12: Laser bar footprint on heat sink with prepared solder voids by using a foil. Darker areas represent a connection between solder and laser bar and brighter areas indicate no connection between laser bar and solder.

The footprint is used to determine the ratio of the contact area to that of the emitters. By comparing the relative contact area with the emitting wavelength, a dependency can be determined. A smaller contact area leads to higher operating temperature.

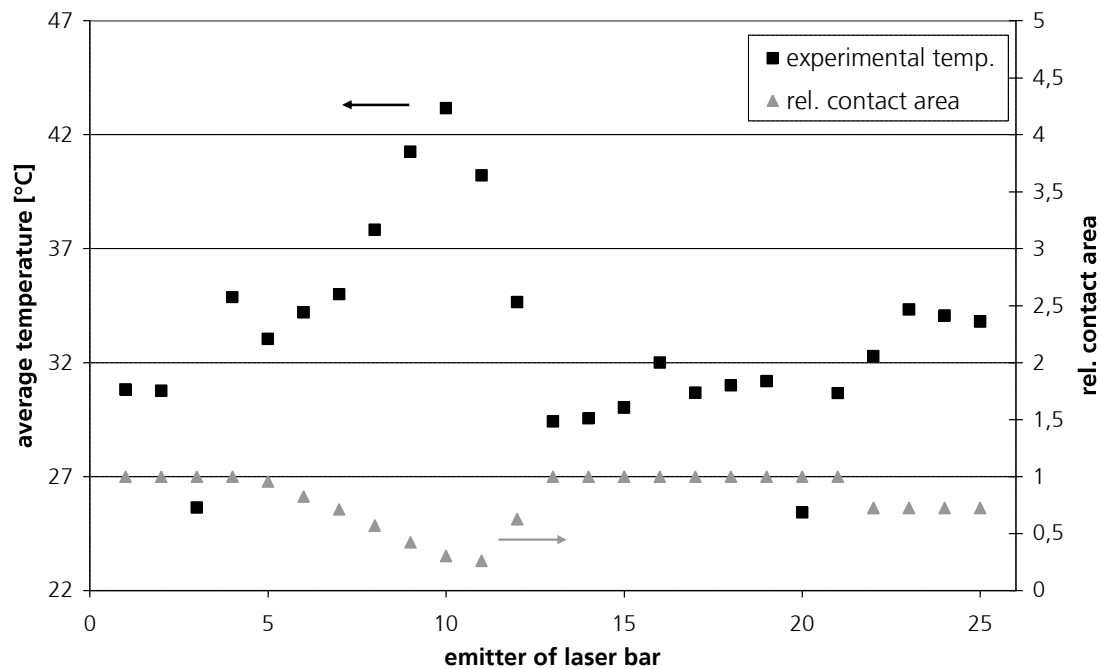


Figure 4-13: Average temperature of the emitters and relative contact area between emitter and heat sink versus the emitters of the laser bar. A smaller contact area leads to a higher operating temperature.

4.2.3. Simulation of Solder Voids

FEM-simulations are a tool to estimate and predict the thermal influence of solder voids. The simulation is compared with experimental results in order to reduce the level of detail the simulation has to be performed to provide realistic information.

A very simple model is to assume a fixed power loss per emitter. This results in homogeneous heat generation of the emitters and is used as a presetting for the simple-model simulation. The simulation with an overall dissipation power of 30 W and solder voids is shown in the upper simulation picture in Figure 4-14. The lower simulation picture takes into account that the power dissipation is inhomogeneous across the bar due to the fact that the contact area between heat sink and bar varies. With the varying contact areas the current distribution and with it the power losses are inhomogeneous. For the "current-dependent" simulation, the current through an emitter depends on the contact area, therefore heat generation is lower for emitters with decreased contact area.

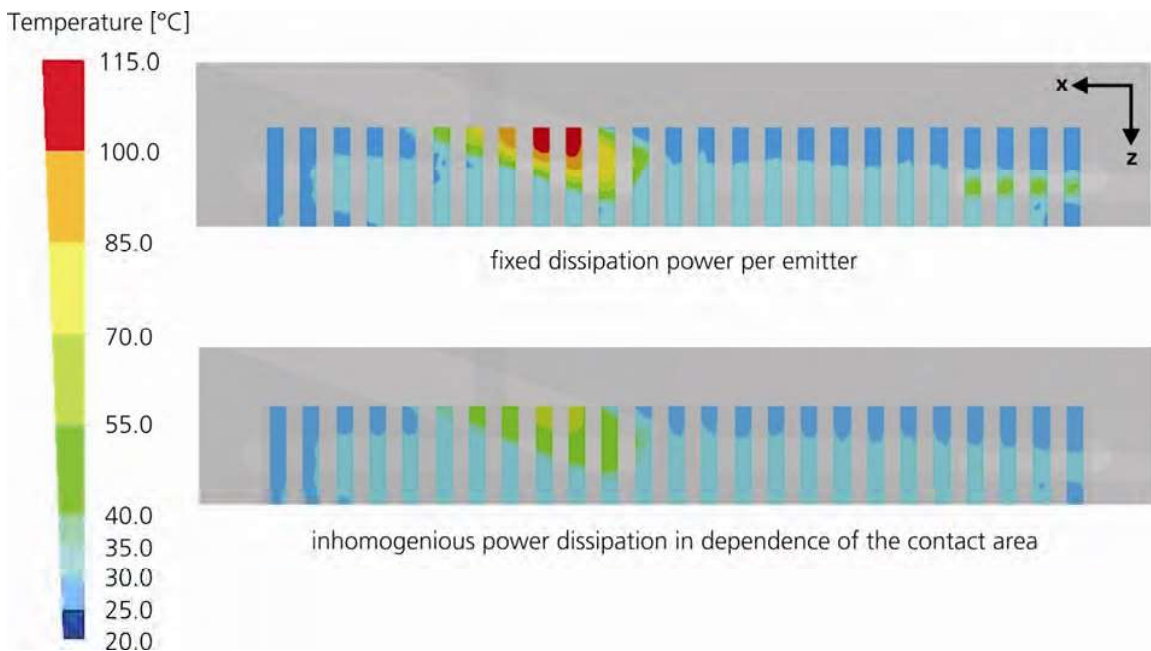


Figure 4-14: Thermal simulation of the emitters of a 50% fill factor bar and a solder layer including voids with a dissipation power of 30 W. The upper simulation is with a fixed power loss per emitter and the lower simulation takes the varying contact area into account.

In both simulations, the solder voids and the geometrical model are the same, but the boundary conditions have been changed. The maximum simulated temperature in the active region is 59 °C for the "current-dependent" dissipation power instead of 115 °C as is the case for "fixed power" dissipation power. This large difference between the two conditions makes the simpler "fixed current" model less desirable than the more detailed "current-dependent" simulation, because this method is more realistic.

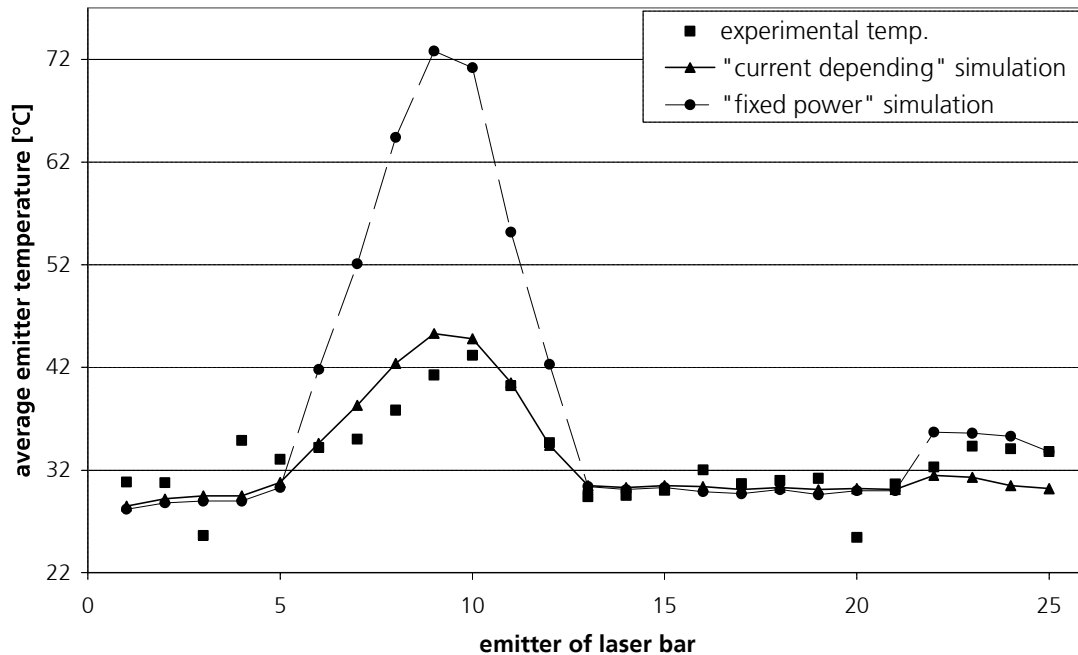


Figure 4-15: Comparison of temperature distribution of "current-dependent" simulation (line), "fixed power" simulation (dotted line), and experiment (dots). The average temperature is plotted versus the emitters of the laser bar.

The comparison between simulation and measurements of a laser bar with known solder voids shows that the simulation, which takes the "current-dependent" power dissipation into account, nearly matches the measured temperature distribution. In this case, the central wavelength of each emitter is compared with the simulated average temperature and not with the simulated maximum temperature of each emitter (Figure 4-15).

For thermal simulations, where an inhomogeneous distribution is expected, the "current-dependent" distribution has to be taken into account for the simulation. The "fixed power" simulation provides results far away from reality.

After verifying the simulation model, the model can be used to estimate the influence of solder voids.

In the following, a diode laser bar with and without solder voids with an overall power loss of 30 W and 60 W are compared (Figure 4-16). The operational temperature of a completely soldered diode laser with a power loss of 60 W is around 45 °C. Solder voids increase the operating temperature of the affected emitters up to 100 °C. It can also lead to catastrophic damage of the laser bar if the void and thereby the temperature is too large.

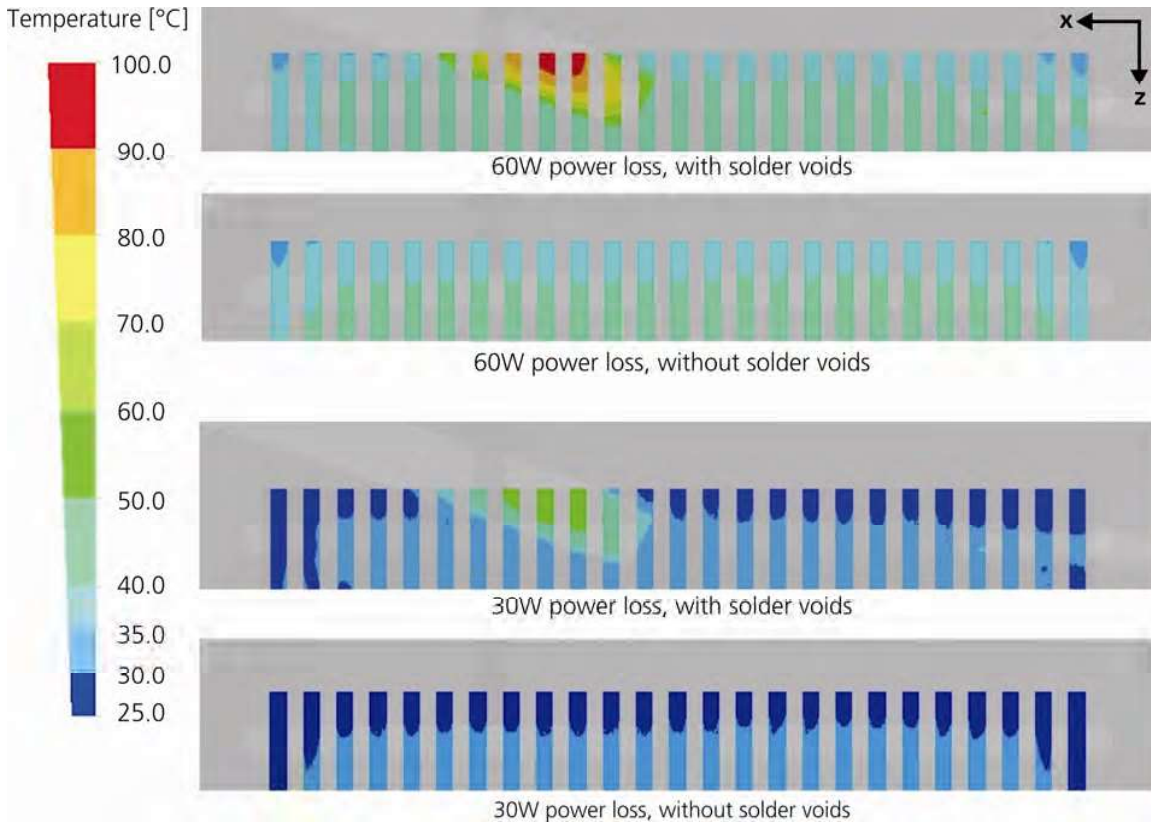


Figure 4-16: Thermal simulation of the emitters of a 50% fill factor bar with a power loss of 30 W and 60 W. The simulation shows for the two different power losses a diode laser with and without solder voids.

Solder voids cannot be inspected visibly without destroying the diode laser. Also, the voids cannot be removed after they appear. As seen, voids lead to side peaks or unusual wavelength distribution of the laser bar. Devices with an inhomogeneous wavelength spectrum likely have an insufficient contact between laser bar and heat sink. Therefore these are candidates for early failure or a short lifetime, due to higher local temperatures of the affected emitters.

4.3. Influence of Solder Layer Thickness

The thermal conductivity of the solder is lower than that of the heat sink material. For example, the thermal conductivity of the common solders such as indium (83 W/mK) and gold-tin (58 W/mK) is 5 to 6 times smaller than the thermal conductivity of copper (394 W/mK). In the following, the influence of the solder thickness is evaluated. Typical thicknesses of evaporated solder layers are about 5 to 7 μm . During the packaging process, the solder layer thickness depends on the downforce. Typically, the downforce is adjusted with weights. The thickness after packaging is then around 3 μm .

4.3.1. Simulation

In order to simulate the influence of the solder thickness, a model of a packaged laser bar with a gold-nickel plated heat sink is chosen. For simulation advantages, only a middle emitter of a laser bar is simulated. This means that the model is cut between the emitters and that these faces are adiabatic. The simulated laser bar has a fill-factor of 50% with an emitter width of 200 μm .

A simplified version of a heat sink is used. Only the metal between the water channels and one emitter of the laser bar are designed for the simulation (Figure 4-17). The heat sink is plated with a 3 μm thick nickel layer. The gold layer is neglected because the thickness is normally less than 150 nm.

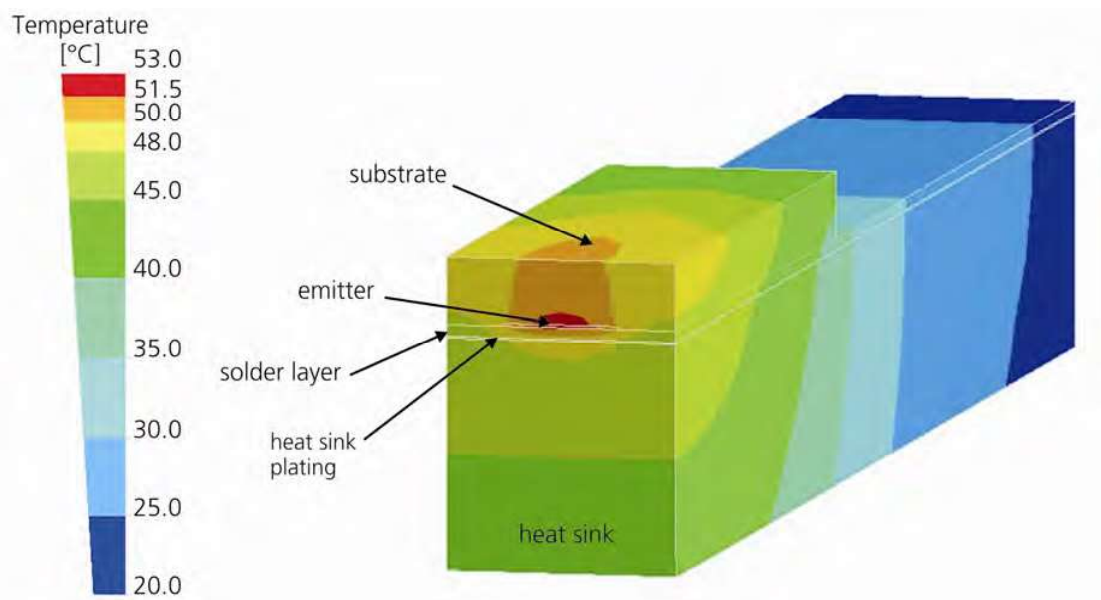


Figure 4-17: Simulated temperature distribution of a middle emitter with a solder layer thickness of 20 μm and a dissipation power of 3 W. The emitter is 200 μm wide and the pitch is 400 μm .

In order to see the influence of solder layer thickness on the operational temperature, different thicknesses are simulated. In this case solder thicknesses of 2, 5, 10, 15, 20, and 50 μm are used. The dissipation power of the emitter is 3 W. The simulation results of the various solder layer

thicknesses can be seen in Figure 4-18. The laser bar substrate is hidden so that the emitter (active region) is visible.

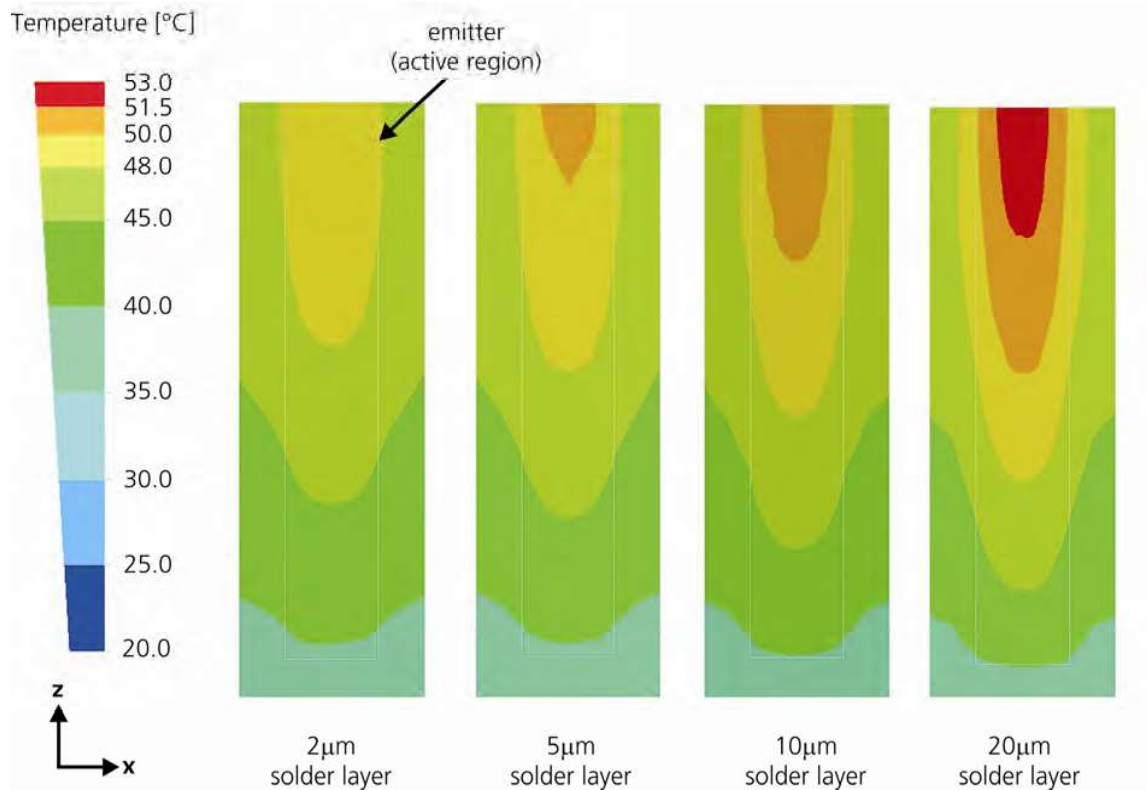


Figure 4-18: Comparison of the emitter temperature in dependence of the solder layer thickness. The laser bar substrate is hidden, so that the active region is visible. The power loss is 3 W. It is a top view and the laser light is emitting at the top of the image.

If the solder layer thickness increases from 2 to 20 μm (ten fold), the temperature rises only 2 $^{\circ}\text{C}$ (Table 4-4). This corresponds to a wavelength shift of 0.5-0.6 nm. By using a solder preform, which has a thickness of 50 μm , the temperature difference compared to a 5 μm thick solder laser is already 4.6 $^{\circ}\text{C}$. Therefore, by using an evaporated solder on heat sinks with typical thicknesses of around 5 μm , the simulation results allow for the following assumption to be made: there is no large temperature effect on the laser bar even if the thickness varies around $\pm 5 \mu\text{m}$.

power loss	solder layer thickness	max. temperature	emitter width	fill-factor
3,0 W	2 μm	50,1 $^{\circ}\text{C}$	200 μm	50%
3,0 W	5 μm	50,3 $^{\circ}\text{C}$	200 μm	50%
3,0 W	10 μm	50,9 $^{\circ}\text{C}$	200 μm	50%
3,0 W	15 μm	51,4 $^{\circ}\text{C}$	200 μm	50%
3,0 W	20 μm	52,1 $^{\circ}\text{C}$	200 μm	50%
3,0 W	50 μm	55,1 $^{\circ}\text{C}$	200 μm	50%

Table 4-4: Overview of the maximum temperature in dependency of the solder layer thickness.

4.3.2. Experiment

The simulation forecasts no significant temperature influence in relation to the solder layer thickness. Due to the fact that the solder layer is very small, the real heat transfer coefficient between the contact surfaces and also the thermal conductivity of the solder with the intermetallic compounds can vary from the values for bulk material.

In order to investigate the influence of solder layer thickness, some diode lasers with a wedge-formed solder layer were produced. The wedge-formed solder is created by placing a 10 μm thick wire as a spacer under one side of the bar. By pushing the laser bar during the soldering process, one side touches the wire and the other side the heat sink (Figure 4-19).

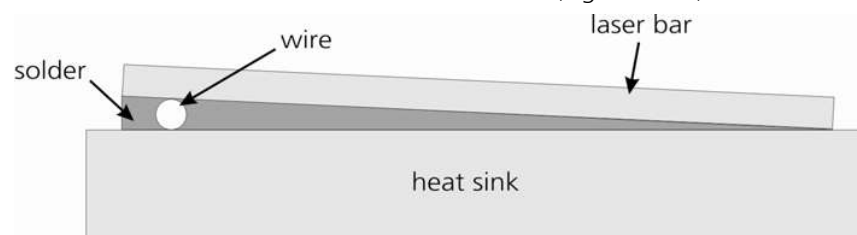


Figure 4-19: Schematic view (front view) of wedge-formed packaged diode laser. A 10 μm thick wire is used as a spacer to create a wedge-formed solder layer.

In Figure 4-20 a mounted laser bar is shown. On the left side there is a wire inside the solder layer and therefore the gap between the heat sink and laser bar is larger than on the right side where no spacer is used.

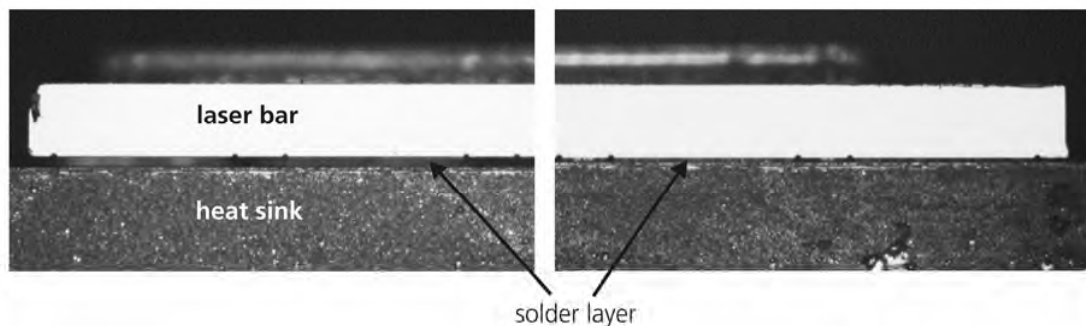


Figure 4-20: Solder layer on the left and right side of a solder wedge-formed mounted diode laser. The solder layer on the left is about 10 μm and on the right 2 μm thick (front view).

The prognosis of the simulation shows only a small thermal shift due to the thicker solder layer. The temperature difference should be below 1 K for a 2 μm and a 10 μm thick solder layer. By measuring the wavelength of each emitter and the thermal wavelength shift, the expected wavelength shift is only 0.3 nm.

The used spectrometer has a resolution of 0.25 nm, so that the expected wavelength shift due to the different solder heights is in the range of the resolution.

The measured wavelength of each emitter is shown in Figure 4-21. The steel wire is on the left. It creates a higher temperature in the region due to the lower thermal conductivity and inadequate thermal contact between the wire and solder. The influence of the different solder thicknesses

can be investigated beginning with emitter eight. A linear fit of the emitter wavelengths between 8 to 20 results in a wavelength slope of 0.005 to 0.020 nm per emitter. By using the theoretical wavelength shift of 0.3 nm/K, a temperature rise of 0.5 to 1.7 K is calculated between the thin and the thicker solder layers. The error range is nearly the same because the wavelength could only be measured with an accuracy of 0.25 nm. This is equivalent to a temperature error of 0.8 K.

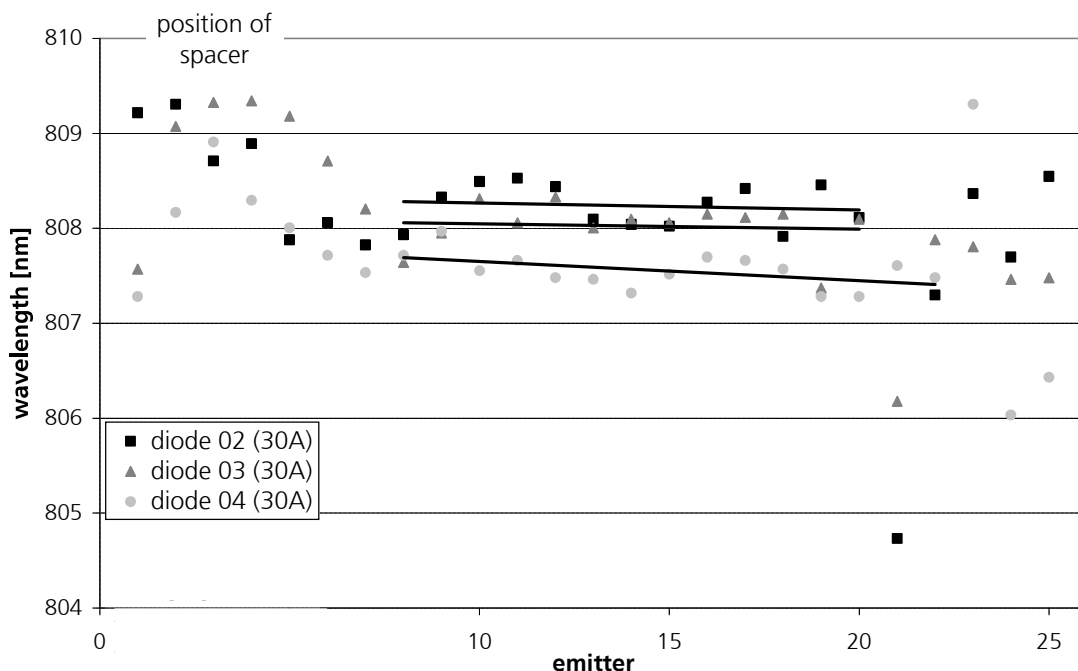


Figure 4-21: Wavelength distribution of 3 packaged diode laser with a wedge-formed solder at 30 A. The solder thickness rises from the right to the left. On the left side 10 μm wire is used as a spacer, causing the higher wavelength. Linear fits show a slight wavelength rise of each diode towards the thicker solder side.

The simulation assumes a temperature difference of 0.8 K between a 2 μm and 10 μm thick solder layer. The results of the measurement are in the same range.

The wavelength depends on the temperature, but also on the mechanical stress.

On the right side of the laser bar the wavelength jumps from one emitter to the next. A wavelength change of 3 nm would represent a temperature change of nearly 7 K. In order to determine if this is a temperature or stress effect, the thermal distribution of the facet is measured with a thermal camera. In Figure 4-22 the thermal image of the front side of the diode layer is shown.



Figure 4-22: Thermal image of diode laser (front view), dark areas are warmer than bright areas, the image is not corrected for the different emission coefficients [measurement performed at MBI].

The temperature of the laser bar is extracted by extracting the gray tones (counts), which are located on the white line ("the measurement region" in Figure 4-22). The gray tones for different driving currents are plotted versus the corresponding lateral position in Figure 4-23.

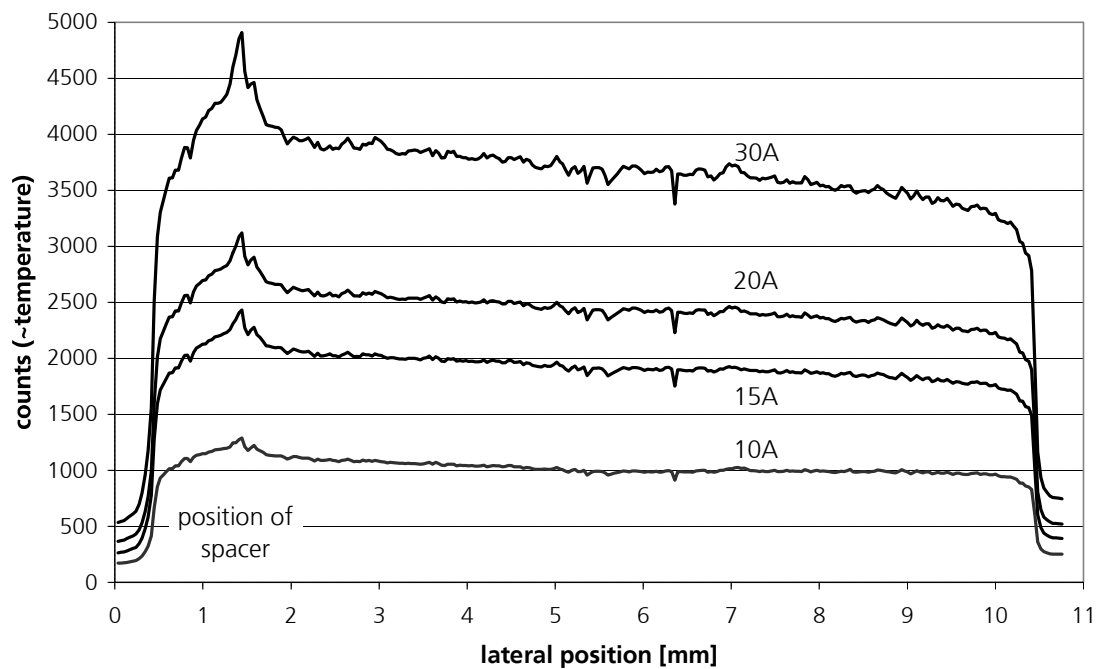


Figure 4-23: Wavelength distribution of packaged diode laser with a solder wedge form. On the left side a $10\mu\text{m}$ wire is used as a spacer, causing the higher temperature [measurement performed at MBI].

At higher currents a small slope is obvious. This means that the laser bar becomes slightly warmer with increasing solder layer thickness. The wavelength jumps in Figure 4-21 are not temperature related, because the thermal camera measures no significant temperature changes of the emitters on the right side, which should occur, if the observed wavelength jumping is temperature related.

The temperature values gathered obtained from the emitter resolved wavelength measurement and from the thermo camera, show the same behaviour. The temperature increase caused by the increased solder layer thickness is very small.

With both methods, the temperature increase at the spacer is obvious. The reason for the temperature increase is the low thermal conductivity of the spacer and poor contact with the solder because the spacer is not coated.

power loss	solder layer thickness	max. temperature		emitter width	fill-factor
		In	AuSn		
3,0 W	2 μm	50,1 °C	50,3 °C	200 μm	50%
3,0 W	5 μm	50,3 °C	50,6 °C	200 μm	50%
3,0 W	10 μm	50,9 °C	51,2 °C	200 μm	50%
3,0 W	20 μm	52,1 °C	53,2 °C	200 μm	50%

Table 4-5: Overview of the simulated maximum temperature in dependency of the solder layer thickness and solder material.

If the indium solder layer thickness varies from 2 to 10 μm , the simulated and also experimental determined temperature changes are about 0.8 °C. If gold-tin solder is used, the temperature change is in the same range. Only if the solder layer thickness increases further, will the lower thermal conductivity of gold-tin in comparison with indium have a greater effect on the maximum temperature (Table 4-5). Therefore no large effects regarding the solder choice are to be expected.

4.4. Thermal Influence on Degradation

In order to estimate the influence of the thermal load on the lifetime, two different sets of laser bars with the same optical output power but different operational temperatures have been aged. In this case, one set is packaged on actively cooled heat sinks and the other set on conductively cooled heat sinks. The cm-bars with 50% fill-factor are operated at 25 W output power. The temperature differences can be calculated by the different operating wavelengths. The wavelengths differ by 8.1nm, which represents a temperature difference of 30 K using a wavelength shift of 0.27 nm/K.

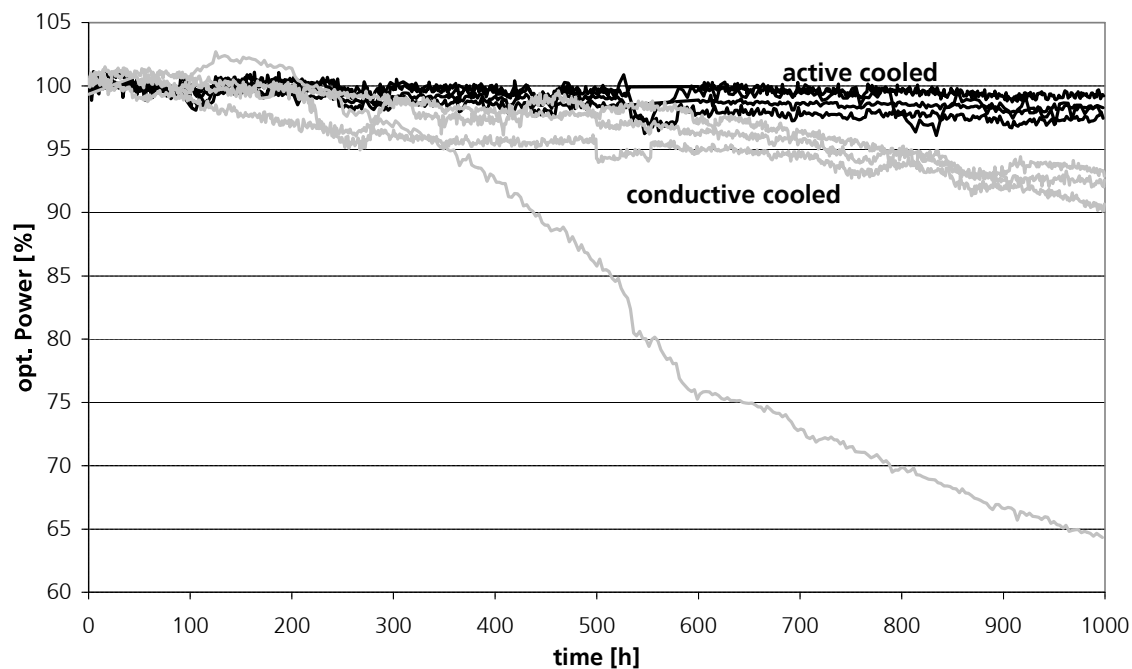


Figure 4-24: Ageing data of actively and conductively cooled packaged diode lasers, which run at the same power level, but different temperatures due to the different cooling method.

It is obvious that the actively cooled diode lasers have a longer lifetime. The average lifetime is 12323 hours. The average lifetime of a set of diode lasers with elevated temperature is 2547 hours, if the early failure is not taken into account. This means that a temperature increase of 30 K reduces the lifetime by nearly 80%.

The activation energy can then be calculated using Formula 3-6.

The calculated activation energy is 0.43 eV, which is in the range of typical values (Chapter 3.3).

5. Mechanical Influence of the Packaging

There are three sources of mechanical stress. The first one is the stress induced during packaging due to the mismatch of the thermal expansion between laser bar and heat sink or submount. The second one is the stress induced during operation due to the inhomogeneous temperature distribution caused by the power loss of the individual emitters of a laser bar. The third one is the average temperature rise during operation, which leads to a reduction of the packaging induced stress. This reduces the temperature shift from melting temperature to operation temperature instead of room temperature. The temperature rise during operation is around 25 °C, which is small compared to the temperature shift of 130 °C (indium) or 260 °C (gold-tin) during the packaging process. Therefore, this influence is not investigated further.

During packaging, the heat sink and laser bar are heated up above the melting temperature of the solder. The laser bar and heat sink connect during cooling, when the solder solidifies. Due to the different thermal expansion coefficients, the laser bar and heat sink shrink at different rates. The mismatch depends on the solidification temperature and the difference of the thermal expansion coefficient.

Due to the substructure of a laser bar, mechanical stress occurs due to the inhomogeneous heat distribution. The local elongation of the material varies due to the variation in temperature. For cooling, an efficient heat sink is needed, so that a strong heat flow with high temperature gradients is present (see Chapter 2.2).

The simulation of packaged bars provides more detailed information about the thermal and mechanical properties of the packaging. In particular, the internal stress distribution along the laser bar dependent upon the different material and soldering parameters can be indicated.

For simulation, the heat sink and laser bar geometry is transferred to a finite element software that is able to calculate temperature distributions, mechanical stress, and deformation for a given set of material parameters and boundary conditions.

5.1. Basic Principle of Mechanical Load

Simulation of a standard copper heat sink is to be carried out, in order to evaluate the stress level during the packaging process and during operation. Therefore, both simulations start with stress free components. The temperature fall during an indium process is 156 °C (solidification point) minus 20 °C (room temperature). For a gold-tin process it is 124 °C higher due to the higher solidification point. An inhomogeneous temperature distribution, identical to that during actual operation, is applied.

In the model, all joints between the different heat sink layers are treated as “hard” joints. No plastic effects or creeping of the solder or the solder material itself are taken into account. Examinations of real heat sinks show, that this is not correct in all cases. As investigations of expansion-matched heat sinks with AlN ceramics inlays show, the deviation between simulation and reality may be quite significant due to partial failure of the joints inside the heat sink. The joints and metallisation of the ceramic could not handle the occurring stress during fabrication.

These three cases are simulated using a GaAs laser bar on a copper heat sink. The power loss of the operating diode laser is 80 W with a maximum temperature of 54.5 °C.

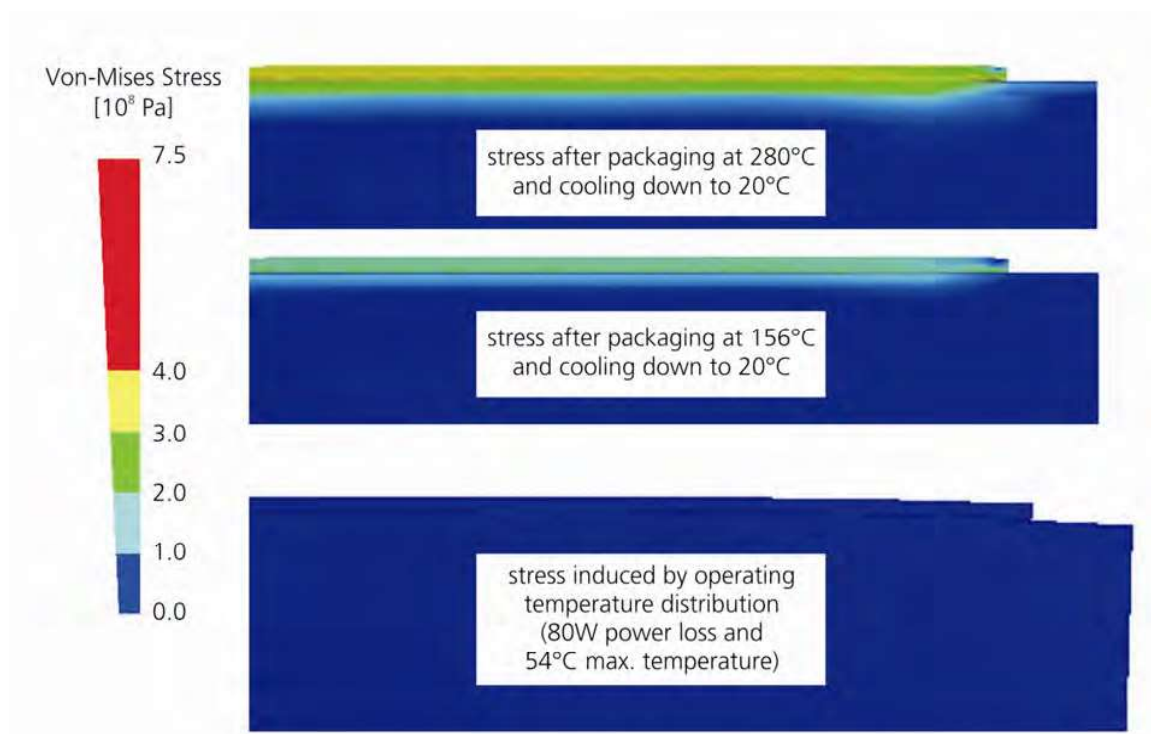


Figure 5-1: Simulation of the occurred Von-Mises stress during indium and gold-tin packaging and operating at 80 W power loss.

In Figure 5-1 the results of the stress simulation are shown. The highest stress level occurs using the gold-tin packaging. The stress caused by a temperature jump of 260 °C for gold-tin is around $7.4 \cdot 10^8$ Pa and the highest operating stress with 80 W power loss is ten times smaller and around $0.7 \cdot 10^8$ Pa. The breaking strength of GaAs is $27 \cdot 10^8$ Pa [27], which is only three times larger than the simulated packaging induced stress of the gold-tin process. The stress caused during operation is mostly located inside the emitters, because they are much warmer compared to the rest of the laser bar. The inhomogeneous temperature distribution is related to the operation of the laser bar and cannot be avoided. Only the maximum temperature can be kept low, thanks to high efficiency cooling of the diode laser bar.

The main stress occurs during the soldering process of the laser bar onto the heat sink. The cooling of copper causes the heat sink to shrink more than the laser bar. Due to this, the laser bar is compressed by the copper heat sink and the heat sink is elongated by the laser bar. This induces compressive stress inside the laser bar and tensile stress inside the heat sink (Figure 5-2).

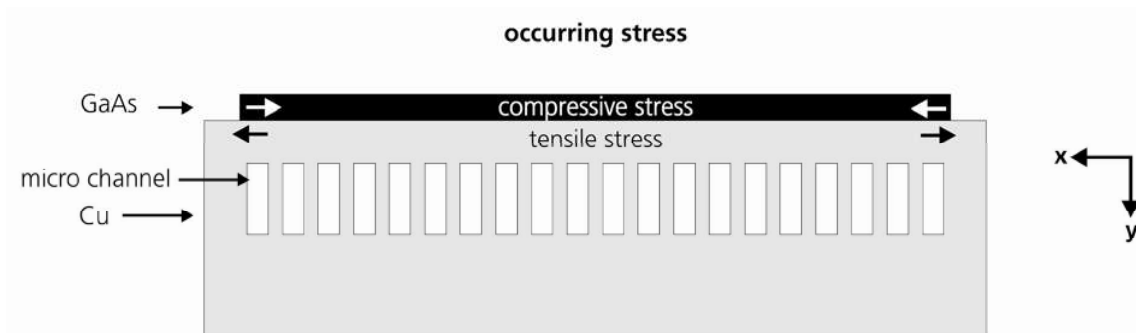


Figure 5-2: Shrinking and stress behaviour during packaging (cooling down) of a laser bar onto a copper heat sink (cross section).

In the case of copper heat sinks, indium is the most common solder, because it is soft, ductile, and can reduce the induced packaging stress of the laser bar by deformation. When using gold-tin solder expansion matched heat sinks or an expansion matched submounts are needed.

5.2. Expansion-Matched Heat Sinks

The main interest of expansion-matching is to avoid stress occurring during the packaging process. The simulation deals with the conditions during heat sink production and the packaging process.

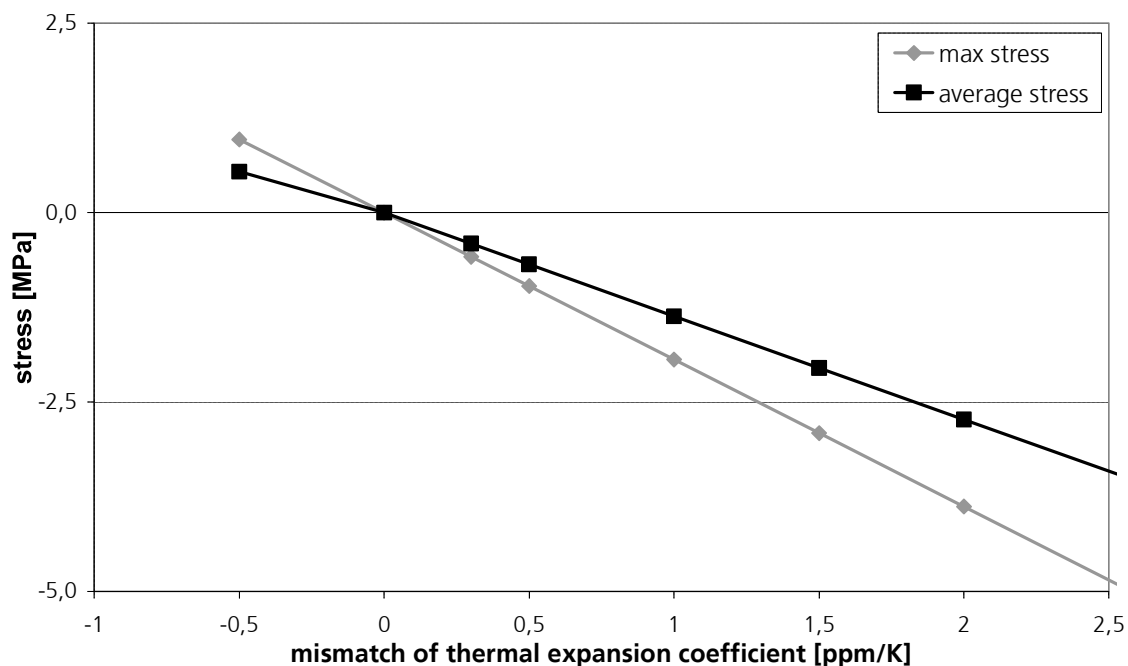


Figure 5-3: Simulated maximum and average stress in the laser bar along lateral direction dependent upon the expansion mismatch.

For these calculations, a simplification 2D simulation is used. With this, a cross section through the package, parallel to the front edge of the heat sink is simulated. In the simulation the connection between laser bar and heat sink is hard, with no ductile behaviour. The shown stress is the stress in y-direction, which represents the longest dimension of the bar and the direction in which the largest stress will occur. The stress in this direction is also the difference in the stress profile between a single emitter and laser bar.

To calculate the stress that occurs when the expansion coefficient of the heat sink varies around that of the GaAs, a bar packaged on an appropriately mismatched heat sink is simulated. GaAs has an expansion coefficient of 6.7 ppm/K. In this case only the stress in lateral direction (x), which is the greatest part due to the longest dimension of the laser bar, is simulated. The resulting stress in the y-direction is about 2 MPa at a 1 ppm/K expansion mismatch. If a copper heat sink is used, the stress in lateral direction is about 20 MPa, which is 100 times smaller than the breaking strength of GaAs. The mechanical stress induced by the packaging process will be reduced by more than a factor of 10, if the expansion coefficient mismatch is below 1 ppm and the relaxation behaviour of the solder is not taken into account. The dependence of the residual stress in the bar on the expansion coefficient mismatch is shown in Figure 5-3.

Materials with a lower thermal expansion coefficient normally have a lower thermal conductivity. If the mechanical stress is lowered due to less expansion of the material, the thermal load increases. Nowadays, novel expansion matching materials are available such as diamond composites, but these are expensive and difficult to machine [47].

The two expansion matched heat sinks ("top-layer" and "sandwich" heat sink) are described in Chapter 2.2.3. In the following, the development and detailed investigation of these two heat sinks are shown.

5.2.1. Design and Simulation

• "Top-Layer" Heat Sink

The "top-layer" heat sink uses an expansion matched material as the top layer on a water cooled micro channel heat sink. Available materials are composite materials of copper with tungsten and molybdenum. A schematic view of the "top-layer" heat sink design is shown in Figure 2-9.

Typical materials are tungsten-copper and molybdenum-copper, which are commercially available as submounts. An overview of the most common materials is shown in Table 5-1.

Material	Thermal conductivity [W/mK]	Thermal expansion coefficient [ppm/K]	Young's Modulus [Gpa]	Electrical characteristic	Supplier
Copper	397	16,6	130	conductor	
BeO	260	6,3	340	insulator	
CuW(10/90)	180	6,5		conductor	Sumitomo
CuW(20/80)	200	8,3		conductor	Sumitomo
CuW(10/90)	180	5,6	306	conductor	BrushWellman
CuW(15/85)	200	7,1	275	conductor	BrushWellman
CuW(10/90)	190	6,4	330	conductor	Polese
CuMo(15/85)	150	7,0	274	conductor	Polese

Table 5-1: Available expansion matched heat sink materials for GaAs (around 6.5 ppm/K) [22],[66],[86].

The top-layer of the heat sink has to be thick enough, so that the CTE of the mounting surface is not influenced by the rest of the heat sink. It also should be not too thick, because then the thermal resistance rises too much. This is due to the fact that the thermal conductivity of expansion matched material is half of that of copper.

The tungsten-copper (10/90) material from the supplier Polese has been chosen due to the fitting expansion coefficient of 6.4 and the high thermal conductivity of 190 W/mK. The material is hard enough so that a 0.4 mm thick top-layer is sufficient to withstand the thermal expansion of the copper body, so that the coefficient of the mounting surface is still fitting.

The following pictures (Figure 5-4) show the intensity of the stress of a packaged diode laser. The top picture is that of a diode laser bar packaged on a standard copper heat sink. The bottom picture is that of an expansion-matched heat sink with a copper body and a top layer made of tungsten/copper.

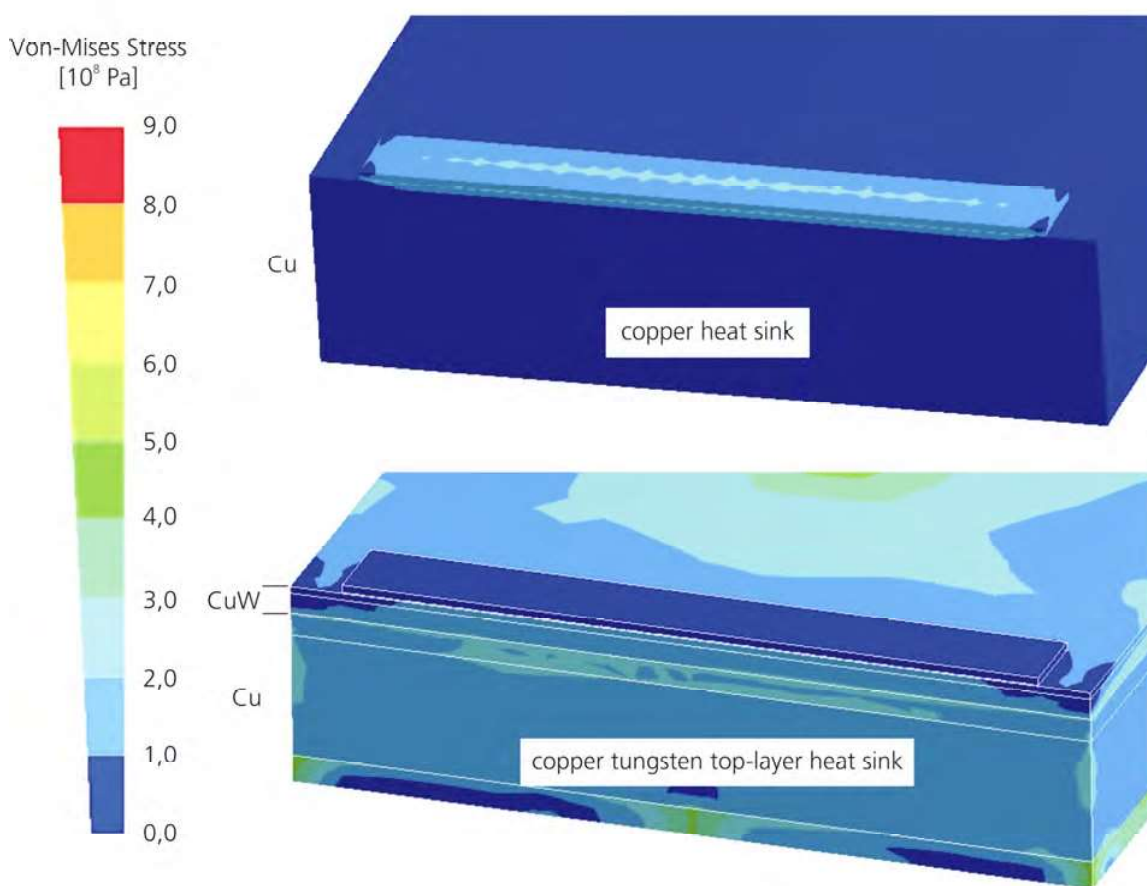


Figure 5-4: Comparison of the packaging induced stress intensity between a copper heat sink package and the "top-layer" heat sink package. No thermal load is present.

After joining the laser bar onto the copper heat sink, the expansion mismatch generates tensile stress in the heat sink because the laser bar with a smaller expansion coefficient reduces the contraction of the copper. Inversely the laser bar is compressed by the copper heat sink. If a top

layer of tungsten/copper were used instead, the bar is not stressed by the soldering process. High stress then exists between the tungsten/copper and the copper sheets in the heat sink. The mechanical stress is moved from the laser bar into the heat sink.

- **"Sandwich" Heat Sink**

The "sandwich" heat sink uses a layer of a low CTE material, which influences the CTE of the copper top layer. To get the right CTE on the mounting surface, the thickness of the top copper layer and that of the low CTE material layer has to be exactly defined. The low CTE material layer must be thick enough to have the strength to influence the top layer. Also, the inner structure of the heat sink should have no effect onto the top layer. But if the low CTE layer is too thick, the thermal resistance increases due to the fact that, the low CTE materials have a lower thermal conductivity than copper. Several simulations are done to find a suitable solution for an expansion matched "sandwich" heat sink. A schematic view of the "sandwich" heat sink design is shown in Figure 2-10.

When simulating the thermo-mechanical stress in a packaged heat sink, the different production steps of the packaging need to be taken into account for the simulation.

The stress and the thermal expansion of the heat sink itself, resulting from the heat sink production process, are simulated. The different layers of the heat sink, made from different materials to achieve expansion matching, are joined at a specified temperature, which is between 600 °C and 1000 °C, depending on the process. During the process of cooling down, stress is generated between layers of different materials due to their different thermal expansion coefficients. This internal stress is a prerequisite for obtaining expansion matching. It leads to reduced expansion of the material with a higher thermal expansion. For the heat sinks considered, the material with the higher expansion coefficient is the base material of the heat sinks, copper. The low-expansion material added to obtain expansion-matching is molybdenum (Mo).

Therefore, the first simulation step results in the calculation of the effective expansion coefficient of the "sandwich" heat sink dependent upon the low expansion material.

The thermal expansion coefficient cannot be obtained directly from the simulation. It is derived from the temperature difference and the correlated heat sink expansion. For stress-free packaging, only the effective expansion coefficient of the heat sink surface in the mounting area, which is an approx. 3 mm deep region at the front edge of the top side, is relevant. The depth of the mounting area is given by the size of the cooled surface, which is given by the length of the micro-channel structure. Since the expansion may be inhomogeneous across this region, the expansion coefficient along the front edge and 2 mm behind the front-edge is calculated.

In order to choose the right material, the CTE of the mounting surface of a heat sink with a 0.1 mm thick top layer and a 0.3 mm thick low CTE material for various low CTE materials are simulated and summarised in Figure 5-5. The simulation shows no major differences in the mechanical behaviour between INVAR, molybdenum, tungsten, and aluminium nitride. For each set the result of the CTE at the front edge and 2 mm behind are shown. Typically the CTE at the front edge is higher, because more solid copper (front side instead of micro channels) is underneath the low CTE material, which influences the CTE at the mounting area.

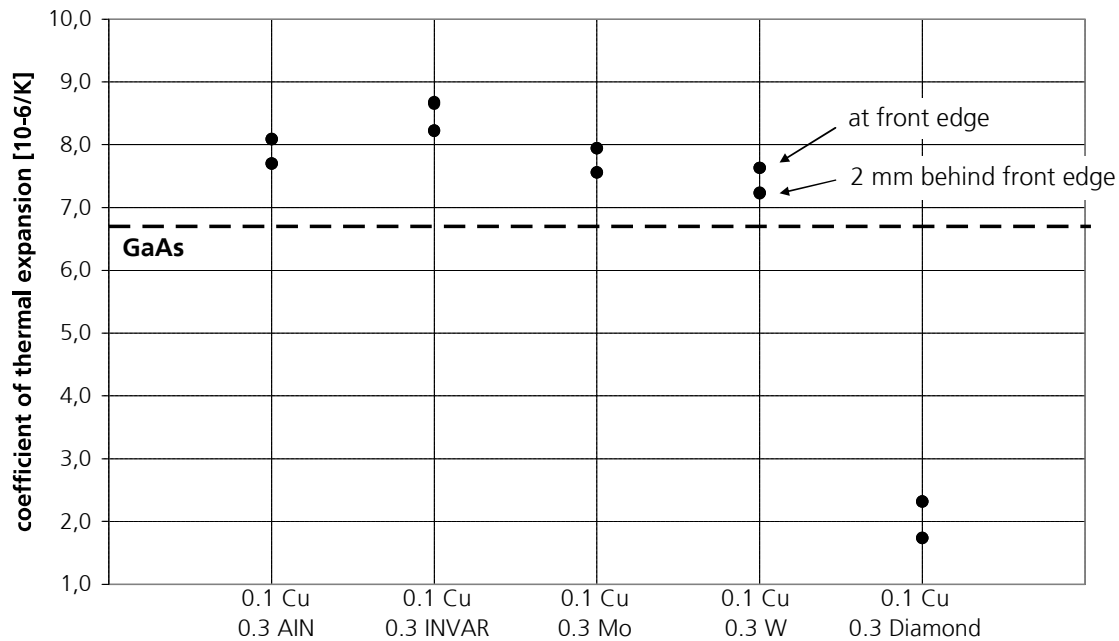


Figure 5-5: Simulated CTE of the "sandwich" heat sink with different low CTE materials. The top layer is always 0.1mm copper and the thickness of the low CTE layer is 0.3 mm. The CTE is calculated at the front edge of the mounting area and 2 mm behind it.

INVAR has a very low thermal conductivity below 20 W/mK and aluminium nitride is an electrical isolator, which can cause problems by using the heat sink as an electrical contact. Tungsten has a bit higher thermal conductivity but is also more expensive and has a slightly lower CTE than molybdenum. By connecting the low CTE material with copper, high stress occurs in the joint of the two materials due to the CTE mismatch. Molybdenum is a bit softer and has a slightly higher CTE, so that the stress in the joint will be lower. For availability reasons molybdenum is chosen for the "sandwich" heat sink. The material properties of the low CTE materials are shown in Table 5-2.

	CTE [ppm/K]	Thermal conductivity [W/m·K]	Elastic Modulus [GPa]	Price [normalized]
INVAR (Fe64/Ni36)	1.7-2.0	13		0.8
Molybdenum	4.9-5.1	138-142	324-347	1.0
Tungsten	4.6	167-173	360-411	1.4
Aluminum Nitride	4.4	175-190		1.8

Table 5-2: Material properties of low CTE material [19],[28]

In order to define the top layer thickness the CTE of copper, top layers with varying thickness on a 0.3 mm thick molybdenum layer are simulated. In Figure 5-6, the CTE dependent upon the copper layer thickness is shown. A 0.1 mm thick layer is the thinnest, which can be easily

fabricated with normal tolerances. For smaller thicknesses, the tolerances have to be smaller, which will increase the fabrication costs exponentially.

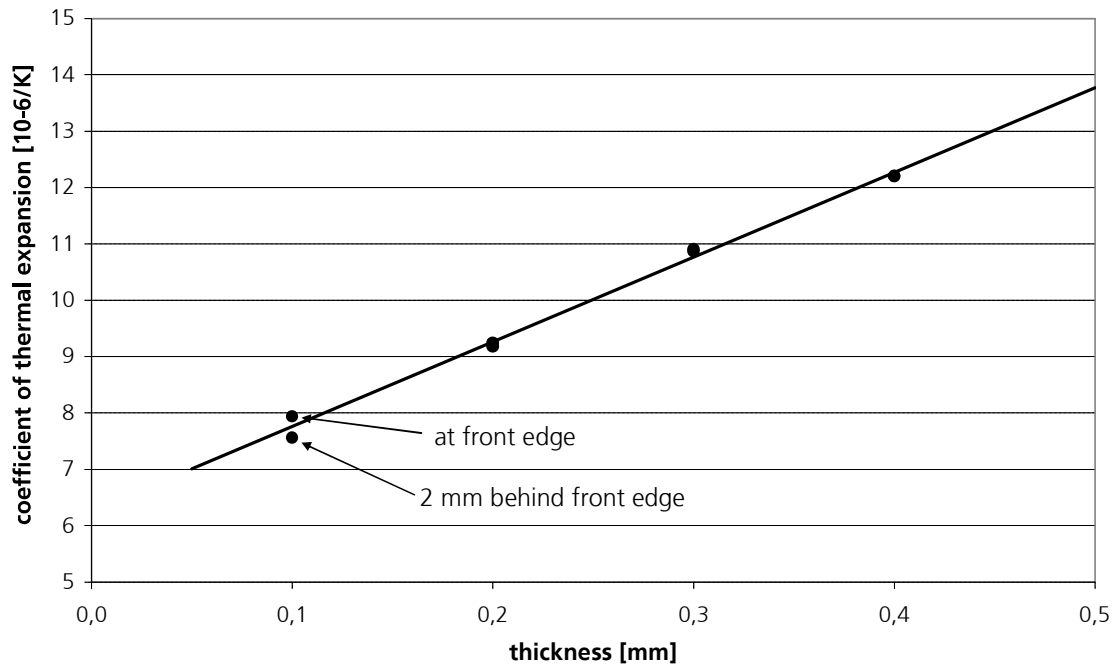


Figure 5-6: Simulated CTE of the packaging surface with copper layers of varying thickness on a 0.3 mm thick molybdenum layer. The CTE is calculated at the front edge of the mounting area and 2 mm behind it.

The best results for thermal expansion matching would be below a 0.1 mm thick top copper layer. Due to the fact, that fabrications of such thin layers are difficult, a 0.1 mm copper top layer with a 0.3 mm molybdenum layer is chosen. The values for the thermal expansion coefficients are slightly above that of GaAs. In reality the fabrication tolerances of the expansion coefficient will vary a bit from heat sink to heat sink. Also, compressive strain is better for the laser bar than tensile strain. Therefore, an increased coefficient is better.

• Simulation results

The simulation shows that the maximum stress intensity in the laser bar, created by packaging, can be reduced by more than a factor of two if the expansion matched heat sinks are used. The simulated maximum stress intensity inside the laser bar mounted onto a copper heat sink is around $3.9 \cdot 10^8$ Pa and for the "sandwich" and "top-layer" heat sink only $1.5 \cdot 10^8$ Pa and $1.4 \cdot 10^8$ Pa. The stress distribution is shown in Figure 5-7. The average stress of a copper mounted bar is around $2 \cdot 10^8$ Pa and $0.5 \cdot 10^8$ Pa for the bars packaged onto an expansion matched heat sink. The stress is decreased by a factor of four.

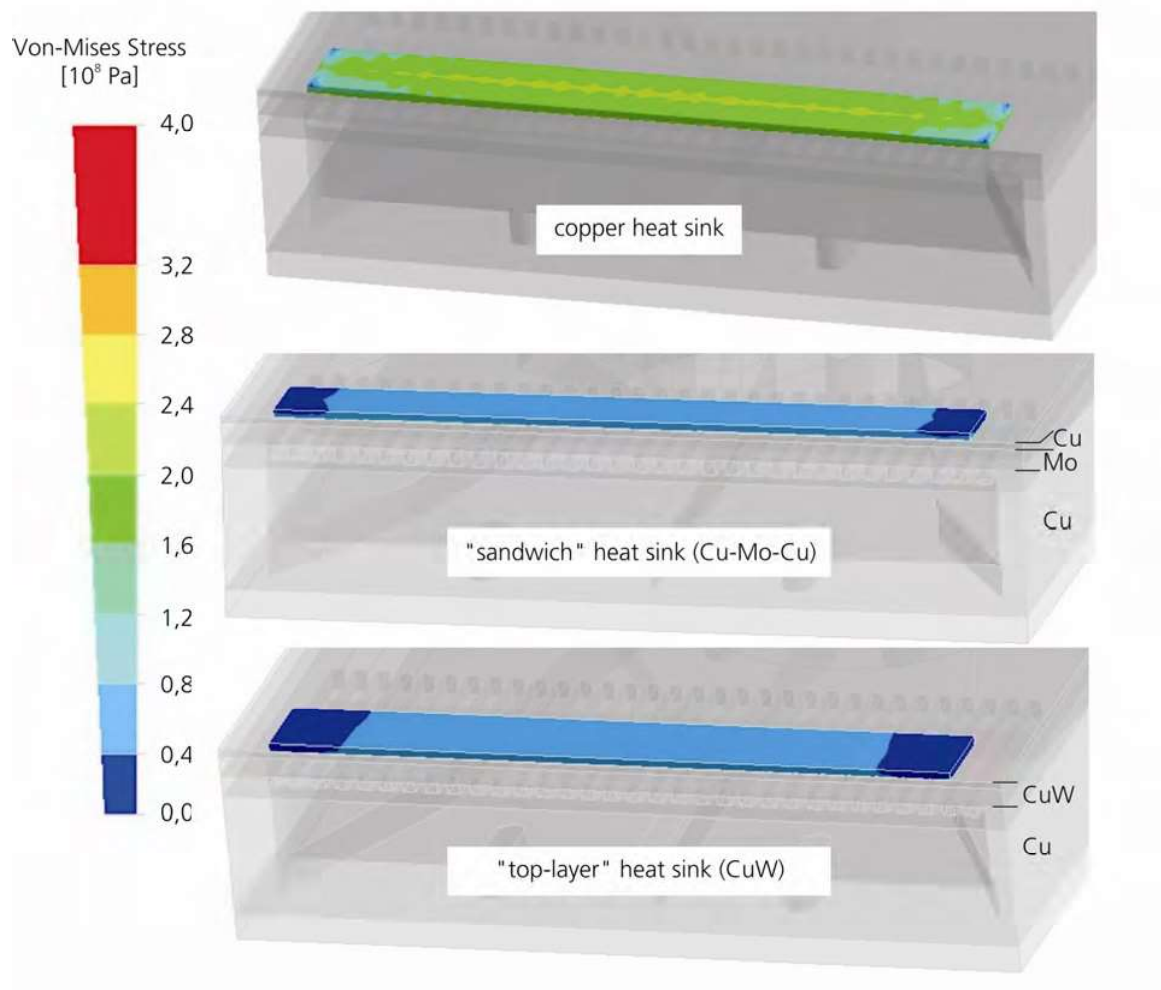


Figure 5-7: Simulated stress intensity of a laser bar for packaging on the copper, "sandwich", and "top-layer" heat sinks. The stress is the packaging stress caused by cooling down from 156°C to 20°C.

5.2.2. Fabrication and Properties

Prototypes of "top-layer" (Figure 5-8) and "sandwich" heat sinks (Figure 5-9) are fabricated using a silver solder diffusion process. The different parts of the heat sink are plated with a thin silver solder layer. A pressing force is applied with a clamping holder, the entire set-up is then all put in a vacuum oven, in order to solder the parts together. [62]

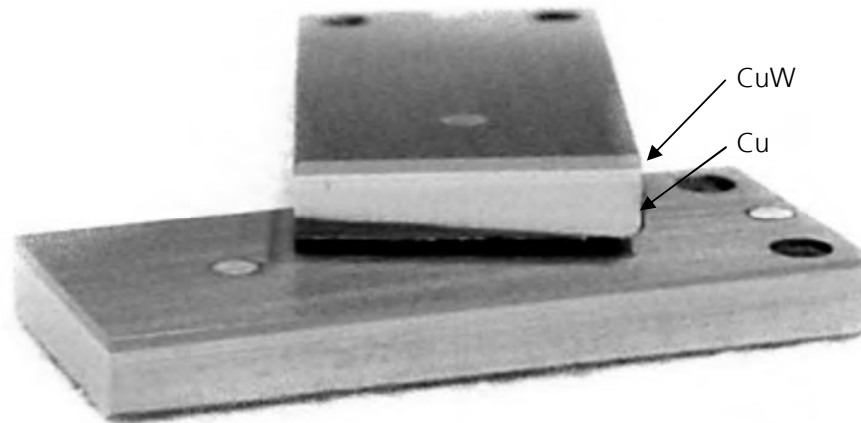


Figure 5-8: Unplated prototype of a "top-layer" heat sink

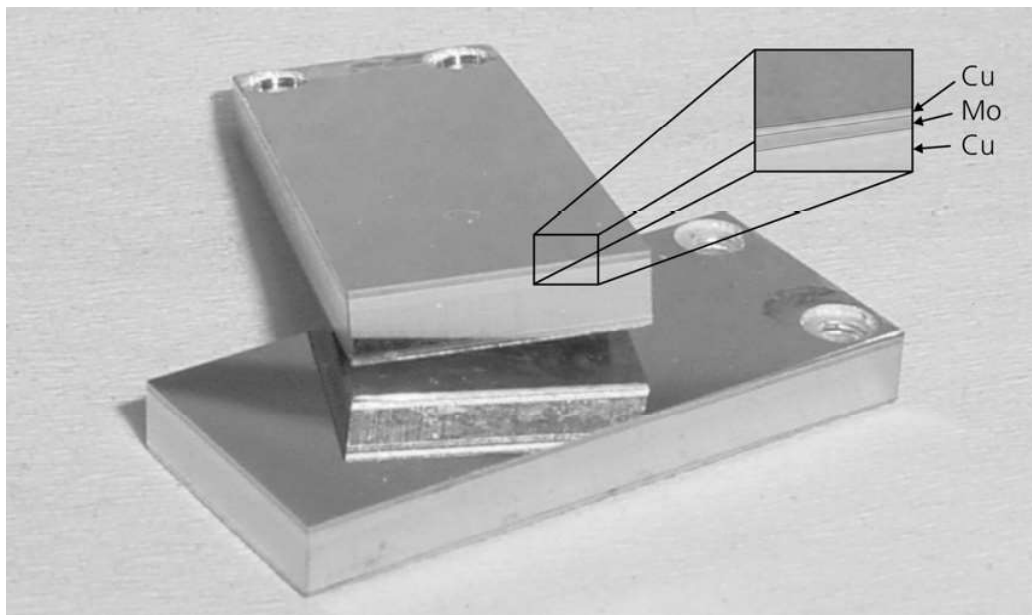


Figure 5-9: Unplated prototype of a "sandwich" heat sink

The expansion coefficient of the heat sinks is measured directly by measuring the length change at different temperatures. The measurements are performed using a measurement microscope. The measured distances at different temperatures are put in relation to the distance at room

temperature. The expansion coefficients can be directly obtained from the slope of the expansion versus temperature curve (Figure 5-10). The measurement accuracy is approx. $1\text{ }\mu\text{m}$, so that the measured distance has an error range of $\pm 2\text{ }\mu\text{m}$ and the maximum temperature difference used is 175 K. The expected expansion is approximately $12\text{ }\mu\text{m}$ over a 10 mm distance. This gives an error of about $\pm 15\%$ for the experimentally determined thermal expansion coefficient.

The expansion measurement is performed at the front edge of the heat sink's top side as well as 2 mm behind the edge, thus characterising the expansion behaviour of the mounting area.

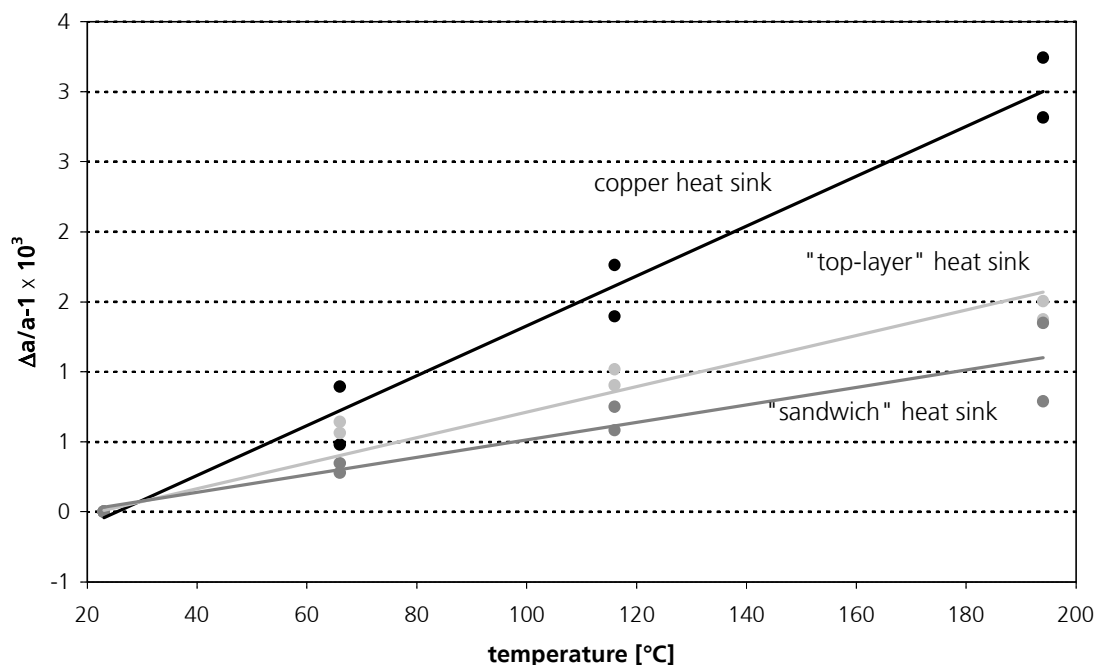


Figure 5-10: Relative expansion as a function of the temperature for copper, "top-layer", and "sandwich" heat sink. The expansion coefficient is given by the slope of the curves. At each temperature a measurement at the front edge and 2mm behind are performed.

Heat sink type	CTE at front edge [ppm/K]	CTE behind edge [ppm/K]	average CTE [ppm/K]	simulated CTE [ppm/K]
copper	16.8 ± 1.3	18.7 ± 1.4	17.8 ± 1.3	
"top-layer"	8.0 ± 1.3	11.5 ± 1.5	9.8 ± 1.4	7.2
"sandwich"	8.1 ± 1.3	6.1 ± 1.2	7.1 ± 1.3	7.7

Table 5-3: Measured and simulated thermal expansion coefficient of a copper, the "top-layer", and the "sandwich" heat sink.

As a reference, copper heat sinks are also measured. In this case the measurement should reveal the expansion coefficient of copper, approx. $16.7 \cdot 10^{-6}\text{ K}^{-1}$. From the measurements, an average value for the expansion coefficient of the copper heat sinks of $17.8 \cdot 10^{-6}\text{ K}^{-1}$ is measured. For the "top-layer" heat sinks, an average expansion coefficient of $9.8 \cdot 10^{-6}\text{ K}^{-1}$ and for the "sandwich" heat sink, an average expansion coefficient of $7.1 \cdot 10^{-6}\text{ K}^{-1}$ is obtained (Table 5-3). The values of

the copper and of the "top-layer" heat sink are above the expected values, but within the error range of 15%. These are likely a measurement error, because measuring the distance with an optical microscope is not very accurate. The smaller value for the "sandwich" heat sink is obvious, because the simulation values were also smaller. For the simulation, copper properties of normal copper are used, but during the fabrication process, the copper is heated and annealed. The elastic modulus decreases by nearly 20%. In general the expansion matched heat sinks reduce the mismatch, which should significantly lower the packaging induced stress.

5.2.3. Stress Level of Laser Bar on Expansion-Matched Heat Sinks

After characterising the expansion matched heat sinks, laser bars are packaged on them, in order to investigate the stress reduction. The biggest part of the packaging induced stress, is the stress in lateral direction along the width of the laser bar. This stress intensity is measured using micro-photoluminescence spectroscopy (Chapter 3.5.2) performed at THALES Research & Technology (TRT).

The shift of the micro-PL peaks along the laser bar is proportional to the mechanical stress. The measurements are not carried out during operation.

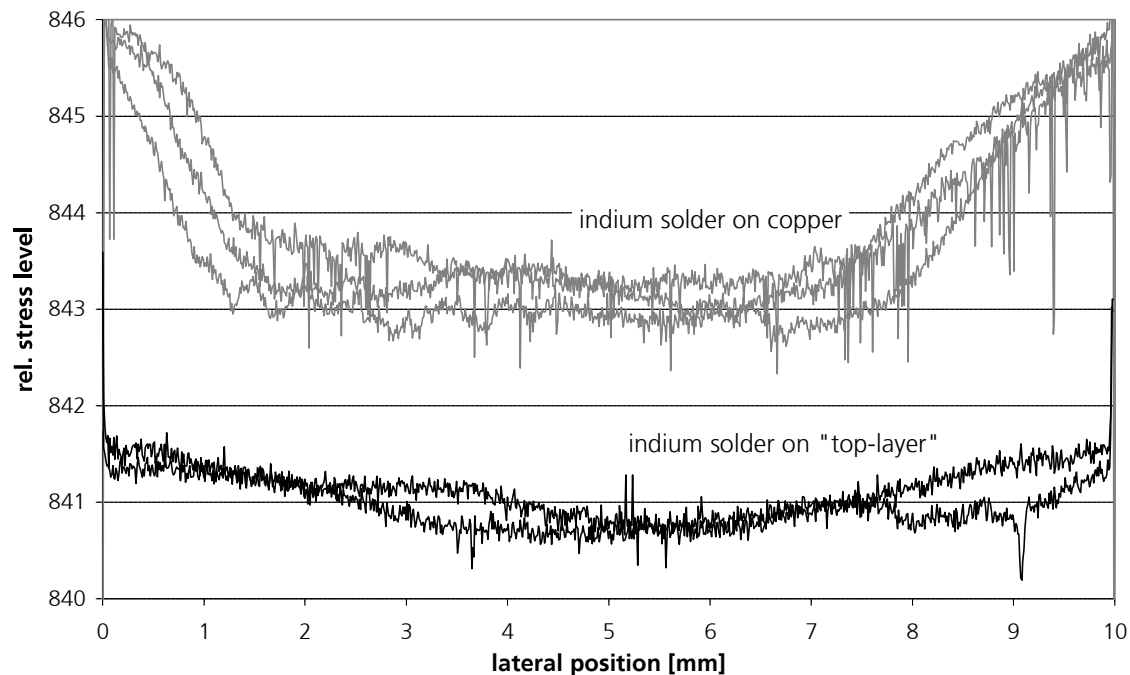


Figure 5-11: Micro-PL stress measurement of indium soldered bars on the "top-layer" and copper heat sinks. The mounted bars are from the same wafer [measurement performed at TRT].

The compared bars are all from the same wafer and are mounted with a standard indium process onto copper and "top-layer" heat sinks. The standard process leads to a thin solder layer with a large amount of intermetallics.

These measurements indicate a large reduction of residual stress, when mounted on the expansion matched "top-layer" heat sinks compared to when mounted on standard copper heat

sinks. The PL wavelength shift is reduced by nearly 3 nm for copper mounted to less than 1 nm for the "top-layer" mounted laser bars. This means, that the stress level is reduced by a factor of three using the Cu-W "top-layer" expansion matched heat sink.

The same measurements are also done for the "sandwich" expansion matched heat sink. The results show a reduction of the PL-wavelength shift from 2 nm for the copper mounted to 1 nm for the "sandwich" mounted laser bars (Figure 5-12). This means, that the stress level is reduced by a factor of 2 using the "sandwich" heat sink.

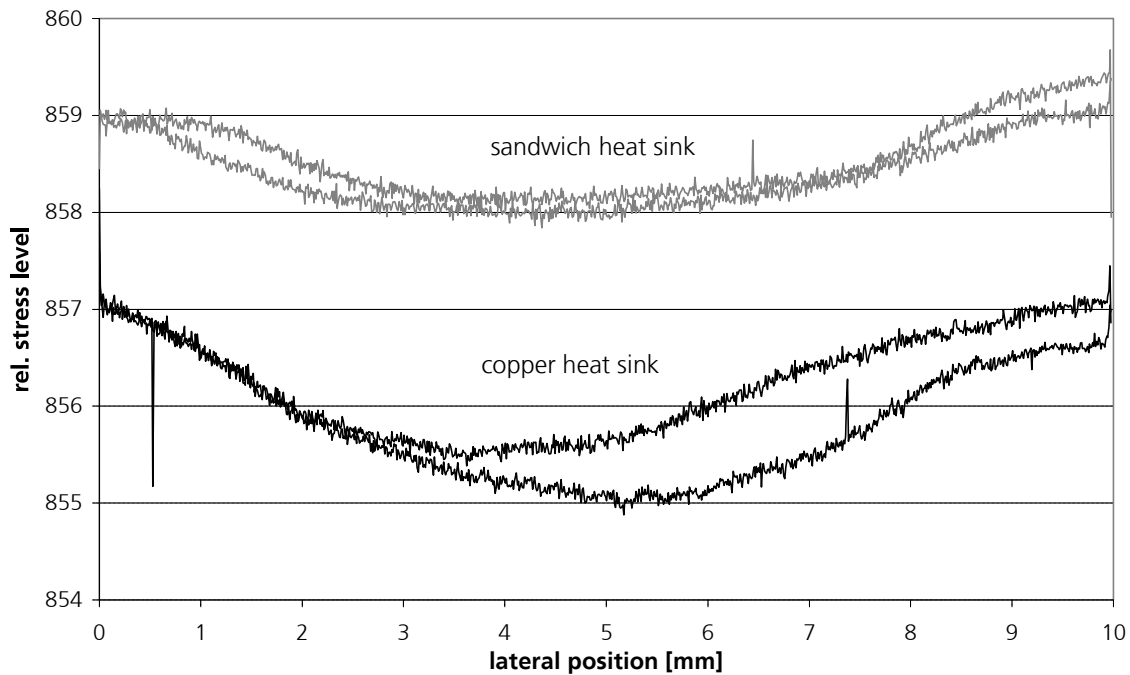


Figure 5-12: Micro-PL stress measurement of indium soldered bars on the "sandwich" heat sink. The mounted bars are from the same waver [measurement performed at TRT].

After mounting a laser bars on copper heat sinks, the largest stress gradient are located at the ends of the bar. As a test, a laser bar is mounted with gold-tin solder on a copper heat sink. The stress is so high, that the laser bar cracks. It even occurred, that the bar spalled at the ends of the laser bar (Figure 5-13). Only the footprint and a part of the metallization of the laser bar remain on the heat sink.

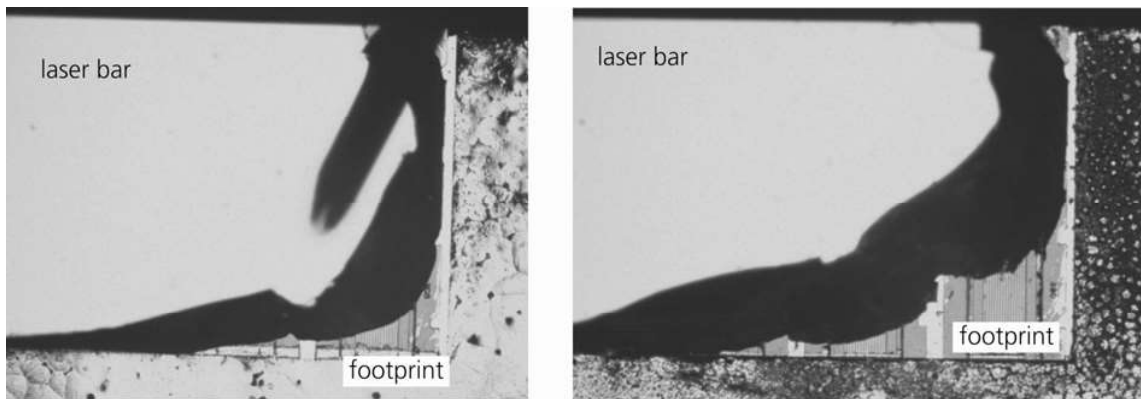


Figure 5-13: Top view of cracked bar (mounted with gold-tin solder on copper), which was spalled at the ends of the bar due to high stress. Left: following the packaging process, right: same bar several minutes later, the edge has cracked further.

In order to demonstrate the influence of the packaging induced stress, the lifetime of diode lasers mounted on copper heat sinks and the "top-layer" expansion matched heat sink are compared. The laser bars are from the same wafer and run at the same power level, so that only the packaging induced stress differs. The chosen power level is high, so that the lifetime will be reduced in order to study the differences between the two different packages in a "shorter" time. Therefore the lifetime is not representative for bars packaged on copper heat sinks.

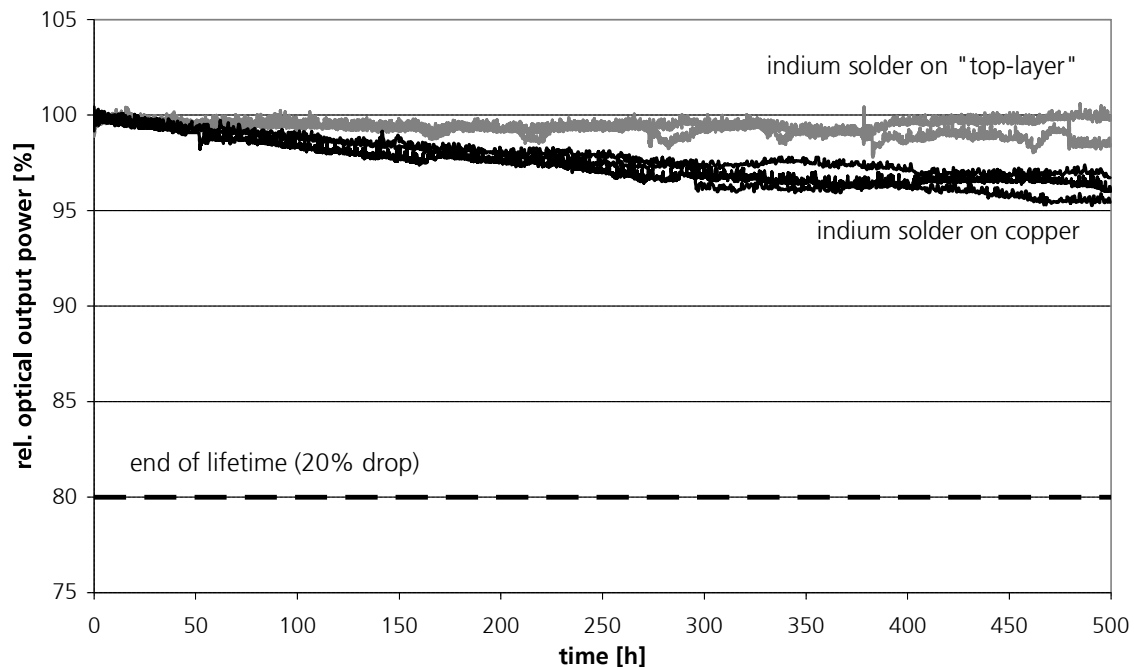


Figure 5-14: Lifetime test of packaged bars with indium on copper and the expansion matched "top-layer" heat sink.

Significant differences can be observed between the two sets of laser bars mounted on copper and "top-layer" heat sinks. The bars mounted with soft solder on the expansion-matched "top-layer" heat sink have a longer lifetime, of about 6100 h. The bars mounted with soft solder on a copper heat sink have a lifetime of about 2700 h, which is less than half. These lifetime tests at high power levels show, that the reduction of packaging induced stress, is the key factor for an increased lifetime.

5.3. Metallurgy of the Solder Interface

The laser bar is soldered on the heat sink and the n-contact sheet on top of it. The soldering connection is established by diffusion of the solder and the material of the contact areas. In this case gold is typically used. The properties of indium and its intermetallics are described in Chapter 2.3.1 and 2.3.5.

Even if the actual soldering process is finished, the diffusion process can still go on at room temperature. Therefore the element distribution directly after the solder process as well as after extended periods of time are of great interest. The rate of diffusion of the contact material and the solder indicated the strength of the connection. No interdiffusion of the solder and contact material indicates a poor connection. A diffusion zone between the solder and the contact surface is an indication of a strong contact. It is also of interest, that pure indium is available after the joining process because indium is ductile and helps to decrease the induced mechanical stress.

5.3.1. Stress Reduction by Solder Creeping

The creep properties depend on the geometry, solder properties, and the already induced stress. The creep behaviour of the solder can help to reduce the stress. Therefore it is important to choose an adequate solder and geometry. The base area is fixed by the laser bar geometry, so that only the thickness of the solder can be varied. The behaviour of indium is investigated, which is the common ductile solder for laser bar packaging, on copper heat sinks.

Indium has the task of reducing the strain by creeping, but this property changes with the fraction of intermetallic compounds (see Chapter 2.3.1).

The influence of the intermetallic compounds on the laser bar solder layer is investigated using shear tests. Solder layers with different thicknesses are manufactured and tested afterwards. The "thick" solder layer is produced with 10 μm thick spacers under each side of the laser bar. The thickness of the spacer varies due to fabrication tolerances. A weight, which presses onto the laser bar during the soldering process, is used to produce the "thin" solder layer. In order to be sure, that the diffusion process took place and is completed, the samples are aged for 100 h at 80 $^{\circ}\text{C}$ in a vacuum oven.

The result of the shear test is shown in Figure 5-15. The displacement is the solder displacement of the laser bar plus the deformation of the whole set-up, especial the sample holder, which is the biggest part. The shear force is much higher for the 2 μm thick solder layer, which has a higher volume fraction of intermetallics. For the 12 μm thick solder layer, the force-displacement curve is typical for materials with excellent creep properties.

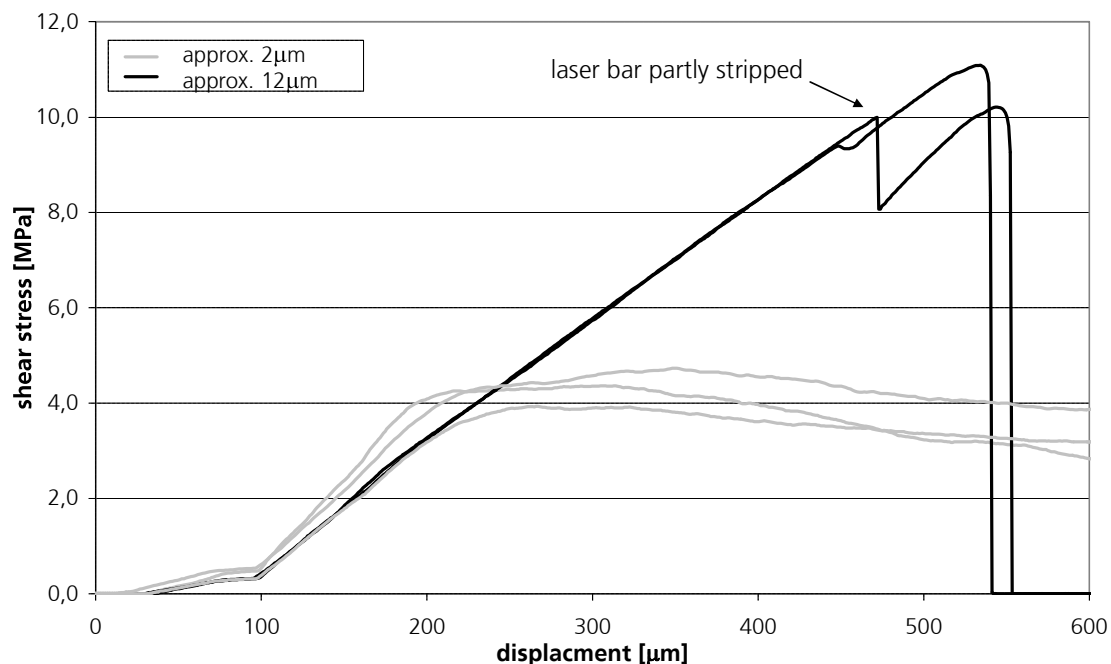


Figure 5-15: Shear test of mounted laser bars with 2 and 12 μm indium solder layers. The shear stress is plotted versus the displacement of the set-up.

The shear stress of the 2 μm thick solder layer increases almost continuously and then the solder layer breaks. The dominant part is the elastic behaviour of the solder. For the 12 μm thick solder layer, the elastic behaviour is dominant until the shear stress reaches 4 MPa. At this point the plastic deformation of the solder dominates and the shear stress does not increase anymore. This is a typical behaviour for materials with excellent creep properties.

In the following the metallurgical composition, especially the fraction of intermetallic compounds is analysed with the dimple grinding technique and EDX-point analysis. The method is described in detail in Chapter 3.6. Investigated is the part of the solder layer that is still connected to the laser bar after shearing.

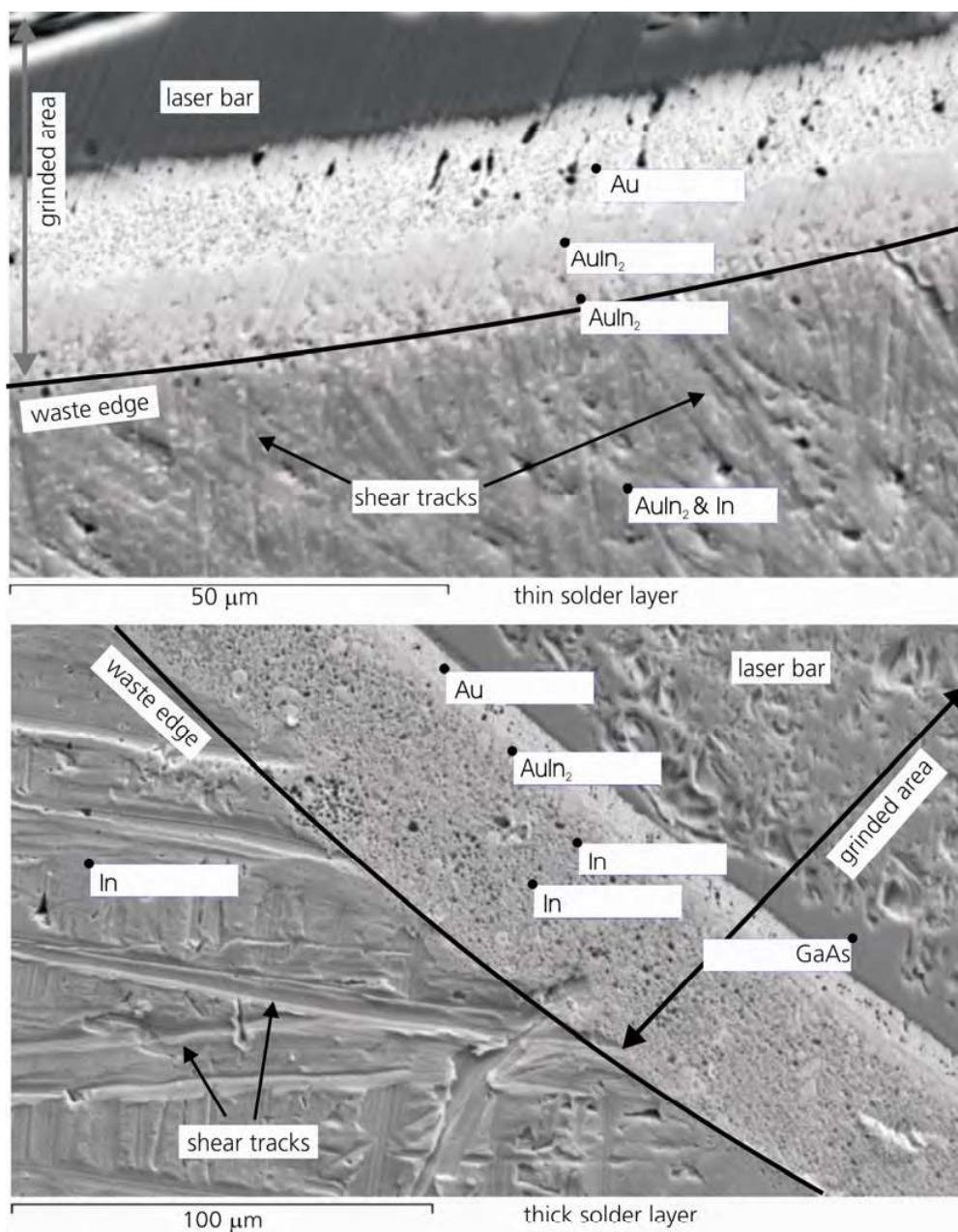


Figure 5-16: SEM image and EDS-point analysis of the "thin" and "thick" indium layer after shear testing. The solder layer side of the laser bar is analysed. Nearly no pure indium could be found in the thin layer. In contrast to the thin layer, pure indium was found in the thick layer. The small black dots in the solder layer are diamond grains from the grinding solution stuck in the indium layer.

The analysis of the material composition of the thin and thick solder layer show, that the thin solder layer contains nearly no pure indium. Many grains as well as a solid layer of AuIn_2 are identified (Figure 5-16, top). The fraction of intermetallic compounds is nearly 100% for the 2 μm

thick solder layer. Over 50% of the 12 μm thickness is still pure indium for the "thick" solder layer sample. On the sheared surface only indium is detected using EDX-point analysis. The shear strength and creep behaviour are strongly connected to the metallurgical composition of the solder layer.

In order to use the advantage of the ductile solder, the solder thickness should be large enough, so that intermetallic compounds cannot grow from the heat sink to the laser bar or the other way around. The process temperature, such as the holding time and maximum temperature have an influence on intermetallic compound growth and formation. Of course the main factor of the intermetallic compound fraction is the available gold, provided by the contact layers of the laser bar and heat sink.

- **Stress influence depending on solder thickness / intermetallic compound**

As already seen, the metallurgical composition of the solder layer influences the properties. These properties also have an influence on stress reduction of the packaging induced stress. Standard ILT plated copper heat sinks and commercial available bars are used for the investigation. Diode lasers with a wedge-formed solder layer, such as the ones introduced in Chapter 4.3, are investigated regarding the mechanical stress. The qualitative stress distribution is determined using the DoP method (Chapter 3.5.3).

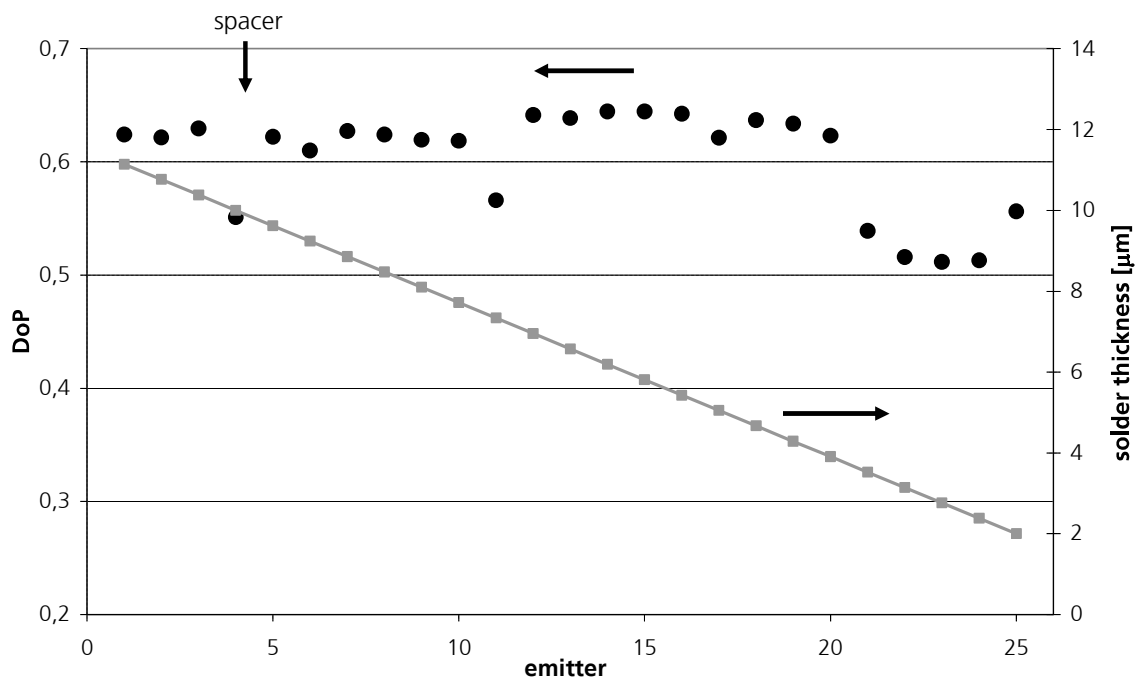


Figure 5-17: DoP of a diode with wedge-formed solder layer. On the left, the solder is 12 μm and on the right 2 μm thick. The DoP value is constant for solder layers thicker than 4 μm .

A uniform distribution, as seen for emitter 1 to 20, represents only the intrinsic stress of the laser bar. The packaging induced stress leads to a change of the DoP value, as seen for emitter 21 to 25. In general, the stress change has no slope proportional to the solder layer thickness. Therefore the solder layer thickness cannot be the direct cause of the higher stress level on the right side.

On the right side, the stress changes significantly for the last 5 emitters. Due to the fact, that the solder layer is small on the right side, a high fraction of intermetallic compounds can harden the thin solder layer, so that the stress cannot be completely relaxed. It looks as though a critical solder layer exists under which the hardening of the intermetallic compound dominates. In this case, the critical thickness is around 4 μm .

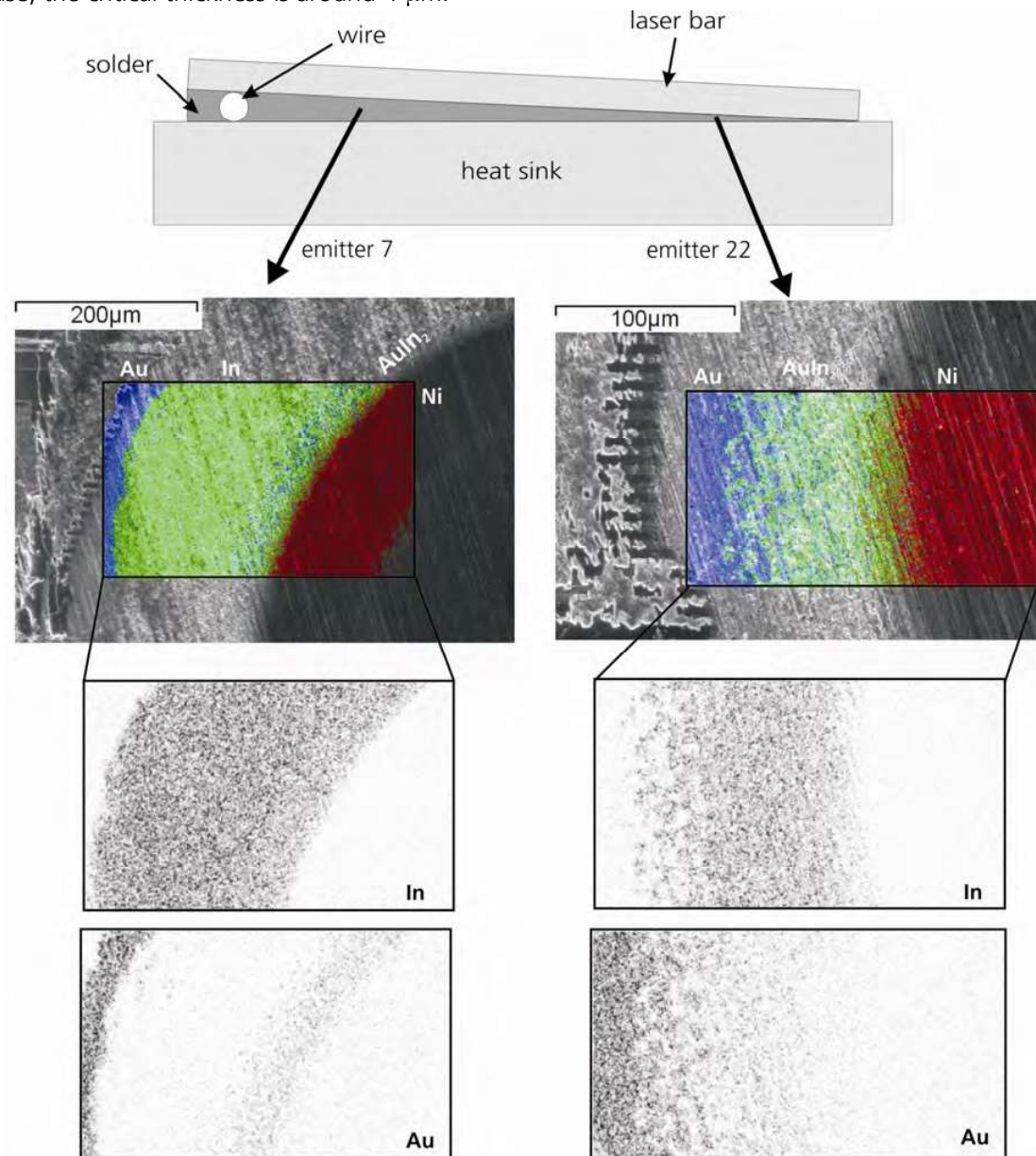


Figure 5-18: EDX-mapping of the solder underneath emitter 7 and 22 of a wedge formed solder laser bar. In the cross section, the laser bar is on the left side and the heat sink is on the right. Darker areas represent a higher amount of the investigated element. On the SEM image, the EDX result is overlaid. Blue represents gold, green indium, and red nickel.

In order to evaluate the different fractions, the solder is analysed metallurgically using EDX. The sample is prepared using the dimple grinding technique.

The metallurgical analysis shows differences in the solder layer composition underneath emitter 7 and 22. The solder layer thickness under emitter 7 is approx. 8 μm and under emitter 22 approx. 2 μm . On the left side of the SEM-images is the laser bar and on the right is the gold nickel plated heat sink (Figure 5-18). In the thin solder layer underneath emitter 22 the gold has diffused through the whole layer. EDX point analysis shows, that a high amount of AuIn_2 intermetallic compounds is present across the whole layer thickness and the AuIn_2 partly connects the laser bar and heat sink. Underneath emitter 7, pure indium regions/layers can still be found. The gold of the laser bar metallisation and heat sink plating were not able to grow the AuIn_2 intermetallic compound through the whole layer. This is shown in the lower left image. The dark region on the left side of the EDX-mapping represents the gold of the laser bar metallisation, and on the right the gold of the heat sink plating. In the middle no dark regions can be found, which means, that there is no gold or gold containing compounds present.

As the analyses show, under emitter 22, a high fraction of the AuIn_2 intermetallic compound is found which affects the plastic deformation properties. The stress due to the expansion mismatch during packaging cannot be completely reduced (see Figure 5-17). Under emitter 7, pure indium regions, with its excellent creep properties, reduce the packaging induced stress. In this investigated case, the amount of gold was not able to establish a gold compound through the whole solder layer. Therefore a critical solder layer thickness of 4 μm for a standard ILT plated heat sink and the commercial available bar could be determined, under which the stress relaxation is dramatically reduced.

- **Relaxation in dependence of solder thickness / intermetallic compound fraction**

Another issue is the time resolved relaxation behaviour of the solder. A short relaxation time is of course better, so that the stress is relaxed fast. In order to investigate the relaxation of stress, strain is induced into a sample while stress distribution is measured after certain time intervals. A wedge-formed solder sample is used to investigate the relaxation behaviour in dependence of the solder thickness.

The sample is heated to 80 °C for 120 h in a vacuum for relaxation of the packaging induced stress, so that the bar is nearly not stressed after this treatment. The sample is then taken out of the oven and cooled down. Cooling of the device induces new strain, due to the expansion mismatch of the laser bar and heat sink, which is similar to the packaging induced stress during the packaging process. The occurring stress, induced by the strain, is measured with the DoP method at certain time intervals after cooling (Figure 5-19).

Emitters with a thicker solder layer, which contain still a pure indium layer, are already relaxed after 1 h. This can be seen, that the emitters have the same DoP value as before. Emitter 4 has a different stress level after 1h, but the spacer is located in this region, which properly influences the relaxation or rather the creeping of the indium solder. After 7h no differences before and after heating could be determined at emitter 4, so that at this time the solder layer is also relaxed here.

The stress level of the last three emitters (23-25) is much higher after 1 h compared to the initial stress. After 7 h and 24 h the DoP value shifts back to the initial value, which means, that the induced stress is slowly relaxing. The initial value differs also from the initial DoP value of the emitters with the thicker solder layer. This means, that a stress level always exists even at the most relaxing state.

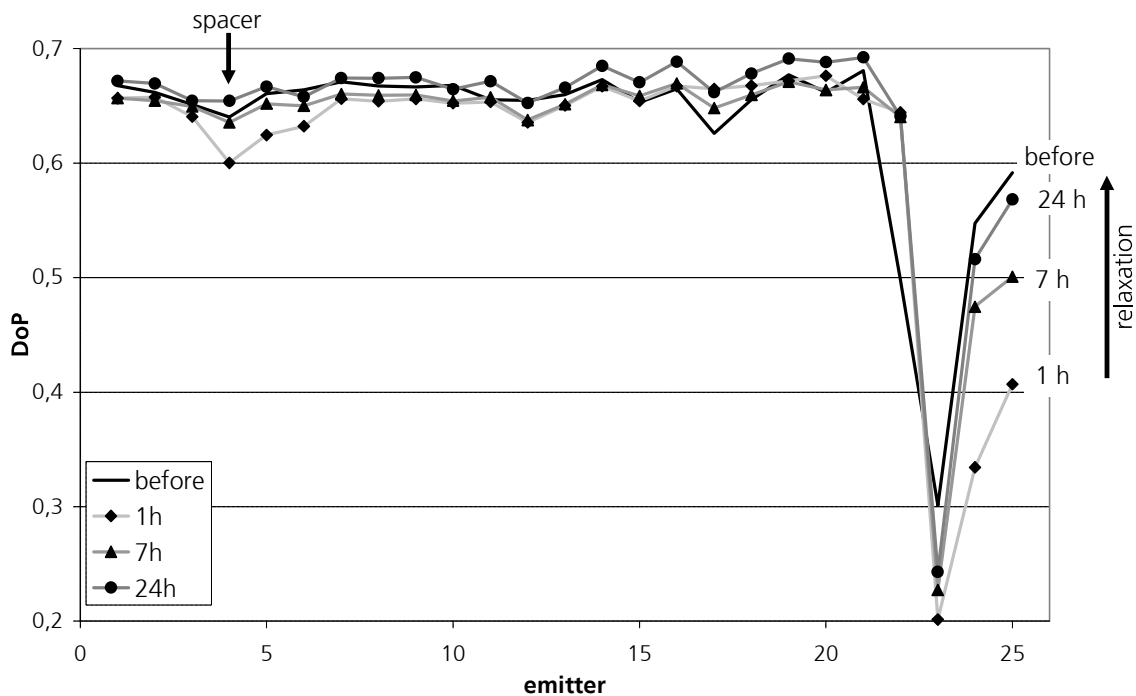


Figure 5-19: Stress distribution of a solder wedge-formed laser bar at 1 h, 7 h and 24 h after heating up to 80 °C for 120 h. The dark line is the initial stress before heating the sample. On the right side the relaxation of the thin solder layer is illustrated.

Therefore thin solder layers underneath the critical thickness with a high fraction of intermetallic compounds should be avoided, because the solder layer reduces the packaging induced stress slower and partially.

In Figure 5-20 the stress distribution of a standard packaged bar with a thin solder layer underneath the critical thickness is compared with an optimised packaged bar. The difference of the package is only the solder layer thickness. The optimised packaged bar uses two spacer on the right and left side of the solder layer in order to obtain at least a 10 µm thick solder layer. The packaging induced stress for the optimised solder varies the DoP value only by about 0.5. The variation of the DoP value of the standard package is in the range of 5.

This shows, that packaging induced stress can be nearly fully relaxed by a solder layer with a thickness above the critical thickness.

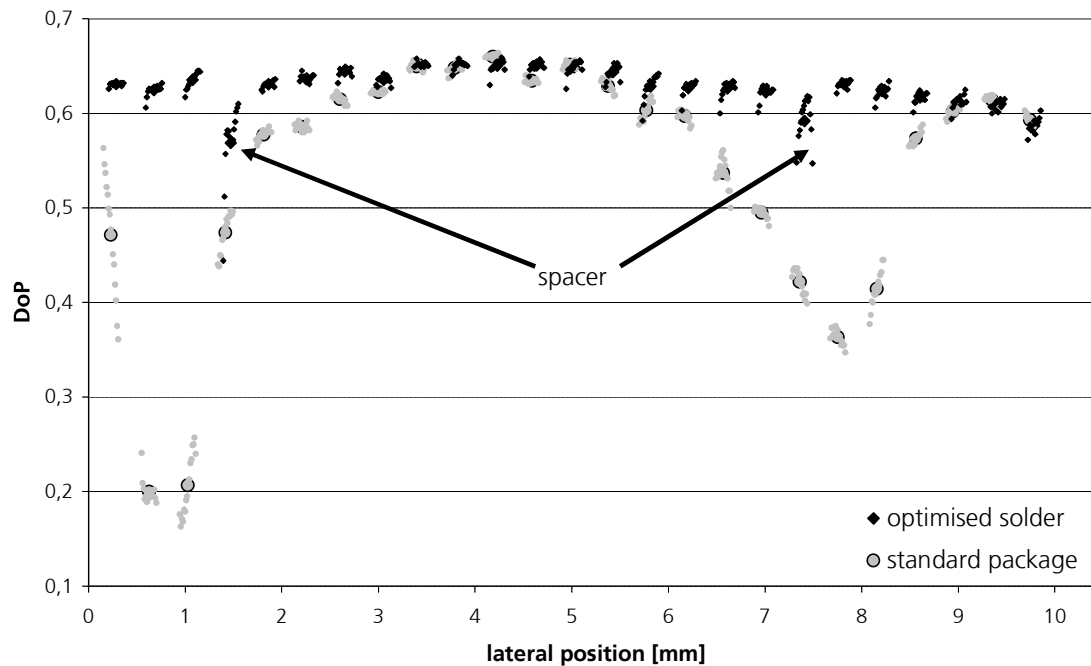


Figure 5-20: DoP distribution of a device with a thin (non optimised) versus an optimised solder layer. The small dots represent the local DoP value and the grey dot is the average of each emitter.

5.3.2. Diffusion Barrier

As already seen in the previous subchapter, the intermetallics of the solder layer can dramatically change the properties of the original solder material. The diffusion is wanted during the soldering process to establish a connection. After establishing the connection, diffusion is unwanted and should not change the solder properties during lifetime. In order to stop the diffusion, especially the diffusion of the heat sink material into the solder, diffusion barriers are used. The diffusion barrier is described in general in Chapter 2.3.5.

The need and benefit of the diffusion barrier is investigated by producing diode lasers without a diffusion barrier.

A heat sink without a diffusion barrier, in this case without nickel and gold, is used to solder a laser bar on top of it. A commercial laser bar with gold plating on the contact surface is used. The diode is packaged with the standard packaging process.

In Figure 5-21 the measured DoP distribution of such bar is shown. The laser bar is under high stress. The laser bar was not specially treated and several days passed after packaging, before the measurements were performed.

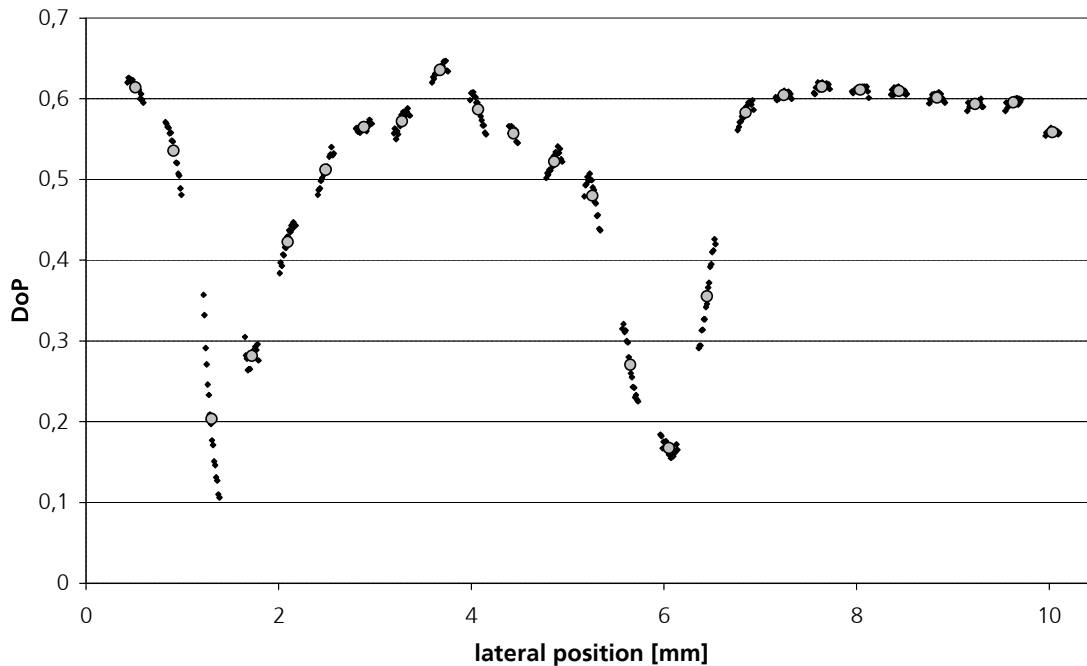


Figure 5-21: DoP distribution of a packaged diode laser without a diffusion barrier. The small dots represent the local DoP value and the grey dots are the average of each emitter.

The DoP value for the packaged bar without diffusion barrier shifts from 0.1 to 0.6, which represents a high amount of packaging induced stress, which is not relaxed by the solder layer.

The solder interface is investigated by dimple grinding and EDX-line scan across the solder layer. On the left side of the SEM-image (Figure 5-22) the laser bar with the gold metallisation can be seen. The gold metallisation is separated by a small platinum layer from the solder interface, so that no more gold can diffuse into it. The copper heat sink is on the right.

Gold grows from the laser bar side into the indium layer and AuIn_2 is formed. From the heat sink side copper diffuses into the indium layer and forms copper-indium compounds. The copper-indium compounds are even found in between the gold indium compound layer (darker spots in the grey AuIn_2 layer). The exact composition of the copper indium intermetallic compound could not be determined with EDX, because the information depth was too large, so that the copper underneath is always also detected. According to information in literature it should be $\text{Cu}_{11}\text{In}_9$ [84].

The solder layer thickness is 3 μm . Even if the solder layer thickness were increased, there would always be enough copper available to transform all indium into a copper-indium composite. These intermetallic compounds even form at room temperature.

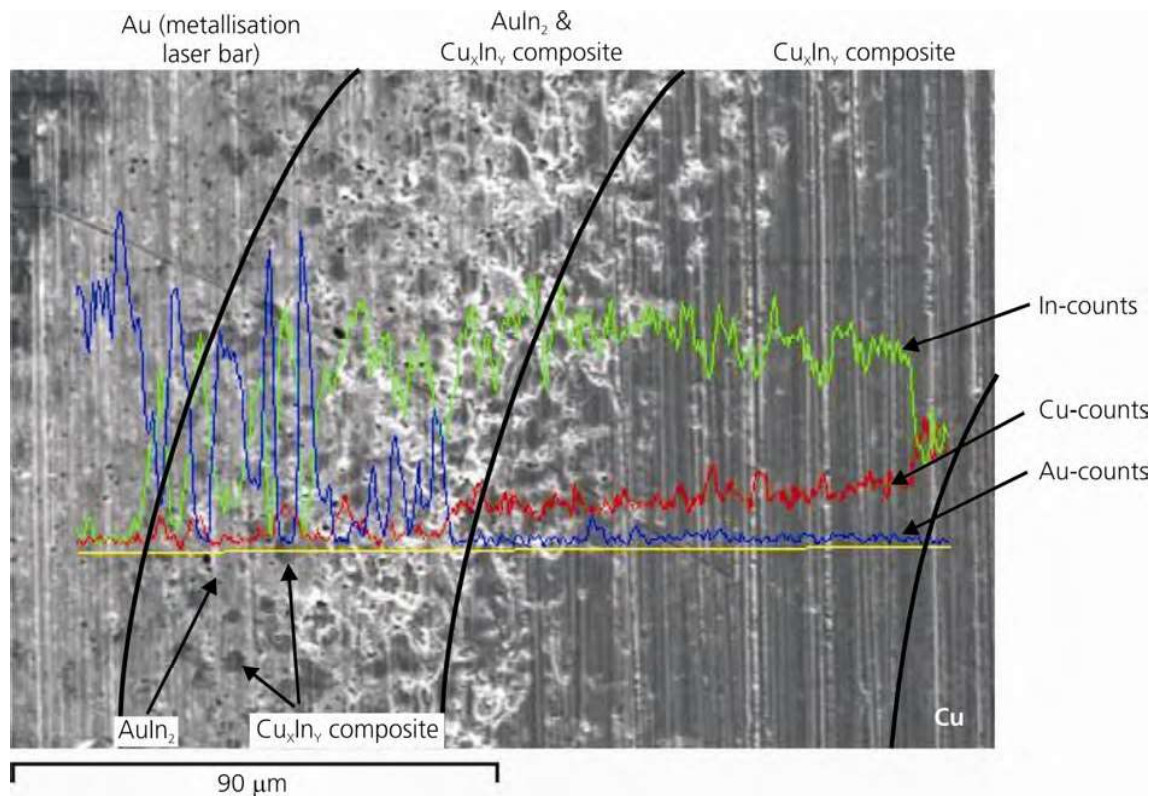


Figure 5-22: SEM image with EDX line-scan of sample without a diffusion barrier. Copper-indium composites have grown through the whole solder layer. Gold also diffuses into the solder layer and builds AuIn₂ intermetallic compounds, but this compound does not reach the heat sink.

Therefore a diffusion barrier is needed, to prevent the heat sink material from diffusing into the solder layer. If a diffusion barrier is used, only the gold contact layer will diffuse into the solder and the diffusion will stop, when no more gold is available.

That the diffusion stops, if the gold layer is used, is investigated with a wedge-formed solder diode laser. A nickel diffusion barrier layer divides the gold contact layer from the copper heat sink. The stress level was measured before and after ageing for 120 h and 250 h at 80 °C in a vacuum oven. If the intermetallic compound would further grow, the induced stress will effect the emitters more and more. As the results in Figure 5-23 shows, the affected region (right side), with DoP levels different from the other emitters on the left side, is not growing. The different stress levels for the stressed emitters (21-25) are due to the different relaxation states (see Chapter 5.3.1 for relaxation behaviour).

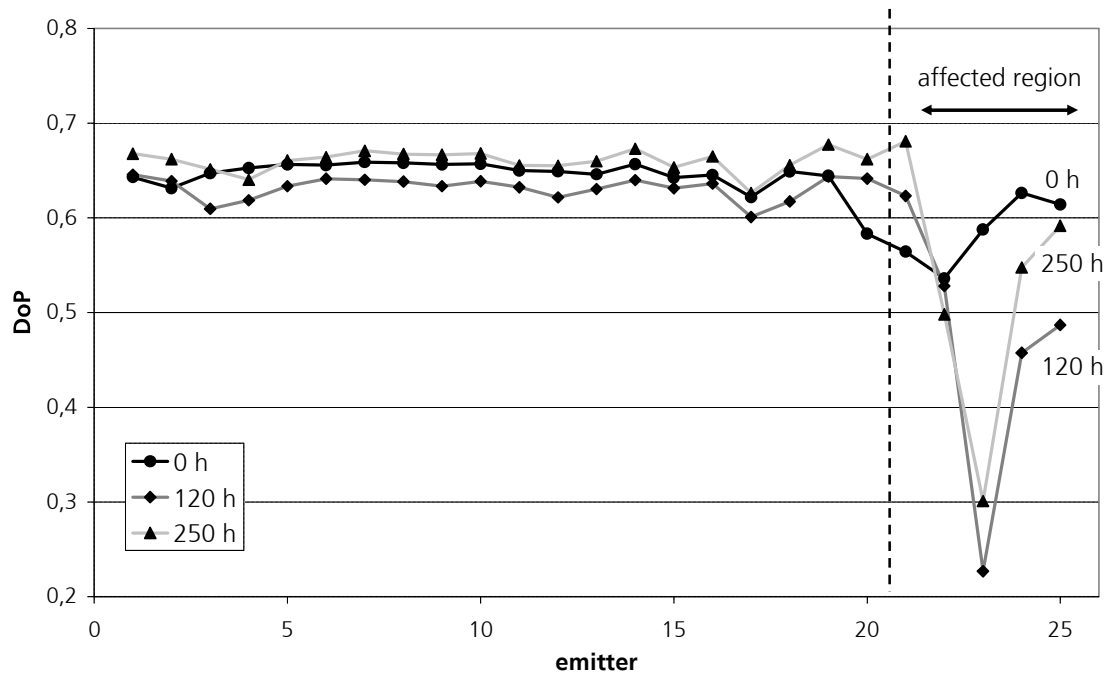


Figure 5-23: DoP distribution after packaging and 250 h ageing of a wedge-formed solder diode laser. The affected region is always the same, no growth can be detected.

Highly stressed laser bars show two downwards directed peaks (see Figure 5-24). The reason cannot be described with the band-gap stress relation described in Chapter 2.1.2, because this model only describes the relation of the heavy-hole and light-hole band regarding the epitaxy produced strain in [001] crystal direction.

It is very probable that the laser could not withstand the stress and, therefore the stress was reduced by dislocation. Also, at these two points, the wavelength varies distinctly from the average wavelength of all emitters. Another indicator is that, the threshold current of these emitters is higher. At 15.8 A only the effected emitters have a lower intensity, which indicated no laser operation. A higher threshold can be created by defects, due to higher non radiating transitions.

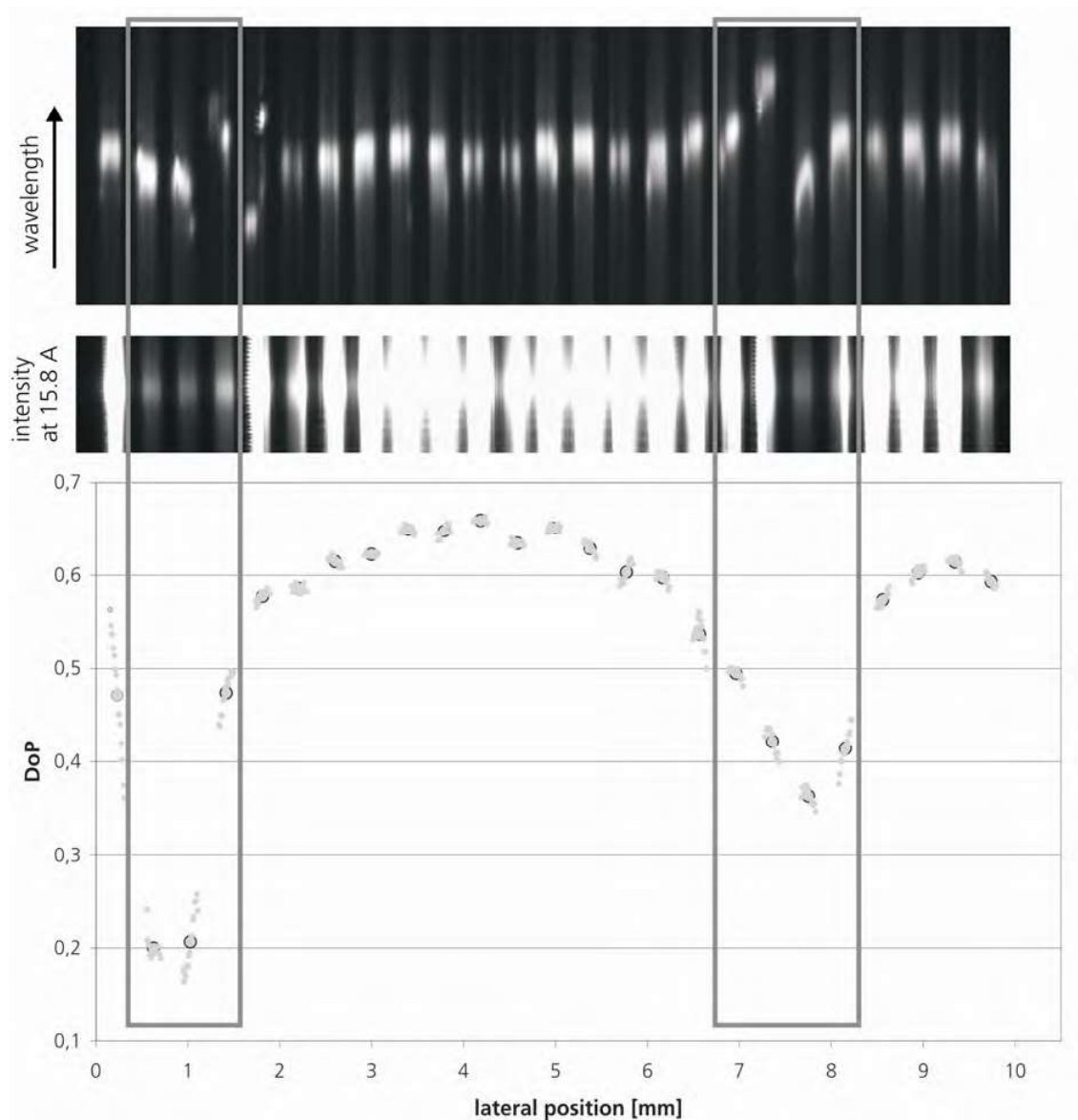


Figure 5-24: Wavelength, intensity around the threshold current and DoP distribution of an diode laser bar mounted with indium on a copper heat sink. In the top image the wavelength distribution versus the lateral position is plotted. In the middle the output intensity (darker represents higher intensity) and in the bottom graph the DoP value is plotted versus the lateral position. All three distributions show a abnormality at the same position (see the gray rectangle).

The thresholds are dependent on the stress level because, typically a certain stress level is used to lower the threshold. All these are indicators for defects and strong stress gradients.

5.3.3. Lifetime Dependent upon different Solder Layer Thickness

A lifetime test of diode lasers with different solder layer thicknesses has been performed to see the influence of the "harder" solder due to the higher fraction of intermetallic compounds. Two sets of diode laser have been packaged. Because the soldering system cannot control the solder layer thickness directly, the pressing force during the packaging process is varied in order to obtain different solder layer thicknesses. Bars from the same wafer are packaged onto conductively cooled heat sinks with a high pressing force and an extremely low force.

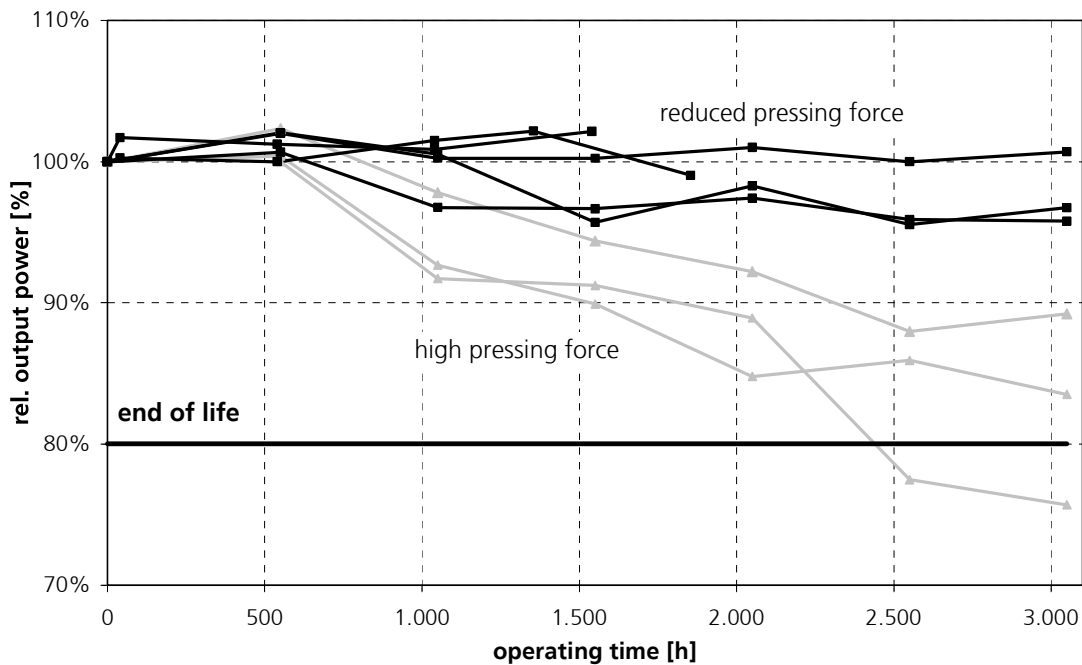


Figure 5-25: Ageing data of two sets of diode laser with varying pressing force during the packaging process. The ageing is done at the nominal output power in continuous wave mode.

The lifetime test shows, that the lifetime of the diode lasers packaged with a lower pressing force are significant longer. The average lifetime for the set of diode laser with high pressing force is 3300 hours and for the set of diode laser with a lower pressing force is 24000 hours.

The mechanical properties of the solder are strongly connected to its metallurgical composition. A high volume fraction of intermetallic compounds change a ductile layer to a brittle one. By reducing the amount of intermetallic compounds, the packaging induced stress nearly disappears due to the plastic deformation of the indium solder layer. The required solder thickness is dependent upon the available amount of gold from the contact layers of the heat sink and laser bar. The wedge-form solder experiments show, that the solder layer should be thicker than the critical thickness, in order to reduce packaging induced stress caused by the hardness of the solder layer (see Chapter 5.3.1). The critical thickness for this investigated case is around 4 μm .

Part III

Outlook

6. Summary

Over the course of last few years, diode lasers have become more and more established as a viable photon source in pumping and direct applications. Increasing the reliability of these devices is necessary as increased reliability reduces costs and makes diode lasers more attractive for use.

High stress levels and high thermal loads are the limiting factors for the lifetime of diode lasers. Large amounts of stress can be caused by the packaging process due to the expansion mismatch of the semiconductor and heat sink materials.

Laser bars are usually mounted with soft solders onto copper heat sinks. Due to the expansion mismatch of the semiconductor and heat sink material, stress is introduced into the laser bar. Ductile solder is used to compensate for the mismatch. By using an expansion matched submount, a brittle solder such as gold-tin can be used. At the same time, due to the lower thermal conductivity of this expansion matched material, the thermal load increases. Here, the effects of expansion matching work against the reduction of the thermal load. For higher reliability of diode lasers, the packaging induced stress and thermal load need to be reduced.

This work describes the thermal and mechanical influence of the packaging process on diode laser bars. To demonstrate this, expansion matched packages using two different types of actively cooled expansion matched heat sinks were developed. The greatest advantage of using expansion matched heat sinks in the submount packaging process is the resultant ease handling due to the fact that the soldering step submount heat sink is eliminated. The integrated design also has the advantage of having low thermal resistance. A "top-layer" heat sink with an expansion matched "top-layer" and a "sandwich" heat sink with a low expansion material inside the heat sink, which influences the CTE of the mounting area, were designed using FEM-simulations.

As the simulated as well as the experimental results show, the performance of the "sandwich" heat sink is better than that of the "top-layer" heat sink. The experimental results are in agreement with the simulated values. The expansion mismatch of the "sandwich" heat sink is nearly 1 ppm/K, instead of the 10 ppm/K mismatch seen in a conventional copper package. The thermal resistance is 0.55 K/W compared to 0.45 K/W seen in the reference copper heat sink. Stress measurements, using micro-PL, show that the stress is also reduced by a factor of 2.5. These results lead to an increase in the lifetime of diode lasers mounted on these expansion matched heat sinks compared to the reference bars packaged on copper heat sinks.

Remains on the solder layer are a common cause for early failure. The remains that lead to an insufficient contact between the laser bar and heat sink were investigated. The influence of solder voids on the thermal behaviour of the laser bar were simulated as well as determined experimentally. The criterion to identify these devices are side peaks, or an unusual shape of the wavelength spectrum.

In order to avoid this source of failure, a gold protection layer process was tested. In the same vacuum in which the solder is deposited onto the heat sink, a thin gold layer is deposited on top of the indium layer. This gold diffuses into the indium and forms the stable compound AuIn_2 , which is not vulnerable to oxidation. This protective layer has no influence on the solder wetting behaviour. Therefore, the standard packaging process, without the critical reduction step, can be applied.

The soft indium solder has the task of reducing the packaging induced stress caused by the expansion mismatch between copper and GaAs during plastic deformation. The possibility of

reducing stress by adapting the solder metallurgy was investigated in detail. During soldering, gold and indium diffuses and establishes a connection. This diffusion takes place at room temperature which allows all of the gold available in the contact plating of the heat sink and the laser bar to diffuse into the indium solder. There, the brittle AuIn_2 intermetallic compound is formed. It is shown that the possibility of plastic deformation decreases with an increase in intermetallic compound fraction. In the investigated case, an indium layer with a thickness of $5\text{ }\mu\text{m}$ is sufficient enough. If the gold fraction in the contact layers is higher, a thicker indium layer or thinner gold contact layer is needed.

The thermal influence of a thicker solder layer is similar to that of a thin solder layer. Simulations and experiments show that the temperature increases caused by increasing the thickness from $2\text{ }\mu\text{m}$ to $10\text{ }\mu\text{m}$ is less than 1 K . Therefore, a thicker solder has a positive influence on the stress relaxation properties of a laser bar while having no influence on the thermal load.

It was also shown, that a thicker solder layer and expansion matched heat sink can lower packaging induced stress.

The increased solder thickness is a way to reduce significantly the packaging induced stress for packages on copper heat sinks and has nearly no effect on the thermal behaviour. But for commercial purposes, a set-up has to be developed to produce solder layers of precisely controlled thicknesses.

The expansion matched heat sink increases the thermal load when compared with copper heat sinks. The FEM-simulations have been confirmed as accurate, so that this simulation tool can be used to design new types of expansion matched heat sinks with advanced materials such as diamond composites. If the mismatch due to novel fabrication techniques can be reduced further, gold-tin rather than indium solder could be used to further improve the long term stability of the laser bar package.

7. Zusammenfassung

Diodenlaser haben sich als Lichtquelle für das optische Pumpen und für die Direktbearbeitung etabliert. Eine Steigerung der Lebensdauer lässt die Kosten weiter sinken und macht den Einsatz der Diodenlaser noch attraktiver.

Thermische und mechanische Spannungen begrenzen die Lebensdauer der Diodenlaser. Die Hauptbeanspruchung entsteht durch die unterschiedliche thermische Ausdehnung während der Montage des Halbleiter- mit dem Wärmesenkenmaterials.

Laserbarren werden typischerweise mit Indiumlot auf die kupfernen Wärmesenken aufgelötet. Durch die unterschiedlichen thermischen Ausdehnungskoeffizienten der Halbleiter- und Wärmesenkenmaterialien werden Spannungen im Laserbarren aufgebaut. Duktile Lote nutzt man, um die Ausdehnungsunterschiede auszugleichen. Schwer verformbare Lote wie Gold-Zinn werden bei der Montage ausdehnungsangepasster Komponenten genutzt. Die geringere thermische Leitfähigkeit der ausdehnungsangepassten Materialien führt zu höheren thermischen Belastungen. Um die Lebensdauer der Diodenlaser zu verlängern, müssen deshalb die bei der Montage induzierten Spannungen verringert werden.

Die vorliegende Arbeit untersucht den thermischen und mechanischen Einfluss des Montageprozesses auf Diodenlaserbarren. Hierfür sind zwei Typen von aktiv gekühlten ausdehnungsangepasster Wärmesenken entwickelt worden. Die Nutzung ausdehnungsangepasster Wärmesenken statt Submounts hat den Vorteil in der Reduzierung der Montageschritte. Ein Vorteil des integrierten Designs ist der geringere thermische Widerstand. Die „top-layer“ Wärmesenke besteht aus einer Deckschicht aus einem ausdehnungsangepassten Material und die „sandwich“ Wärmesenke besteht aus einer dünnen kupfernen Deckschicht, die durch ein Material mit geringerer thermischer Ausdehnung beeinflusst wird. Die Wärmesenken wurden mittels FEM-Simulationen ausgelegt.

Die simulierten und auch die experimentell ermittelten Ergebnisse zeigen, dass die "sandwich" Wärmesenke leistungsfähiger als die "top-layer" Wärmesenke ist. Die experimentellen Ergebnisse stimmen dabei mit den simulierten Werten überein. Die Ausdehnungsunterschied der "sandwich" Wärmesenke beträgt rd. 1 ppm/K anstatt 10 ppm/K bei konventionellen Kupferwärmesenken. Der thermische Widerstand liegt bei 0,55 K/W im Vergleich zu 0,45 K/W für den Referenzdiodenlaser, der auf einer Kupferwärmesenke montiert ist. Spannungsmessungen mit Mikro-Photolumineszenz zeigen eine Absenkung um den Faktor 2,5. Diese Effekte steigern die Lebensdauer der auf ausdehnungsangepassten Wärmesenken montierten Diodenlaser im Vergleich zu den Referenzdiodenlasern, die auf Kupferwärmesenken montiert sind.

Frühe Ausfälle sind häufig auf Rückstände auf der Lotschicht zurückzuführen. Die Rückstände verschlechtern den Kontakt zwischen Laserbarren und Wärmesenke. Dies ist genauer untersucht worden. Der Einfluss der Lotfehler auf das thermische Verhalten der Laserbarren ist simuliert als auch experimentell bestimmt worden. Nebenmaxima und ungewöhnliche Spektren der Laserbarren sind ein Indiz für solch unvollständige Lötverbindungen.

Um diese Fehler zu vermeiden ist ein Gold-Schutzschicht-Prozess getestet worden. Dazu wird im gleichen Vakuum sowohl die Lotschicht auf die Wärmesenke als auch eine dünne Goldschicht auf die Lotschicht aufgebracht. Das Gold diffundiert ins Indium und bildet eine stabile AuIn₂ Verbindung, welche kaum oxidiert. Die Schutzschicht hat dabei keinen Einfluss auf das Benetzungsverhalten des Indiumlotes. Damit kann der Montageprozess ohne den kritischen Reduktionsschritt ausgeführt werden.

Die Aufgabe des Weichlotes Indium ist die Reduzierung der induzierten Montagespannungen durch plastische Verformung. Die Möglichkeiten der Spannungsreduzierung durch Änderung der Lotzusammensetzung sind im Detail untersucht worden. Während des Lötvorganges diffundieren Gold und Indium zusammen und bilden eine Verbindung. Die Diffusion findet schon bei Raumtemperatur statt. Das zur Verfügung stehende Gold diffundiert vollständig in die Indiumlotschicht und bildet die spröde intermetallische Phase AuIn₂. Es wurde gezeigt, dass die plastische Verformung mit ansteigendem Anteil der intermetallischen Phase abnimmt. Im untersuchten Fall ist eine Lotschicht von 5 µm ausreichend, damit die intermetallische Phase keinen Einfluss auf das plastische Verhalten hat. Ist der Goldanteil der Kontaktflächen größer, wird eine dickere Indiumschicht benötigt.

Der thermische Einfluss der dickeren Lotschicht ähnelt der dünneren. Simulationen und Experimente haben gezeigt, dass der Temperaturanstieg bei einer Lotschichtdickenänderung von 2 µm auf 10 µm kleiner als 1 K ist. Eine dickere Lotschicht hat damit einen positiven Einfluss auf die Spannungsminderung, wobei die thermische Belastung sich nicht erhöht.

Es ist gezeigt worden, dass sowohl eine dickere Lotschicht als auch ausdehnungsangepasste Wärmesenken die bei der Montage erzeugten mechanischen Spannungen reduzieren.

Die dickere Lotschicht senkt die mechanischen Spannungen ohne das thermische Verhalten der Baugruppe zu beeinflussen. Für kommerzielle Anwendung muss aber noch eine Anlage entwickelt werden, die die Lotschichtdicke präzise während des Montageprozesses steuert.

Die ausdehnungsangepassten Wärmesenken erhöhen die thermische Belastung im Vergleich zu Kupferwärmesenken. Die FEM-Simulationen haben sich bewährt und ermöglichen mit der Nutzung neuartiger Materialien, wie Diamantverbundwerkstoffe, die Entwicklung besserer ausdehnungsangepasster Wärmesenken. Wenn der Ausdehnungsunterschied zwischen Laserbarren und Wärmesenke weiter verkleinert wird, wird sich das Gold-Zinn Lot wegen der besseren Langzeitstabilität durchsetzen.

Part IV

Appendix

8. Material Properties

- Copper

Properties of Copper E-Cu57 (2.0060)	
Density at 20°C	8,93 g/cm ³
Thermal Expansion Coefficient	16,8 µm/K (20-100°C) 17,3 µm/K (20-200°C) 17,7 µm/K (20-300°C)
Melting Point	1083 °C
Thermal Conductivity	394 W/(m·K) (20°C) 385 W/(m·K) (100°C) 381 W/(m·K) (200°C)
Specific Heat at 20°C	386 J/(kg·K)
Tensile strength (20°C)	300 MPa
Elastic Modulus at 20°C	130 GPa 110 GPa (annealed)
Poisson's	0,34 [19]
Shear Modulus	48 GPa
Electrical Resistance	1,7 nΩ·m

Table 8-1: Properties of copper ([17]if not otherwise specified)

- GaAs

Properties of GaAs	
Density at 20°C	5,316 g/cm ³
Thermal Expansion Coefficient	6,86 µm/K
Melting Point	1238 °C
Thermal conductivity	46 W/(m·K) (20°C)
Specific Heat at 20°C	350 J/(kg·K)
Elastic Modulus at 20°C	<100> 85 GPa <110> 121 GPa <111> 140 GPa
Poisson's	<100> 0,31 [48]
Shear Modulus	32,8 GPa [48]

Table 8-2: Properties of GaAs ([27][48]if not otherwise specified)

- Gold / Tin

Properties of eutectic Au80Sn20	
Density at 20°C	14,7 g/cm ³ [11] 14,5 g/cm ³ [81]
Thermal Expansion Coefficient at 20°C	16 µm/K [11] 15,9 µm/K [81]
Melting Point	280 °C
Thermal Conductivity	58 W/(m·K) [11] 57 W/(m·K) [81]
Tensile strength (20°C)	275 MPa
Elastic Modulus at 20°C	68 GPa [11]
Poisson's at 20°C	0,405 [11]
Shear Modulus	25 GPa [11]
Electrical Resistance	16 nΩ·m [11]

Table 8-3: Properties of Au80Sn20 ([11], [81] if not otherwise specified)

- Indium

Properties of Indium	
Density at 20°C	7,30 g/cm ³
Density at 164°C	7,02 g/cm ³
Thermal Expansion Coefficient at 20°C	24.8 µm/K [34] 33 µm/K [19],[80]
Melting Point	156,6 °C
Boiling Point	2072 °C
Specific Heat at 25°C	233 J/(kg·K)
Latent Heat of Vaporization	1959,4 kJ/kg [34] 1970 kJ/kg [19] 2019 kJ/kg [80]
Thermal Conductivity	81,8 W/(m·K) (300K) [80] 83,7 W/(m·K) (273K) [34]
Tensile Strength	1,6 MPa (295K) 15,0 MPa (76K) 31,9 MPa (4K) [34]
Compressive Strength	2,14 MPa [34]

Elastic Modulus at 20°C	12,7 GPa [34] 11 GPa [19],[80]
Poisson's at 20°C	0,45 [19],[34]
Bulk Modulus	35,3 GPa [34]
Tensile Modulus	10,6 GPa [34]
Mohs Hardness	1,2 [80]
Brinell Hardness	8,83 MPa [80]
Electrical Resistance	8,8 nΩ·m [28]

Table 8-4: Properties of Indium ([19], [34], [80] if not otherwise specified)

- Molybdenum

Properties of Molybdenum	
Density	10,2 g/cm ³
Thermal Expansion Coefficient at 20°C	4,9 μm/K
Thermal Conductivity	142 W/(m·K)
Elastic Modulus at 20°C	347 GPa
Poisson's at 20°C	0,3

Table 8-5: Properties of Molybdenum [19]

- Nickel

Properties of Nickel	
Density	8,9 g/cm ³
Thermal Expansion Coefficient at 20°C	13,3 μm/K
Thermal Conductivity	92 W/(m·K)
Elastic Modulus at 20°C	216 GPa
Poisson's at 20°C	0,31

Table 8-6: Properties of Nickel [19]

- Polyimide (DuPont Kapton®)

Properties of Polyimide	
Density	1,4 g/cm ³
Thermal Expansion Coefficient at 20°C	20 μm/K
Thermal Conductivity	0,12 W/(m·K)
Specific Heat	1090 J/(kg K)
Elastic Modulus at 20°C	2,5 GPa
Poisson's at 20°C	0,34

Table 8-7: Properties of Polyimide [20]

- Tungsten / Copper

Properties of W90Cu10 (T700)	
Density	17,1 g/cm ³
Thermal Expansion Coefficient at 20°C	6,4 µm/K
Thermal Conductivity	195 W/(m·K)
Elastic Modulus at 20°C	330 GPa

Table 8-8: Properties of W90Cu10 [52]

9. Abbreviation and Symbols

Abbreviation	Definition
AES	Auger Electron Spectroscopy
COMD	Catastrophic Optical Mirror Damage
CTE	Thermal expansion coefficient
CW	Continuous wave
DoP	Degree of Polarisation
EDX	Energy Dispersive X-Ray Spectroscopy
ESCA	Electron Spectroscopy for Chemical Analysis
ESD	Electrostatic Discharge
FEM	Finite Element Method
FWHM	Full width half maximum
HPDL	High Power Diode Laser
IAF	Fraunhofer Institute for applied physics (Freiburg)
ILT	Fraunhofer Institute for Laser Technology (Aachen)
IR	Infrared
L	Liquid
LI	Light -current
LIV	Light-current voltage
MBI	Max Born Institute (Berlin)
MeO	Metal Oxide
MTTF	Mean Time To Failure
PC	Personal Computer
PCS	Photo-Current Spectroscopy
PDT	Photo dynamic therapy
PL	Photoluminescence
PVD	Physical Vapour Deposition
qw	Quantum well
qwc	Quasi continuous wave
R&D	Research and Development
RMS	Root-Mean-Square
SAM	Scanning Acoustic Microscope
SEM	Scanning Electron Microscope
TE	Transversal electric polarisation

TEC	Thermoelectric cooler
TM	Transversal magnetic polarisation
TRT	Thales Research & Technology
XPS	X-Ray Photoelectron Spectroscopy

Symbol	Definition
a_{epi}	Lattice parameter, epitactical layer
a_{sub}	Lattice parameter, substrate
c	Speed of light
C	Elastic modulus tensor components
C_{ijkl}	4 th -Order Tensor
e	Elementary Charge
E	Gap energy
E_0	Energy gap at 0K
E_C	Energy gap, lowest conduction band
E_g	Energy gap
E_{HH}	Energy gap, heavy-hole
E_{LH}	Energy gap, light-hole
E_{SO}	Energy gap, split-off band
h	Plank's constant
H	Isotropic strain part
I	Current
I_{TE}, I_{TM}	Transversal electric polarised and transversal magnetic polarised intensity
I_{th}	Threshold Current
$I_{thermal}$	Thermal Impedance
k_B	Boltzmann constant
m^*	Effective mass
n	Stress exponent for creeping
P	Power
P_{heat}	Heating power
P_{loss}	Lost power
P_{opt}	Optical output power
Q	Aktivation energy
r_f	Front tracking ratio

r_r	Rear tracking ratio
R_{th}	Thermal resistance
S	Uniaxial strain part
T	Absolute temperature
T_0, T_1	Characteristic temperature
$T_{coolant}$	Coolant temperature
$T_{heat\ sink}$	Heat sink temperature
T_{laser}	Operating temperature of the mounted diode laser bar
T_{ref}	Reference temperature
$T_{without}$	Temperature without thermal load
U	Voltage
V_F	Forward Voltage
w	Width
ΔE_{hh}	Energy shift, heavy-hole band
ΔE_{lh}	Energy shift, light-hole band
$\dot{\epsilon}$	Creep velocity
$\Delta\lambda$	Spectral width or wavelength shift
α	Material constant
β	Reaction rate
ϵ	Strain
ϵ_{kl}	Strain tensor
η	total efficiency
η_d	Slope efficiency
λ_c	Central wavelength
λ, λ_{laser}	Wavelength of the laser
λ_{peak}	Peak wavelength
λ_{pulse}	Pulse wavelength
$\lambda_{without}$	Wavelength at the temperature without thermal load
σ	Stress
σ_{ij}	Stress Tensor

10. Literature

- [1] B. **Adolphi** und G. **Blassek**: "Oxidation von Indium und eutektischen Indiumlegierungen"; Mat.-wiss. u. Werkstofftech. 24, 8-11, 1993
- [2] J. **Bardeen** and W. **Shockley**: " Deformation Potentials and Mobilities in Non-Polar Crystals"; Phys. Rev. 80, 72-80 (1950)
- [3] Ludwig **Bergmann**, Clemens **Schaefer**, Lehrbuch der Experimentalphysik Band 6 Festkörper, de Gruyter, Berlin, 1992
- [4] Mark L. **Biermann** et al.: "Spectroscopic method of strain analysis in semiconductor quantum-well devices" J. Appl. Phys. 96, 4056-4065 (2004)
- [5] Jens **Biesenbach**: "Konfektionierung von Hochleistungs-Diodenlasern", Dissertation RWTH Aachen, Shaker Verlag, Aachen, (2002)
- [6] G.L. **Bir**, G.E. **Pikus**: "Symmetry and strain-induced effects in Semiconductors"; John Wiley & Sons, New York (1974)
- [7] J. **Bjøntegaard** et al.: "Low Temperature Interdiffusion in Au/In Thin Film Couples"; Thin Solid Film, 101; p. 253-262 (1983)
- [8] G **Blasek**, W. **Werner** und S. **Franz**, Dresden: "Lotwerkstoffe auf Indiumbasis – Eigenschaften Kristallwachstum intermetallischer Verbindungen"; VDI Berichte Nr. 933; 1991
- [9] **Coherent**: "Datasheet of Conduction-Cooled CW and QCW Packaged Bars" (2004)
- [10] Larry A. **Coldren**, Scott W. **Corzine**: "Diode Lasers and Photonic Integrated Circuits"; John Wiley & Sons; 1995
- [11] **Cookson Electronics Assembly Materials**: "Product Bulletin Eutectic Gold/Tin Solder"; www.alphametals.com; 2005
- [12] Paul **Crump** et al.: "Diode laser efficiency increases enable >400-W peak power from 1-cm bars and shows clear path to peak powers in excess of 1-kW"; Proc. of SPIE Vol. 6104 610409-1 (2006)
- [13] **curamik electronics gmbh** "Laser Diode Cooler", Prospekt
- [14] **c ´ t magazin für computer technik**: "Der leise PC"; Heft 17 p.118; 2001
- [15] Robert **Darveaux** and Iwona **Turlik**: "Shear Deformation of Indium Solder Joints"; IEEE Transactions on components, Hybrids, and Manufacturing Technology, Vol. 13, No4 (1990)
- [16] **Department of Defense**: "Test Method Standard Microcircuits MIL-STD-883E"; (1996)
- [17] **Deutsches Kupfer-Institut**: "Werkstoffdatenblatt E-Cu57", Düsseldorf
- [18] R. **Diehl**: "High-Power Diode Lasers, Fundamentals, Technology, Applications"; Springer Verlag, 2000
- [19] **Doduco KG**: "DODUCO Data Book 2nd edition"; Pforzheim; 1983
- [20] **DuPont**: PyraluxProductProperties.pdf; <http://www.pyralux.dupont.com> (2006)

- [21] Thomas **Ebert**: "Optimierung von Mikrostrukturkühlern zur Steigerung der Ausgangsleistung von Hochleistungsdiodenlasern"; Dissertation RWTH-Aachen; Shaker Verlag; Aachen; 1998
- [22] **Elementsix**: company website: <http://www.e6.com> (2006)
- [23] **Encyclopedia.com**: <http://encyclopedia.com/html/i1/indium.asp> (2005)
- [24] **Feinwerktechnik Wittemann GmbH**: <http://www.feinwerktechnik-wittemann.de> (2005)
- [25] Mark A. **Fritz**, Daniel T. **Cassidy**: "Extraction of bonding strain data in diode lasers from polarization-resolved photoluminescence measurements"; Microelectronics Reliability 44; p 787-796 (2004)
- [26] M. **Fukuda**: "Reliability and Degradation of Semiconductor Lasers and Leds"; Artech House, Boston (1991)
- [27] G. **Gerlach**, W. **Dötzel**: "Grundlagen der Mikrosystemtechnik"; Hanser Lehrbuch (1996)
- [28] **Goodfellow GmbH**: <http://www.goodfellow.com> (2005)
- [29] **G. Gottstein**: "Physikalische Grundlagen der Materialkunde"; Springer Verlag (2001)
- [30] **GSFC NASA Advisory**: "Indium Solder Encapsulating Gold Bonding Wire Leads to Fragile Gold-Indium Compounds and Unreliable Condition that Result in Wire Interconnection Rupture"; NA-GSFC-2004-01, Goddard Space Flight Center
- [31] Anquiang **He**, Barbara **Djurfors**, Siamak **Akhlaghi** and **Douglas G. Ivey**: "Pulse Plating of Gold-Tin Alloys for Microelectronic and Optoelectronic Applications"; Best paper published in Plating and Surface Finishing Journal, 2002
- [32] S. **Hengesbach**: "Thermische Simulation von passiven Wärmesenken für Diodenlaserbarren"; Studienarbeit an der RWTH, 2005
- [33] J.J. **Hughes**, D.B. **Gilbert**, and F.Z. **Hawrylo**: "Measurement of the Thermal Resistant of Packaged Laser Diodes", in RCA Review Vol. 46 June 1985, pp. 200-213
- [34] **Indium Corporation of America**: <http://www.indium.com> (2005)
- [35] **Indium Corporation Knowledge Base**: <http://knowledge.indium.com> (2006)
- [36] **INTEL** Website: <http://www.intel80386.com/cpuheat.html> (2005)
- [37] J. **Jandeleit** et al.: "Fabrication and characterization of high power diode lasers"; Proceedings ISPA'99, SPIE, Vol. 3896, pp.65-70 (1999)
- [38] M. **Jansen**, P. **Bournes** et al.: "High performance laser diode bars with aluminium-free active regions"; Optics Express 3; Vol. 4, No.1, 1999
- [39] Jane E. **Jellison**: "Gold-Indium Intermetallic Compounds: Properties and Growth Rates" Code 313: Materials Control and Applications Branch (MC&AB) (1979)
- [40] **JENOPTIK Laserdiode GmbH**: Product sheet of "actively cooled cw and qcw diode lasers without collimation"; <http://www.jold.com> (2006)
- [41] Lawrenc A. **Johnson**: "Laser diode burn-in and reliability testing"; IEEE Communications Magazine (Feb. 2006)
- [42] Yu. I. **Khait** et al.: "Kinetic model for gradual degradation in semiconductor lasers and light-emitting diodes"; Appl Phys. Lett 53 (22), p2135-2137 (1988)

- [43] S.R. **Kisting**, P.W. **Bohn** et al.: "High precision temperature- and energy-dependent refractive index of GaAs determined from excitation of optical waveguide eigenmodes"; Appl. Phys. Lett. 57 (13), 24.September 1990
- [44] **Kugler GmbH**: "Katalog Laseroptik und Systemkomponenten", <http://www.kugler-precision.com> (2005)
- [45] Chin C. **Lee**: "Fluxless bonding technology for high power laser diode arrays" ; Final Report 1998-99 for MICRO Project 98-089
- [46] Chin C. **Lee**, Chen Y **Wang**, Goran **Matijasevic** and Steve S. **Chan**: "A new Gold-indium eutectic Bonding Method"; Material Research Society, Vol. 254; 1992
- [47] M. **Leers** et al.: "Expansion-matched passively cooled heatsinks with low thermal resistance for high-power diode laser bars"; Proceedings of the SPIE, Volume 6104, pp. 20-29 (2006)
- [48] M. **Levinshtein**, S. **Rumyantsev**, and M. **Shur**: "Handbook Series on Semiconductor Parameters0 , Vol 1 "; World Scientific Publishing Company (1996)
- [49] Chien-Chih **Liu** et al.: "The Microstructure Investigation of Flip-Chip Laser Diode Bonding on Silicon Substrate by Using Indium-gold Solder"; IEEE Transactions on Components and Packaging Technologies, Vol. 26, No. 3 (2003)
- [50] Dirk **Lorenzen**: "Methoden zur zuverlässigkeitsorientierten Optimierung der Aufbau- und Verbindungstechnik von Hochleistungs-Diodenlaserbarren", Dissertation TU Berlin, Verlag Dr. Köster, Berlin, 2003
- [51] B.N. **Lucas** and W.C. **Oliver**: "Indentation Power-Law Creep of High-Purity Indium"; Metallurgical and Material Transactions A, Vol. 30A, p 601-610 (1999)
- [52] Arndt **Luedtke**: "Thermal Management Materials for High-Performance Applications"; Advanced engineering materials 6, No.3, p. 142-144, 2004
- [53] E. **Martin**, J.P. Landesman et al.: " Microphotoluminescence mapping of packaging-induced stress distribution in high-power AlGaAs laser diodes"; Applied Physics Letters, Vol. 75, 2521-2523 (1999)
- [54] T.B. **Massalski**: "Binary alloy phase diagrams", American Society for Metals; Metals Park, Ohio; 1986
- [55] **OSRAM Opto Semiconductors**: <http://www.osram-os.com> (2005)
- [56] **OSRAM Opto Semiconductors**: "Datasheet of un-mounted laser bars, 50% fill-factor: SPL BG91-2S" (2005)
- [57] S. **Paul**, J.B. **Roy** and P.K. **Basu**: "Empirical expressions for the alloy composition and temperature dependence of the band gap and intrinsic carrier density in $Ga_xIn_{1-x}As$ ", J. Appl. Phys. 69; p. 827; 1991
- [58] W. **Pittroff** et al.: "Mounting of Laser Bars on Copper Heat sinks Using Au/Sn Solder and CuW Submounts"; Proceedings - Electronic Components & Technology Conference 52nd; p. 276-281; (2002)
- [59] W. **Pittroff** et. al.: "Mounting of High power Laser Diodes on boron Nitride Heat Sinks Using an Optimized Au/Sn Metallurgy", IEEE Trans. on Advanced Packaging, Vol. 24, No. 4, p. 434-441 (2001)

- [60] **Reliasoft Corporation**: "Accelerated Life Testing Reference"; (Rev. 2001) / <http://www.weibull.com>
- [61] Franz **Rinner**: "Verbesserung der Langzeitstabilität von InGaAs/AlGaAs Hochleistungs-Diodenlasern"; Dissertation RWTH Aachen; Shaker Verlag, Aachen; 2003
- [62] Christian **Scholz** et al.: "Mechanical stress-reducing heat sinks for high-power diode lasers "; Proceedings of the SPIE, Volume 5336, pp. 176-187 (2004)
- [63] R.L. **Sellin** et al.: "High-reliability MOCVD-grown quantum dot laser", Electronics Lessters Vol. 38 No. 16 (2002)
- [64] V. **Simic** and Z. **Marinkovic**: "Thin film interdiffusion of Au and In at room temperature"; Thin solid films, p57-61, 41, 1977
- [65] Jasprit **Singh**: "Semiconductor Optoelectronics, Physics and Technology", McGRAW-HILL , Inc. (1995)
- [66] **Sumitomo Electric Industrie, LTD**: company website: <http://www.sumitomoelectricusa.com> (2006)
- [67] B. **Sumpf** et al.: "High-power 980nm quantum dot broad area lasers"; Electronics Letters Vol. 39 No. 23 (2003)
- [68] **Telcordia GR-468-CORE**, "Generic Reliability Assurance Requirements for Optoelectronic Devices Used In Telecommunications Equipment (a module of RQGR, FR-796) Bellcore, Issue 1, December 1998
- [69] J.W. **Tomm** et al.: "Transient thermal tuning properties of single emitters in actively cooled high-power cm-bar arrays"; SPIE Proc. 5336; p.125-131 (2004)
- [70] J.W. **Tomm** et al.: "Quantitative strain analysis in AlGaAs-based devices"; Applied Physics Letters; Vol. 82, no 23 (2003)
- [71] J.W. **Tomm** et al.: "Spatially resolved spectroscopic strain measurement on high-power laser diode bars"; J. Appl. Phys. 93, p. 1354-1362 (2003)
- [72] J.W. **Tomm** et al.: "Direct spectroscopy measurement of packaging-induced strains in high-power diode arrays"; Proc. SPIE 3626 (1999)
- [73] J.W. **Tomm** and J. Jiménez: "Quantum-Well Laser Array Packaging" McGraw-Hill Professional (2006)
- [74] Y.P. **Varshni**: "Temperature dependence of the energy gap in semiconductors"; Physica 34, p149-154, 1967
- [75] Ramnath **Venkatramon**, James R. **Wilcox**, and Stephen R. **Cain**: "Experimental study of the kinetics of transient liquid phase solidification reaction in electroplated gold-tin layers on copper", Metallurgical and Materials Transactions A, Vol. 28A, p.699-706, March 1997
- [76] T. **Westphalen**: "Untersuchung von Hochleistungs-Diodenlaserbarren mittels Einzelemitter-aufgelöster Charakterisierung" Diplomarbeit am Lehrstuhl TOS der RWTH-Aachen (2006)
- [77] Markus **Weyers**: "GaAs-based high power laser diodes", 11th European Workshop on MOVPE, Lausanne June 5th-8th 2005

- [78] C. E. T. **White** and H. **Okamoto**. "Phase Diagrams of Indium Alloys and their Engineering Applications"; ASM International (1992)
- [79] Nicolas **Wiedmann**: "Hochleistungsdiodenlaser für Hochtemperaturanwendung"; Dissertation RWTH Aachen; Shaker Verlag, Aachen; 2002
- [80] **Wikipedia**, the free encyclopaedia: <http://www.wikipedia.org> (2005, 2006)
- [81] **Williams Advanced Materials inc**: <http://www.williams-adv.com> (2005)
- [82] R. **Xia** et al: "Mounting-induced Strain Threshold for the Degradation of High-Power AlGaAs Laser Bars", IEEE Photonics Technology Letters, Vol. 15, No. 7 (2002)
- [83] Chi **Yan** et al.: "Observing lateral temperature and refractive index profiles in an optical pumped midinfrared laser through temporally and spatially resolved spectra"; Appl. Phys. Lett. 71 (21); 1997
- [84] C.L. **Yu** et al.: "Intermetallic Compounds Formed at the Interface between Liquid Indium and Copper Substrates"; Journal of Electronic Materials, Vol. 31, No.5 (2002)
- [85] U.**Zeimer** et al: "Insitu characterization of strain distribution in broad-area high-power lasers under operation by high-resolution x-ray diffraction and topography using synchrotron radiation"; J. Phys. D: Appl. Phys. 32; 1999
- [86] Carl H. **Zweben**: "New material options for high-power diode laser packaging"; Proceedings of SPIE; Volume 5336, High-Power Diode Laser Technology and Applications II, June 2004, pp. 166-175

Acknowledgements

The work was done at the Fraunhofer Institute for Laser Technology.

In particular, I would like to thank Prof. Dr. R. Poprawe M.A. for the topic, supervision, and support of my work. Prof. Dr. P. Loosen I would like to thank for the thorough review of my thesis.

I am grateful for Dr. Konstantin Boucke's review of my thesis, as well as many very helpful and supportive discussions, which helped me to move forward with my work.

To my colleagues of the Fraunhofer ILT department "Laser Components" I have to say thank you for your support. In particular Wolfgang Brandenburg for his encouraging words, Carsten Heuer and Michael Janßen for their introduction in mechanical drawings and design, Michael Leers for the interesting dialogs about the FEM-simulations, Anja Seidel for the packaging of many laser bars with all the different packages, Natascha Schwanen for the numerous hours in front of the SEM (REM), and Thomas Westphalen for the special characterisation of the diode lasers.

I am grateful to Daniel, my brother in-law, for the time consuming final correction of my English grammar and spelling and to my wife Pamela, for the repeated correction of the many rough drafts of my dissertation.

I thank my parents and my wife for their understanding of this endeavour, which has consumed much of my time throughout the last years.

Jens Tom (MBI) and Myriam Oudart (TRT) I would like to thank for their interesting dialogs and the stress measurements, which was supported by the European Commission through the IST projects WWW.BRIGHT.EU (IST-511722) (2004-2006) (<http://www.bright-eu.org>) and POWERPACK (IST-2000-29447) (2001-2004).

In closing, I would like to thank all the persons not mentioned here, who have contributed to my work. Thank you.

Curriculum Vitae

Christian Scholz, born August 26, 1973 in Duisburg, Germany

1980 – 1984	Attended elementary school GGS Großenbaumer Allee, Duisburg (Germany)
1984 – 1993	Attended high school Steinbart-Gymnasium, Duisburg (Germany)
1993 – 1994	Community service for the Protestant Church community Duisburg-Innenstadt, Duisburg (Germany)
1994 – 2000	Studied physics at RWTH Aachen University of Technology, Aachen (Germany)
04.07.2000	Finished with Diploma in Physics. Diploma Thesis at Fraunhofer Institute for Laser Technology: "Investigation of the joint between laser bar and copper micro-channel heat sink".
2000 – Present	Scientist at Fraunhofer Institute for Laser Technology, Department of Laser Components, Aachen (Germany)